UNIVERSITEIT VAN PRETORIA
UNIVERSITY OF PRETORIA
YUNIBESITHI YA PRETORIA
Denkleiers • Leading Minds • Dikgopolo tša Dihlalefi

Wall Heat Transfer Coefficient in a Molten Salt Bubble Column

by

Petrus Jabu Skosana

A dissertation submitted in partial fulfilment of the requirements for the degree

Master of Engineering (Chemical Engineering)

in the

Department of Chemical Engineering
Faculty of Engineering, the Built Environment and Information Technology

University of Pretoria

Pretoria

October 2014

Wall Heat Transfer Coefficient in a Molten Salt Bubble Column

Author : Petrus Jabu Skosana
Supervisor : Prof. Mike Heydenrych
Co-supervisor : Dr David Van Vuuren
Department : Chemical Engineering, University of Pretoria
Degree : Master of Engineering (Chemical Engineering)

SYNOPSIS

The Council for Scientific and Industrial Research (CSIR) is developing a novel process to produce titanium metal at a lower cost than the current Kroll process used commercially. The technology initiated by the CSIR will benefit South Africa in achieving the long-term goal of establishing a competitive titanium metal industry.

A bubble column reactor is one of the suitable reactors that were considered for the production of titanium metal. This reactor will be operated with a molten salt medium. Bubble columns are widely used in various fields of process engineering, such as oxidation, hydrogenation, fermentation, Fischer–Tropsch synthesis and waste water treatment. The advantages of these reactors over other multiphase reactors are simple construction, good mass and heat transfer, absence of moving parts and low operating costs.

High heat transfer is important in reactors when high thermal duties are required. An appropriate measurement of the heat transfer coefficient is of primary importance for designing reactors that are highly exothermic or endothermic.

An experimental test facility to measure wall heat transfer coefficients was constructed and operated. The experimental setup was operated with tap water, heat transfer oil 32 and lithium chloride–potassium chloride (LiCl–KCl) eutectic by bubbling argon gas through the liquids. The column was operated at a temperature of 40 ^{o}C for the water experiments, at 75, 103 and 170 ^{o}C for the heat transfer oil experiments, and at 450 ^{o}C for the molten salt experiments. All the experiments were run at superficial gas velocities in the range of 0.006 to 0.05 m/s. Three heating tapes, each connected to a corresponding variable AC voltage controller, were used to heat the column media.

Heat transfer coefficients were determined by inducing a known heat flux through the column wall and measuring the temperature difference between the wall and the reactor contents. In order to balance the system, heat was removed by cooling water flowing through a copper tube on the inside of the column. Temperature differences between the column wall and the liquid were measured at five axial locations.

A mechanistic model for estimating the kinematic turbulent viscosity and dispersion coefficient was developed from a mechanism of momentum exchange between large circulation cells. By analogy between heat and momentum transfer, these circulation cells also transfer heat from the wall to the liquid.

There were some challenges when operating the bubble column with molten salt due to leakages on the welds and aggressive corrosion of the column. The experimental results were obtained when operating the column with water and heat transfer oil. It was found that the heat transfer coefficient increases with superficial gas velocity. The values of the heat transfer coefficient for the argon–water system were higher than those for the argon–heat transfer oil system. The heat transfer coefficients were also found to increase with an increase in temperature. Gas holdup increased with the superficial gas velocity. It was found that the estimated axial dispersion coefficients are within the range of those reported in the literature and the ratios of dispersion coefficients are in agreement with those in the literature. The estimated kinematic turbulent viscosities were comparable with those in the literature.

Keywords: Bubble column; molten salt; heat transfer coefficient; gas holdup; dispersion coefficient.

ACKNOWLEDGEMENTS

- I would like to express my sincere gratitude to the Department of Science and Technology for providing the funding for this research project and to the CSIR for the use of its facilities.
- I would like to thank the following people for their contribution:
  - I want to express my sincere gratitude to Dr David Van Vuuren, who is my manager at the CSIR and was my co-supervisor for this project. His constructive criticism, stimulating discussions and constructive suggestions were of great value in accomplishing this work. I also want to thank him for his patience and for motivating me when the going got tough.
  - I want to thank Prof. Mike Heydenrych of the University of Pretoria, who was my supervisor, for his patience and understanding in all the challenges we came across and for his guidance and support through the project.
  - I want to thank my colleague, Mr Dannie Snyman, for his help with all the electrical connections for the experimental setup.
  - I appreciate the assistance I received from the staff at the CSIR mechanical workshop with the mechanical design, machining and welding of the equipment.
  - Finally I want to thank my family for their support, encouragement and understanding throughout my studies.

CONTENTS

SYNOPSIS ..... **i**

ACKNOWLEDGEMENTS ..... **iii**

LIST OF FIGURES ..... **vii**

LIST OF TABLES ..... **ix**

NOMENCLATURE ..... **xi**

CHAPTER 1: INTRODUCTION **1**

1.1 Motivation and background 1

1.2 Research problem 3

1.3 Aims and objectives 4

1.4 Structure of the dissertation 4

CHAPTER 2: LITERATURE REVIEW **6**

2.1 Heat transfer coefficient 6

2.1.1 Theory of heat transfer 6

2.1.1.1 Conductive heat transfer 6

2.1.1.2 Convective heat transfer 7

2.1.1.3 Wall heat transfer in bubble columns 8

2.1.2 Heat transfer correlations 8

2.1.3 Experimental methods 12

2.1.4 Effect of operating parameters on heat transfer coefficient 14

2.1.4.1 Superficial gas velocity 14

2.1.4.2 Liquid properties 15

2.2 Gas holdup 15

2.2.1 Gas holdup theory 15

2.2.1.1 Flow regimes 15

2.2.1.2 Prediction of gas holdup 17

2.2.3 Gas holdup correlations 20

2.2.2 Measuring equipment and techniques 23

2.2.2.1 Overall gas holdup 23
2.2.2.2 Level expansion method 24
2.2.4 Effect of operating parameters on gas holdup 29
2.2.4.1 Superficial gas velocity 29
2.2.4.2 Operating temperature 29
2.3 Axial dispersion coefficient 30
2.3.1 Circulation patterns 30
CHAPTER 3: EXPERIMENTAL SETUP AND PROCEDURE 33
3.1 Experimental setup 33
3.1.1 Column 35
3.1.2 Gas supply 35
3.1.3 Gas distributor 35
3.1.4 Heat transfer section 36
3.1.5 Modified experimental setup 38
3.2 Experimental procedure 39
3.2.1 Heat transfer coefficient 39
3.2.1.1 Column operated with water 40
3.2.1.2 Column operated with heat transfer oil 40
3.2.1.3 Column operated with molten salt mixture 41
3.2.2 Gas holdup 41
3.3 Experimental understanding 41
3.3 1 Impact of cooling water 41
3.3.2 Comparison between stainless steel and copper bubble column 42
3.3.3 Modelling of the temperature profile in the thermowell 44
CHAPTER 4: RESULTS AND DISCUSSION 49
4.1 Heat transfer coefficient 49
4.1.1 Column operated with water 49
4.1.2 Column operated with heat transfer oil 52
4.1.3 Column operated with molten salt mixture 54

4.2 Gas holdup 56
4.2.1 Column operated with water 56
4.2.2 Column operated with heat transfer oil 57
4.3 Mechanistic model for dispersion coefficients 58
4.3.1 Liquid flow model 58
4.3.2 Model for turbulent viscosity and dispersion coefficients 62
4.3.3 Model verification 66
CHAPTER 5: CONCLUSIONS AND RECOMENDATIONS 72
REFERENCES 74
APPENDICES 84
Appendix 1: Experimental data for heat transfer coefficient measurements 84
Appendix 2: Experimental data for gas holdup measurements 91
Appendix 3: Data for mathematical modelling of dispersion coefficients 94
Appendix 4: Calculation of experimental and percentage error 99
Appendix 5: Temperature difference between the column centre and the liquid–film interface 101
Appendix 6: Derivation of gas holdup equation 107
Appendix 7: Calibration 110
Appendix 8: Gas distributor design 113
Appendix 9: Calculations of the mass of LiCl and KCl in the eutectic mixture 116
Appendix 10: Photograph of the bubble column test rig 118

LIST OF FIGURES

Figure 2.1: Schematic representation of the temperature profile in a bubble column (Dhotre et al., 2005) 8

Figure 2.2: Schematic diagram of the experimental apparatus for heat transfer coefficient measurements in the bubble column (Hikita et al., 1981) 12

Figure 2.3: Heat transfer section of the bubble column (Hikita et al., 1981) 13

Figure 2.4: Types of flow regime in bubble columns (Shaikh & Al-Dahhan, 2007) 16

Figure 2.5: Comparison of the overall gas holdup measured by the pressure drop and the bed expansion method (Zhang et al., 2003) 23

Figure 2.6: Gas holdup as a function of superficial gas velocity obtained by using the level expansion and pressure difference methods (Fransolet et al., 2001) 24

Figure 2.7: Schematic diagram of gas holdup and liquid velocity profile 31

Figure 2.8: Liquid circulation patterns in bubble columns 32

Figure 3.1: Schematic diagram of the experimental setup 33

Figure 3.2: Photograph of the experimental setup 34

Figure 3.3: Perforated plate showing the arrangement of the orifices 36

Figure 3.4: Gas distributor fitted with ¼ in. stainless steel tubing 36

Figure 3.5: Thermocouples soldered to the wall of the copper pipe 37

Figure 3.6: Schematic diagram of the modified experimental setup 39

Figure 3.7: Temperature profile between spacing of heating elements for a stainless steel pipe 43

Figure 3.8: Temperature profile between spacing of heating elements for a copper pipe 44

Figure 3.9: Thermowell used for temperature measurements 45

Figure 3.10: Temperature profile for stainless steel and copper thermowells 48

Figure 4.1: Different runs for measuring the heat transfer coefficient 50

Figure 4.2: Comparison of experimental heat transfer coefficient with the literature for measurements in water medium 51

Figure 4.3: Comparison of experimental heat transfer coefficient with the literature for measurements in water medium in the modified experimental setup[1] 52

Figure 4.4: Heat transfer coefficient at different temperatures 53

Figure 4.5: Comparison of heat transfer coefficients with the literature for measurements in heat transfer oil medium 54

Figure 4.6: Copper pipe damaged by leakage of molten salt 55

Figure 4.7: Experimental setup before salt leakage (new test rig) 55

Figure 4.8: Experimental setup after salt leakage 56

Figure 4.9: Comparison of experimental results for gas holdup with the literature 57

Figure 4.10: Experimental gas holdup at heat transfer oil 57

Figure 4.11: Schematic diagram depicting the momentum exchange between circulation cells 63

Figure 4.12: Comparison of predicted and experimental kinematic turbulent viscosity 67

Figure 4.13: Variation of axial dispersion coefficient with the column diameter 68

Figure 4.14: Predicted axial dispersion coefficient 69

Figure 4.15: Experimental axial dispersion coefficients from the literature (Baird & Rice, 1975) 70

Figure A6.1: Column level before and after bubbling 107

Figure A7.1: Brass block that ensures uniform temperature 110

Figure A7.2: Water bath used for calibrating the thermocouples 111

Figure A10.1: Photograph of the bubble column test rig with thermal insulation 118

LIST OF TABLES

Table 2.1: Summary of the heat transfer correlations investigated by various researchers . 10

Table 2.2: Summary of the gas holdup correlations investigated by researchers 20

Table 2.3: Level measuring techniques (Omega, 2001) 26

Table 3.1: Physical properties of the liquids 35

Table 4.1: Comparison of heat input and heat output 49

Table 4.2: Temperature difference measured at different axial positions of the heating zone for u_G = 0.031 m/s 49

Table 4.3: Ratios of axial to radial dispersion coefficient 71

Table A1.1: Data for the column operated with water at 40 °C and $u_G = 0.006$ m/s 84

Table A1.2: Data for the column operated with water at 40 °C and $u_G = 0.016$ m/s 84

Table A1.3: Data for the column operated with water at 40 °C and $u_G = 0.024$ m/s 85

Table A1.4: Data for the column operated with water at 40 °C and $u_G = 0.033$ m/s 85

Table A1.5: Data for the column operated with water at 40 °C and $u_G = 0.040$ m/s 85

Table A1.6: Data for the column operated with water at 40 °C and $u_G = 0.047$ m/s 86

Table A1.7: Data for the column operated with water at 40 °C and $u_G = 0.051$ m/s 86

Table A1.8: Data for the column operated with heat transfer oil at $T = 75$ °C ($u_G = 0.007$ m/s) and 103 °C ($u_G = 0.009$ m/s) 87

Table A1.9: Data for the column operated with heat transfer oil at $T = 75$ °C ($u_G = 0.017$ m/s) and 103 °C ($u_G = 0.019$ m/s) 87

Table A1.10: Data for the column operated with heat transfer oil at $T = 75$ °C ($u_G = 0.027$ m/s) and 103 °C ($u_G = 0.029$ m/s) 88

Table A1.11: Data for the column operated with heat transfer oil at $T = 75$ °C ($u_G = 0.0035$ m/s) and 103 °C ($u_G = 0.038$ m/s) 88

Table A1.12: Data for the column operated with heat transfer oil at $T = 75$ °C ($u_G = 0.041$ m/s) and 103 °C ($u_G = 0.045$ m/s) 89

Table A1.13: Data for the column operated with heat transfer oil at $T = 75$ °C ($u_G = 0.046$ m/s) and 98 °C ($u_G = 0.05$ m/s) 89

Table A1.14: Data for the column operated with heat transfer oil at $u_G = 0.049$ m/s 90

Table A2.1: First run for the column operated with water at 40 °C 91

Table A2.2: Second run for the column operated with water at 40 °C 92

Table A2.3: Third run for the column operated with water at 40 °C 93

Table A2.4: Data for the column operated with heat transfer oil at 170 °C 93

Table A7.1: Temperature difference for thermocouples inserted into water 111

Table A7.2: Calibration of a thermowell 112

NOMENCLATURE

A	heat transfer area	[m^2]
A_r	area ratio of nozzle to column	[–]
a_S	empirical constant	[–]
C_B	concentration for substance B	[kmol/m^3)]
C_P	specific heat capacity of the liquid	[kJ.kg^{-1}.K^{-1}]
C_{PS}	average slurry concentration	[kg(solid)/kg(slurry)]
$C_{P,sl}$	specific heat capacity of the slurry	[kJ.kg^{-1}.K^{-1}]
d_b	bubble diameter	[m]
D_C	column diameter	[m]
D_n	nozzle diameter	[m]
D_o	orifice diameter	[m]
d_o	hole diameter of the distributor	[m]
d_P	diameter of cylindrical probe	[m]
d_S	sparger diameter	[m]
E_r	radial dispersion coefficient	[m^2/s]
E_Z	axial dispersion coefficient	[m^2/s]
g	gravitational acceleration	[m/s^2]
$\dot{G}$	mass flux across the curved surface where the liquid velocity is zero	[$kg.s^{-1}.m^{-2}$]
ΔH	height difference between the two pressure transducers	[m]
H	gas–liquid dispersion height or depth of the dip tube in gas–liquid dispersion	[m]
h	heat transfer coefficient	[$W.m^{-2}.K^{-1}$]
H_{mano}	head of the manometer	[m]
H_0	gas-free liquid height	[m]
H_r	ratio of height to diameter	[–]
h_S	stagnation point heat transfer coefficient	[$W.m^{-2}.K^{-1}$]
h_W	wall heat transfer coefficient	[$W.m^{-2}.K^{-1}$]
I	vibration intensity	[m/s]

j_{GL}	drift flux	[m/s]
k	thermal conductivity	[W.m^{-1}.K^{-1}]
ΔL	distance between the measured temperature difference	[m]
L_j	liquid jet length	[m]
$m_{upwards}$	liquid mass flowrate in the upwards direction of the circulation cell	[kg/s]
n	constant in gas holdup equation	[–]
N	number of data points	[–]
$\dot{N}_B$	molar flow of substance B	[kmol/s]
P	pressure	[Pa]
P_e	electrical power	[W]
P_m	energy dissipation rate per unit mass	[m^2/s^3]
P_S	vapour pressure of the liquid phase	[Pa]
P_{tip}	pressure at the tip of the bubbler	[Pa]
P_{top}	pressure at the surface of the liquid	[Pa]
P_v	power dissipation rate per unit mass	[m^2/s^3]
Q	rate of heat transfer	[W]
Q_{loss}	heat loss from the heating element to the surrounding environment	[W]
r	radial coordinate	[m]
r_o	column radius where liquid velocity is zero	[m]
R	column radius	[m]
s	standard deviation of the data	
S_b	cross-sectional area ratio of the column and the distributor for the tapered bubble column	[–]
T_B	bulk liquid temperature	[^{o}C]
T_W	surface temperature	[^{o}C]
ΔT	temperature difference	[^{o}C]
ΔT_i	temperature difference at ΔL	[^{o}C]
u	interstitial liquid velocity	[m/s]
u_G	superficial gas velocity	[m/s]
u_{Gr}	superficial gas velocity in the riser	[m/s]

u_L	superficial liquid velocity	[m/s]
u_{Lb}	rise velocity of large bubble	[m/s]
u_{mG}	minimum superficial gas velocity for no weeping	[m/s]
u_S	superficial gas velocity through the column	[m/s]
u_{Sb}	rise velocity of small bubble	[m/s]
u_{trans}	transition velocity	[m/s]
u_W	liquid interstitial velocity at the wall	[m/s]
V_G	gas volume	[m^3]
V_j	jet velocity at nozzle exit	[m/s]
V_L	liquid volume	[m^3]
ΔV	voltage difference	[mV]
V_o	critical weep velocity	[m/s]
x	heat transfer path	[m]
$\bar{x}$	mean of the data	
x_i	individual data point	
z	critical value for a 95% confidence level	[–]
Z	distance from the tip of a dip tube to the bottom of the column	[m]
ΔZ	height of recirculation cell	[m]

Dimensionless numbers

Ar	Archimedes number	$D_C^3 \rho_L^2 g / \mu_L^2$
Eo	Eotovs number	$D_C^2 \rho_L g / \sigma_L$
Fr	Froude number	$u_G^2 / g d_b$
Fr'	modified Froude number	$\left(V_o^2 / d_o g\right) \times \left[\rho_G / (\rho_L - \rho_G)\right]^{5/4}$
Mo	Morton number	$g \mu_L^4 / \rho_L \sigma_L^3$
N	number of holes	[–]
Nu	Nusselt number	hL / k_L
Pr	Prandtl number based on liquid properties	$C_P \mu_L / k_L$

Pr_{sl}	Prandtl number based on slurry properties	$C_{Psl}\mu_{sl}/k_{sl}$
Re	Reynolds number based on liquid properties	$u_G D_C \rho/\mu$
Re_{sl}	Reynolds number based on slurry properties	$u_G D_C \rho_{sl}/\mu_{sl}$
St	Stanton number	$h/\rho_L C_P U_G \mu_L$
St_{sl}	Stanton number based on slurry properties	$h/\rho_{sl} C_{psl} U_G$
Su	Suratmann number of liquid	$\rho_L \sigma_L D_n/\mu_L^2$
We_o	Weber number at the critical weep point	$\rho_G d_o V_o^2/\sigma_L$

Greek letters

α	thermal diffusivity	[m^2/s]
δ	distance travelled by lump of fluid for it to change momentum	[m]
ε_{av}	average gas holdup	[–]
ε_G	gas holdup as a function of a column radius	[–]
$\bar{\varepsilon}_G$	average gas holdup	[–]
ε_{Gr}	gas holdup in the riser	[–]
ε_L	liquid holdup	[–]
ε_S	solid holdup	[–]
ε_{trans}	gas holdup at the transition velocity	[–]
μ	mean value for the continuous variable x	
μ_L	viscosity of the liquid phase	[kg.m^{-1}.s^{-1}]
μ_t	turbulent viscosity	[kg.m^{-1}.s^{-1}]
μ_{sl}	viscosity of slurry	[kg.m^{-1}.s^{-1}]
ρ_{av}	average suspension density	[kg/m^3]
ρ_{disp}	density of the gas–liquid dispersion	[kg/m^3]
ρ_G	gas density	[kg/m^3]
ρ_L	liquid density	[kg/m^3]
ρ_S	solid density	[kg/m^3]

ρ_{sl}	density of the slurry	[kg/m^3]
ρ_{water}	density of water in the manometer	[kg/m^3]
σ_L	surface tension of the liquid	[N/m]
τ	shear stress	[kg.m^{-1}.s^{-2}]
τ_W	shear stress at the wall	[kg.m^{-1}.s^{-2}]
υ	kinematic viscosity	[m^2/s]
υ_L	kinematic viscosity of a liquid	[m^2/s]
υ_M	molecular kinematic viscosity	[m^2/s]
υ_t	turbulent kinematic viscosity	[m^2/s]
ϕ_L	solid-phase volume fraction	[–]

Subscripts

b	bubble
B	bulk
C	critical or column
G	gas
GL	gas liquid
i	insulation
j	jet
L	liquid
Lb	large bubble
M	molecular
n	nozzle
o	orifice
P	probe
PS	solid particles
r	radial coordinate or riser
S	solid or stagnant
Sb	small bubble
Sl	slurry
t	tip or turbulent
W	wall
Z	axial coordinate

CHAPTER 1: INTRODUCTION

1.1 Motivation and background

The Council for Scientific and Industrial Research (CSIR) is developing a novel process to produce titanium metal at a lower cost than the current Kroll process used commercially. The technology initiated by the CSIR will benefit South Africa in achieving the long-term goal of establishing a competitive titanium (Ti) metal industry.

Ti is usually produced by the reduction of titanium tetrachloride ($TiCl_4$) with magnesium to form titanium metal and magnesium dichloride as given by Equation 1.1, named the Kroll process (Takeda & Okabe, 2006).

$$TiCl_4(g) + 2Mg(l) \longrightarrow Ti(s) + 2MgCl_2(s) \qquad [1.1]$$

The ongoing research at the CSIR is aimed at producing titanium metal by continuous reduction of $TiCl_4$ with a certain alkali or alkali earth metal (Van Vuuren, Oosthuizen & Heydenrych, 2011). This reaction is exothermic and takes place in a molten salt medium. The overall process for the CSIR–Ti technology is believed to be cheaper than the Kroll process. The CSIR–Ti process will be continuous, in contrast to the Kroll process which is operated in batches. A bubble column reactor is one of the suitable reactors that are being considered by the CSIR for the reduction reaction to take place. Because of the exothermic nature of the reduction reaction, the cooling jacket needs to be installed for heat recovery. The design of a reactor cooling jacket requires data for heat transfer coefficients.

Bubble columns are widely encountered in industrial fields of process engineering, such as fermentation processes, hydrometallurgical processes, petrochemical processes and waste water treatment (Degaleesan, Dudukovic & Pan, 2001). Bubble columns are also used for chemical processes such as oxidation, chlorination, alkylation, polymerisation and hydrogenation reactions. Other processes that employ bubble columns include the hydrotreating and conversion of petroleum residues, and direct and indirect liquefaction in the production of liquid fuels from coal. The bubble column has also been identified as a suitable type of reactor for a variety of gas conversion processes involving the production of liquid fuels from synthesis gas, such as the Fischer–Tropsch process and the synthesis of methanol.

These systems can be operated in either a continuous or a semi-batch mode. In a three-phase system, fine solid particles are present in bubble columns. The solid particles can be either catalysts, biomass, mineral particles and reactants or products of a reaction (Todt, Lucke, Schugerl et al., 1977). In the continuous mode, a gas and liquid either flow cocurrently up or countercurrently. In the latter case, a gas is flowing in the upward direction while a liquid is flowing downwards. In the semi-batch mode, a liquid is stationary inside the column while a gas is flowing upwards.

Bubble columns possess wider industrial applications than other multiphase reactors such as fluidised bed reactors, packed bed reactors, trickle bed reactors and continuous stirred tank reactors due to the benefits they provide. These include the following (Joshi, Vitankar, Kulkarni et al., 2002; Ruthiya, 2005; Tiefeng, Jinfu & Yong, 2007; Vinit, 2007; Singh & Majumder, 2010):

- Ease of construction since they contain only a cylindrical vessel, a gas distributor and a few internals.
- Low maintenance costs due to the absence of moving parts.
- Isothermal conditions.
- High mass and heat transfer rates.
- Online catalyst addition and removal.
- Large liquid residence time which is suited to slow reactions.
- Higher effective interfacial area and liquid mass transfer coefficients.

However, there are some drawbacks in this reactor which include bubble coalescence, back mixing which negatively affects the conversion of the reactants, low catalyst loading, the fact that catalyst deactivation can increase if the solids concentration is increased, and difficult separation of fine particles from the liquid phase (Gandhi & Joshi, 1999). Although bubble columns are often preferred over other types of reactor, their design is still a challenging task due to:

- Their hydrodynamics are complex.
- There is a lack of hydrodynamic data over a wide range of operating conditions.
- Most of the reported data are for air–water systems at room temperature.
- There are still some difficulties with accurate experimental and measuring techniques for bubble columns.

Due to their industrial importance and wide applicability, their design and scale up has received attention for many years (Kantarci, Borak & Ulgen, 2005a). Moreover, the continuous research in this field has led to the application of computational fluid dynamics

(CFD) which is the computational tool that uses numerical methods and algorithms to model fluid dynamics problems (Cartland Glover, Generalis & Thomas, 2000; Delnoij, Kuipers & Van Swaaij, 1997; Rampure, Mahajani & Ranade, 2009; Van Baten, Ellenberger & Krishna, 2003). CFD methods can be combined with experimental data to model hydrodynamic correlation to cover a wider range of experimental conditions. CFD methods can thus improve the applicability of a correlation in predicting the hydrodynamic parameters.

The hydrodynamics of bubble columns have been extensively documented in the literature (Gandhi, Prakash & Bergougnou, 1999; Mudde & Saito, 2001; Soong, Harke, Gamwo et al., 1997). The hydrodynamic parameters typically considered in bubble columns are: (a) bubble sizes; (b) flow regime; (c) gas holdup; (d) liquid-side mass transfer coefficient; (e) heat transfer coefficient; and (f) axial dispersion coefficient. Flow regimes, bubble sizes and their distribution, and gas holdup are the primary design parameters, while mass and heat transfer coefficients, gas–liquid interfacial areas and axial dispersion coefficients are the secondary design parameters needed for developing correlations and for the performance evaluation of bubble columns (Ghosh & Upadhyay, 2007). The performance of a bubble column is highly dependent on these hydrodynamic parameters. It is, therefore, imperative to conduct thorough measurements and data analysis of these parameters.

1.2 Research problem

Much of literature has been reported on the heat transfer coefficient measured from the heat flux induced by an immersed heater or heated column wall, and the corresponding temperature difference between the heated surface and the column dispersion (Li & Prakash, 1997; Jhawar & Prakash, 2007; Wu, Al-Dahhan & Prakash, 2007; Deckwer, Loulsl, Zaldl et al., 1980b; Fair, Lambright & Andersen, 1962; Hikita, Asai, Kikukawa et al., 1981). These measurements were done mostly for water, aqueous and hydrocarbon liquid systems, but few if any have been reported on heat transfer coefficient measurements using molten salts at high temperatures.

Heat transfer in bubble columns is assumed to be analogous to heat transfer in pipe flow. In bubble columns operated in a heterogeneous flow regime, circulation cells are present which exchange momentum in a similar way to liquid eddies in the case of a pipe flow. Similar to pipe flow, there is an analogy between mass, momentum and heat exchange in bubble columns. Therefore, the heat is transferred from the wall to the bulk of the liquid by the momentum exchange in circulation cells.

However, little work was done previously on the modelling of turbulent viscosities and dispersion coefficients caused by the momentum exchange of the circulation cells. In addition to the measurement of the heat transfer coefficient, a mechanistic model for dispersion coefficients will be developed.

1.3 Aims and objectives

The main aim of this research project is to measure the wall heat transfer coefficient in a bubble column operated with different molten salt media.

The research objectives are:

- To study the effect of superficial gas velocity on the heat transfer coefficient and the gas holdup.
- To compare the experimental results with those in the literature.
- To develop a mechanistic model for dispersion coefficients from an analogy with momentum exchange between circulation cells.

1.4 Structure of the dissertation

Chapter 1 gives the motivation for this work and background on bubble columns. The aims and objectives of the research are also explained.

Chapter 2 is a literature study on the heat transfer coefficient, the gas holdup and the axial dispersion coefficient. Sections 2.1 to 2.3 are structured as follows:

- Heat transfer coefficient:
  - Studies the reported literature for the heat transfer coefficient.
  - Studies different experimental setups for measuring the wall heat transfer coefficient.
- Gas holdup:
  - Studies different techniques for measuring the gas holdup.
  - Studies different experimental setups for measuring the wall heat transfer coefficient.
- Axial dispersion coefficient:
  - Studies the mechanism of liquid circulation in bubble columns.

Chapter 3 explains the methodology used for measuring the heat transfer coefficient and the gas holdup.

Chapter 4 discusses the experimental results obtained for the heat transfer coefficient and the gas holdup. The theoretical work on modelling the dispersion coefficients is also explained.

Chapter 5 draws conclusions from the findings of the study and gives recommendations that should be taken into consideration when measuring the wall heat transfer coefficient in bubble columns.

CHAPTER 2: LITERATURE REVIEW

2.1 Heat transfer coefficient

One advantage of bubble columns is their high rates of heat transfer. Heat transfer in bubble columns is 20–100 times greater than in single-phase flow (Chen, Hasegawa, Tsutsumi et al., 2003; Joshi, Sharma, Shah et al., 1980; Kantarci et al., 2005a), which promotes fast removal or addition of heat. Proper implementation of heat transfer coefficient measurements is, therefore, crucial for the design and optimisation of bubble columns to ensure the appropriate removal or addition of heat. In many instances the amount of heat removed or added to the column is of importance in order to maintain catalyst activity, reaction integrity and product quality (Gandhi & Joshi, 2010).

Heat transfer in bubble columns has been studied by several investigators. Measurements of heat transfer coefficients in bubble columns can be divided into two methods (Kantarci et al., 2005a): (a) heat transfer from the heated column wall to the contents and (b) heat transfer from an immersed heater to the contents. The experimental study for this work focused only on heat transfer from the column wall. Wall heat transfer coefficients in a bubble column can be measured by employing a heat source and then measuring the energy input and temperature difference between the surface of the heat source and the column dispersion.

2.1.1 Theory of heat transfer

Heat is the energy transferred from a hot system to a cold system as a result of a temperature gradient. Consequently, there cannot be any heat transfer in the case of a zero temperature gradient. Generally, heat can be transferred in three different modes, namely conduction, convection and radiation (Cengel, 2003: 17). Only conductive and convective heat transfer are discussed in this section.

2.1.1.1 Conductive heat transfer

Conductive heat transfer is the energy transfer between fundamental particles in a solid, liquid or gas as a result of the interaction and temperature difference between the particles (Cengel, 2003: 18). Generally, if a hot object is brought into contact with a cold object, the hot object becomes cooler while the cold object becomes warmer. Therefore, heat has been transferred from the hot to the cold object. Conduction in solids is a result of vibration between particles in a lattice and energy transport by free electrons. In gases and liquids, conduction is due to collision and diffusion of the molecules during their random motion. It

must be noted that heat is transferred by conduction in gases and liquids only if a fluid is stationary.

Heat transfer by conduction is represented by Fourier's law of heat conduction as given by (Cengel, 2003: 18):

$$Q = -kA\frac{dT}{dx} \quad [2.1]$$

where Q is the heat transfer rate in the x direction and proportional to the temperature gradient $\frac{dT}{dx}$ in same direction, k is the thermal conductivity and A is the heat transfer area. The negative sign in Equation 2.1 denotes that heat is transferred in the direction of decreasing temperature. Thermal conductivity is the measure of a material's ability to conduct heat. Materials with high values of thermal conductivity are good conductors of heat, while those with low values of thermal conductivity are poor conductors of heat. Thermal conductivity is a function of temperature and it also varies with pressure for gases.

2.1.1.2 Convective heat transfer

Convective heat transfer occurs when heat is transferred from a solid surface and an adjacent fluid that is in motion, and it increases with fluid velocity (Cengel, 2003: 25). Similarly, heat transfer during phase change between a vapour and a liquid is by convection due to the motion of vapour bubbles and liquid droplets during vaporisation and condensation respectively. It must be noted that heat transfer is by convection in multiphase systems such as bubble columns due to the presence of a moving fluid. Convection is called forced convection if the fluid is forced by means of mechanical equipment. Otherwise, it is natural convection in the case of free motion of the fluid.

Convective heat transfer from a surface to a fluid is represented by Newton's law of cooling, as follows (Cengel, 2003: 26):

$$Q = hA\left(T_W - T_B\right) \quad [2.2]$$

where Q is the convective heat transfer rate, T_W is the wall temperature, T_B is the bulk liquid temperature and h is the heat transfer coefficient which depends on the conditions in the boundary layer. The conditions in the boundary layer are influenced by surface

geometry, the nature of the fluid motion and the range of fluid thermodynamic and transport properties.

2.1.1.3 Wall heat transfer in bubble columns

In bubble columns, heat can be transferred by conduction through the column wall, then by convection from the wall surface to the column dispersion (Dhotre, Vitankar & Joshi, 2005). The temperature gradient for wall-dispersion heat transfer of an externally heated bubble column is illustrated in Figure 2.1. Temperature is high at the wall inner surface and decreases in the boundary layer until it becomes uniform in the column dispersion.

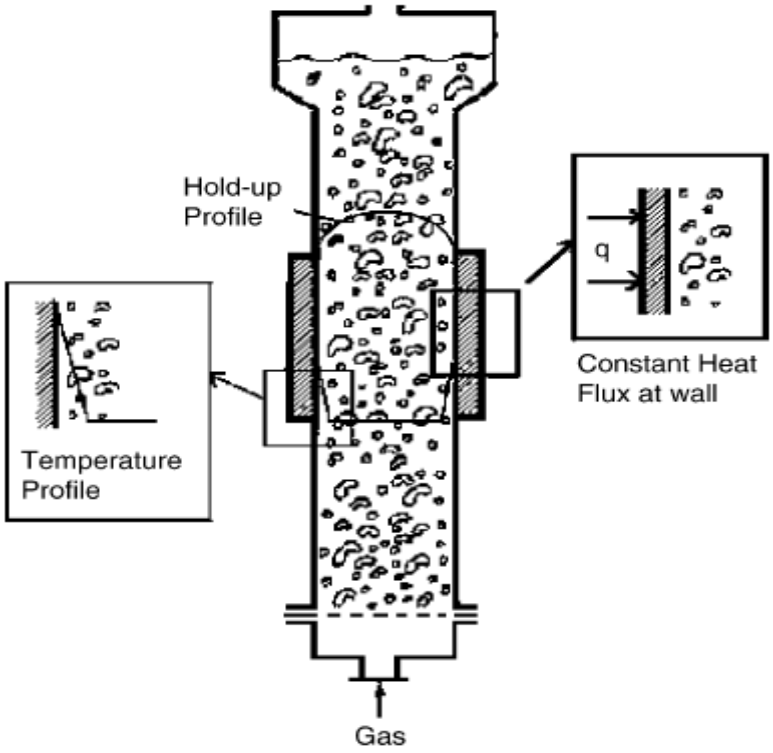

Figure 2.1: Schematic representation of the temperature profile in a bubble column (Dhotre et al., 2005)

2.1.2 Heat transfer correlations

Heat transfer correlations are used in the design of bubble columns to estimate the heat transfer coefficient. Equation 2.3 is a general formula for many heat transfer correlations for different column conditions (Kantarci, Ulgen & Borak, 2005b).

$$St = C_1 \left(\mathrm{Re}\, Fr\right)^{C_2} \mathrm{Pr}^{C_3} \left(\frac{x}{H}\right)^{C_4} \left(\frac{r}{R}\right)^{C_5} \qquad [2.3]$$

The use of the dimensionless parameters, namely Re and Fr, Pr, x/H and r/R, reflects the effects of superficial gas velocity, liquid phase properties, axial position and radial position of an internal heater respectively on the heat transfer coefficient. The effect of column diameter and sparger design is not included in Equation 2.3 because of their small effect on the heat transfer coefficient (Joshi et al., 1980; Kantarci et al., 2005b). Parameters C_1, C_2, C_3, C_4 and C_5 can be determined from the measured data by using non-linear regression methods.

These correlations are empirical and they have limitations in their application, such as (Dhotre et al., 2005; Hulet, Clementy, Tochonz et al., 2009):

- There are limitations to the original range of experimental conditions:
  - This implies that the values of constants C_1, C_2, C_3, C_4 and C_5 will differ outside the range of experimental conditions in which they were determined.
- Limited data are sometimes used for the development of correlations.
- Some important variables may be missing in the correlation.
- Each correlation is dependent on a particular system and the properties of a gas–liquid system.
- Most of the correlations are derived under steady-state conditions and thus they cannot be applied during unsteady-state conditions.
- There are uncertainties in the application of three-phase correlations to two-phase systems and vice versa.

The limitations of these correlations will introduce inaccuracies when determining the heat transfer coefficient. Data modelling techniques can be employed to cover a wide range of the data and to partially overcome these limitations. Modelling techniques such as artificial neural networks and support vector regression have been reported in the literature (Al-Hemiri & Ahmedzeki, 2008; Chen et al., 2003; Gandhi & Joshi, 2010). Previous work on heat transfer correlations in bubble columns is listed in Table 2.1.

Table 2.1: Summary of the heat transfer correlations investigated by various researchers

Researcher	System	Height/Diameter ratio	Sparger	Range of u_G	Operating conditions	Correlation
Fair et al. (1962)	Air–water	10 ft/18 in. and 10 ft/42 in.	Perforated plate Baffles	0–0.5 ft/s	–	$^1h = 1200u_G^{0.22}$
Kast (1963)	Air–water/ isopropanol	4 m/0.29 m	–	0.0025–0.06 m/s		$\frac{h_W}{\rho_L C_P u_G} = 0.1\left[\left(\frac{\rho_L D_C u_G}{\mu_G}\right)\left(\frac{u_G^2}{gD_C}\right)\left(\frac{\mu_L C_P}{k_L}\right)^2\right]^{-0.22}$
Hart (1976)	Air–water and ethylene glycol	42/4 in.	¼ in. o.d. single nozzle	0.0001–0.8 ft/s	160 and 183 °C	$\frac{h}{C_P u_s \rho_L}\left(\frac{c_P \mu_L}{k_L}\right)^{0.6} = 0.125\left(\frac{u_S^3 \rho_L}{\mu_L g}\right)^{-0.25}$
Deckwer (1980a)	–	4.1 cm	Porous sparger of 75 µm	0–3.3 cm/s	143–270 °C 400–1 100 kPa	$St = -0.1\left(\mathrm{Re}\, Fr\, \mathrm{Pr}^2\right)^{0.25}$
Hikita et al. (1981)	Air–water sucrose, methanol	162/10 and 240/19 cm	Nozzle	0.04–0.4 m/s	25–45 °C	$\frac{h_w}{\rho_L C_p u_G}\left(\frac{C_p \mu_L}{k_L}\right)^{2/3} = 0.411\left(\frac{u_G \mu_L}{\sigma_L}\right)^{-0.851}\left(\frac{\mu_L^4 g}{\rho_L \sigma_L^3}\right)^{0.308}$
Yang et al. (2000)	Nitrogen–Paratherm heat transfer fluid glass beds	1.37/0.1016 m	Perforated plate Square pitched holes 1.5 mm diameter	0–20 cm/s	0.1–4.2 MPa 35–81 °C	$St_{sl} = 0.037\left[\left(\mathrm{Re}_{sl}\, Fr\, \mathrm{Pr}_{sl}^{1.87}\right)\left(\frac{\bar{\varepsilon}_G}{1-\bar{\varepsilon}_G}\right)\right]^{-0.22}$

Li & Prakash (2001)	Air–water glass beds	2.4/0.28 m	Six arm, 6 mm diameter	0.05–0.3 m/s	23 °C	[2] $h = 0.1\left[k_{sl}\rho_{sl}C_{p,sl}\left(\frac{P_v}{\mu_{sl}}\right)^{0.5}\right]^{0.5}$
Cho et al. (2002)	Air–liquid	2.5/0.152 m	Nozzles	0.02–0.12 m/s	0.1–0.6 MPa	[3] $h = 11710 u_G^{0.445}\mu_L^{-0.060}P^{0.176}$
Li & Prakash (2002)	Air–water glass beds	2.4/0.28 m	Six arm, four 1.5 mm diameter holes	0.05–0.3 m/s	23 °C	[4] $\frac{h_S d_P}{k} = a_S(\mathrm{Pr})^{0.4}\left(\frac{u_L d_P}{v}\right)^{0.5}$
Kantarci et al. (2005b)		60/17 cm	2 mm holes, 60° from each other	0.03–0.2 m/s	296–318 K	

$$St = C_1(\mathrm{Re}\,Fr)^{C_2}\,\mathrm{Pr}^{C_3}\left(\frac{x}{H}\right)^{C_4}\left(\frac{r}{R}\right)^{C_5}$$

Air–water	Air–water– cell 0.1% + 0.4%
$C_1 = 0.164$; $C_2 = -0.30$; $C_3 = -1.01$; $C_4 = -0.054$; $C_5 = -0.009$	$C_1 = 0.098$; $C_2 = -0.26$; $C_3 = -0.54$; $C_4 = -0.07$; $C_5 = -0.013$
Air–water – cells 0.1%	**Air–water – cells 0.4%**
$C_1 = 0.090$; $C_2 = -0.26$; $C_3 = -0.54$; $C_4 = -0.07$; $C_5 = -0.013$	$C_1 = 0.102$; $C_2 = -0.26$; $C_3 = -0.54$; $C_4 = -0.07$; $C_5 = -0.013$

Jhawar & Prakash (2007)	Air–water	2.5–0.15 m	Fine sparger, pore size 15 µm and coarse sparger	0.05–0.4 m/s	22 °C	[5] $h = 8.65\left(\frac{u_G}{\bar{\varepsilon}_G}\right) + 3.32$ $\frac{u_G}{\bar{\varepsilon}_G} \le 0.3 m/s$ [5] $h = 2\left(\frac{u_G}{\bar{\varepsilon}_G}\right) + 3.3$ $\frac{u_G}{\bar{\varepsilon}_G} \ge 0.3 m/s$

Units of variables in the correlations: 1, h (Btu/h).Ft^{2}.$^{-o}$F, U_G (ft/s); 2 (SI Units); 3 (SI Units); 4 (SI Units); 5 (SI Units)

2.1.3 Experimental methods

Much literature has been reported on heat transfer coefficient studies where heat transfer coefficients were measured between the surface of an immersed object and the column dispersion (Li & Prakash, 1997; Jhawar & Prakash, 2007; Wu, Al-Dahhan, & Prakash, 2007).

In this study experimental investigations were, however, done on a column wall to dispersion heat transfer. Cho, Yang, Eun et al. (2005), Deckwer et al. (1980b), Fair et al. (1962), Hikita et al. (1981), Kim, Cho, Lee et al. (2002), Sada, Katoh, Yoshil et al. (1984), and Terasaka, Suyama, Nakagawa et al. (2006) reported the addition of heat through the wall of bubble columns. Among the authors who reported on heat transfer studies, the measurement of the heat transfer coefficient through the walls of a column was studied by Hikita et al. (1981), Fair et al. (1962) and Hart (1976).

Experiments carried out by Hikita et al. (1981) were conducted using two bubble columns. The first column had an internal diameter (i.d.) of 10 cm, a height of 162 cm and was made of acrylic resin. The other column was made of transparent vinyl chloride resin and the column dimensions were 19 cm i.d. and 240 cm in height. Gas was dispersed using a single-nozzle sparger in which two nozzles of 0.9 and 1.3 cm i.d. were used for the 10 cm column. Three nozzles of 1.31, 2.06 and 3.62 cm i.d. were used for the 19 cm column. The nozzles were located 5 cm above the bottom plate of the column.

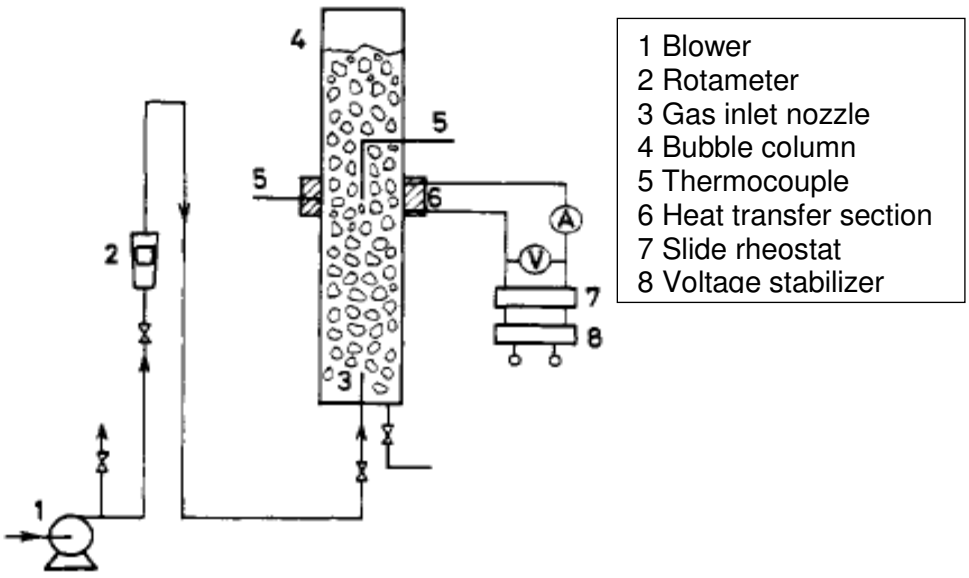

Figure 2.2: Schematic diagram of the experimental apparatus for heat transfer coefficient measurements in the bubble column (Hikita et al.*, 1981)*

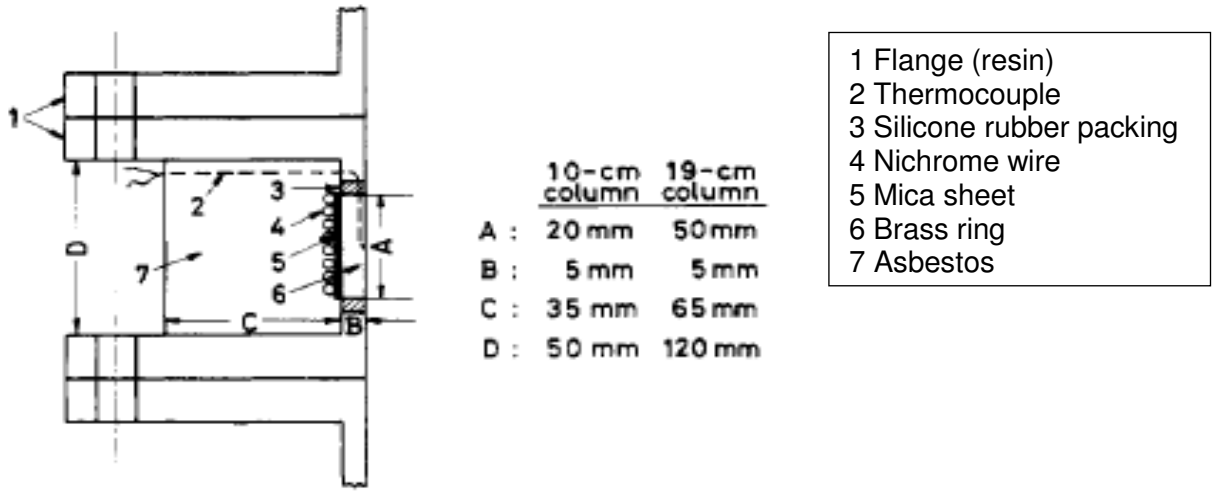

Figure 2.3: Heat transfer section of the bubble column (Hikita et al.*, 1981)*

As shown in Figures 2.2 and 2.3, heat was supplied through the walls of the column with an electric heater located at a certain height above the gas distributors. The heat transfer section was made from brass rings wrapped with mica sheet for insulation purposes. The heating element was made from nichrome wire, wrapped around the brass section and insulated with asbestos to reduce the heat loss to the surrounding air. The temperature of the brass section (i.e. the wall temperature) was measured by four and eight copper–constantan thermocouples of 0.2 mm diameter for the 10 cm and 19 cm columns respectively. The thermocouples were located in the middle of the brass section and were connected to a digital multi-thermometer. The column temperature was also measured with copper constantan thermocouples inserted at the column axis at the same level as the heat transfer section. The rate of heat transfer was measured from amperage and voltmeter readings by applying Joule's law. The temperature difference was limited to 3–10 °C to avoid the variation of liquid physical properties along the heat transfer path.

Hart (1976) measured wall heat transfer in a bubble column consisting of a 609.6 mm section of 99.06 mm i.d. copper pipe with butt-joined fibreglass ends These ends were installed in order to reduce the axial heat leak from the copper section, thus allowing a more accurate determination of the heat transfer area. The copper section was wrapped with glass tape to insulate, electrically, it from the heating element. The heating element was 12.7 mm x 0.0508 mm chromel-A tape which was wrapped around the glass-covered copper section with a spacing of about 6.35 mm between wraps.

Temperature and flowrate measurements determined the heat flux and the temperature difference between the liquid and the column wall. In this way, the heat transfer coefficient

could be determined. With a 10 A Powerstat, the heating element could deliver a heat flux up to about 9 464 W/m^2 through the inside area of the copper pipe. Nine thermocouples were installed at equal intervals along the column wall. They were inserted into small holes drilled to within about 0.4 mm of the inside pipe wall. The holes were then filled with lead shot which was tapped gently with a punch, causing the lead to flow into every cavity. Soldering could not be used because of the fibreglass ends.

2.1.4 Effect of operating parameters on heat transfer coefficient

2.1.4.1 Superficial gas velocity

The effect of superficial gas velocity on the heat transfer coefficient has been reported by many researchers. An increase in the heat transfer coefficient with superficial gas velocity is reported in the literature (Daous & Al-Zahrani, 2006; Wu & Al-Dahhan, 2012; Kantarci et al., 2005b; Fazeli, Fatemi, Ganji et al., 2008).

Wu & Al-Dahhan (2012) studied heat transfer coefficients in a mimicked slurry bubble column of a mixture of air, C_9–C_{11} n-paraffin mixture and a Fischer–Tropsch catalyst. Heat was supplied to the column with the aid of a heat transfer probe placed at the centre of the column. For both the wall and centre regions of the column, the heat transfer coefficient initially increased with the superficial gas velocity and then levelled off at higher gas velocities. The authors explained that at low superficial gas velocities, bubbles with relatively small diameters are uniformly distributed across the column cross-section and slowly move along the column axis. As the superficial gas velocity increases, large bubbles are formed and most of them rise through the core region of the column at a high bubble rise velocity. The higher bubble rise velocity results in an increase in surface renewal and a decrease in the film thickness at the probe surface, which can significantly increase the heat transfer coefficient. On the other hand, small bubbles in the wall region move downwards with liquid circulation. This is what causes the difference in heat transfer coefficient between the wall and centre region.

Daous & Al-Zahrani (2006) carried out heat transfer studies in a bubble column and a slurry bubble column equipped with a single gas nozzle as a sparger. They found that increasing the superficial gas velocity increases the rising velocities of bubbles, which in turn enhances the heat transfer coefficient.

A different phenomenon was reported by Li & Prakash (1997) in a slurry bubble column of an air–water–glass beads system. They reported an increase in the heat transfer coefficient, which then decreases above a superficial gas velocity of 0.2 m/s.

2.1.4.2 Liquid properties

Cho et al. (2002) performed heat transfer studies in a pressurised bubble column. They reported a decrease in the heat transfer coefficient with increasing liquid viscosity. The bubble sizes increase with an increase in liquid viscosity. The rising velocities of large bubbles decrease their residence time and thus reduce the gas holdup and hence the heat transfer coefficient.

2.2 Gas holdup

Gas holdup indicates the gas volume inside the column and it determines the required total column volume (Dhotre, Ekambara & Joshi, 2004). Gas holdup can also be used to estimate average residence time, average interfacial area, average interstitial velocity and pressure drop (Dhotre et al., 2004; Kumar, Moslemian & Dudukovic, 1997).

2.2.1 Gas holdup theory

2.2.1.1 Flow regimes

The bubble dynamics result in different flow regimes in bubble columns and gas holdup behaves differently in various flow regimes. The flow regimes encountered in bubble columns are bubbly flow, slug flow, churn-turbulent flow and annular flow, as shown in Figure 2.4 (Shaikh & Al-Dahhan, 2007). The flow regimes most frequently reported in the literature are the bubbly flow (homogeneous), transition and churn-turbulent (heterogeneous) regimes (Shaikh & Al-Dahhan, 2005).

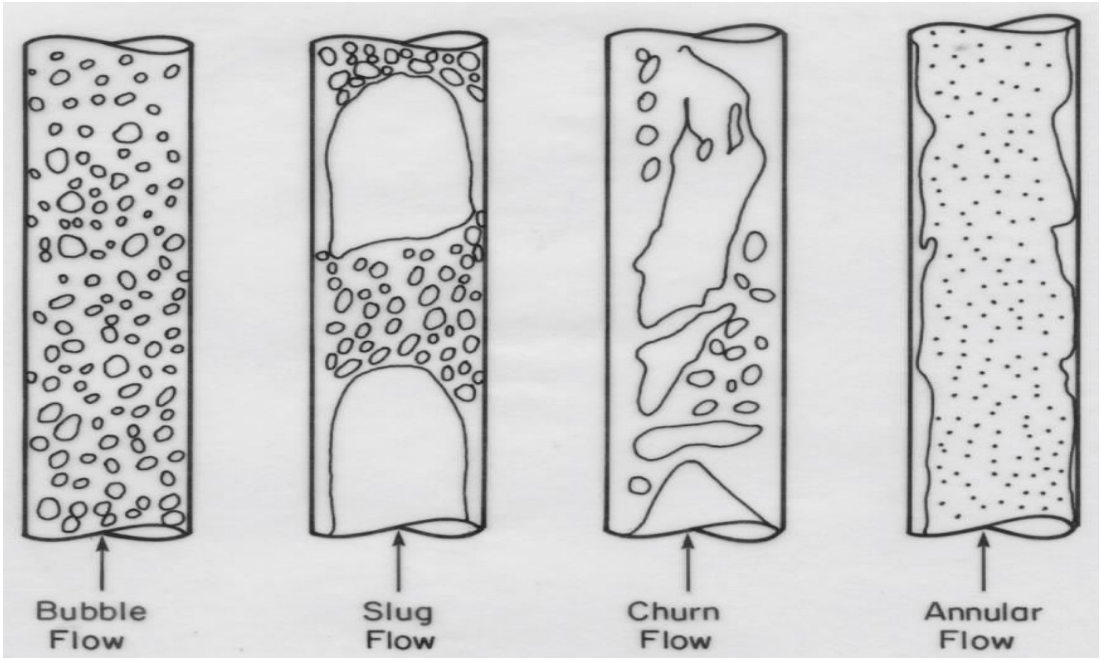

Figure 2.4: Types of flow regime in bubble columns (Shaikh & Al-Dahhan, 2007)

Homogeneous flow regime: This occurs when gas-dispersion plates with small, closely spaced orifices are employed and it is encountered at low superficial gas velocities which form a uniform flow of small nearly spherical bubbles (Ruzicka, Zahradnik, Drahos et al., 2001). The bubbles rise upwards with small vertical and horizontal fluctuations. There is little bubble coalescence and breakup and can thus they can be neglected in this flow regime (Mena, Ruzicka, Rocha et al., 2005). Moreover, narrow bubble size distribution is encountered and the bubbles are monodispersed. Gas holdup in this flow regime is uniformly distributed in the radial direction and hence liquid circulation is insignificant.

Transition flow regime: This is the flow regime in which the first large bubble is observed (Krishna, Wilkinson & Van Dierendonck, 1991). The velocity at which this first large bubble is observed is called the transition velocity. Significant liquid circulation patterns develop at superficial velocities beyond the transition velocity. The transition from the homogeneous to the heterogeneous flow regime depends on the superficial gas velocity, sparger design, fluid properties, slurry concentration and the column diameter.

Heterogeneous flow regime: This is produced by either (a) plates with small and closely spaced orifices at high gas flowrates, or (b) plates with large orifices (above 1.6 mm) at any gas flowrate (Ruzicka et al., 2001). This flow regime occurs at superficial gas velocities beyond the transition velocity, forming a mixture of large and small bubbles. It is characterised by bubble breakup and bubble coalescence. Coalescence of small bubbles

results in the formation of large bubbles (Mena et al., 2005). Operating in this flow regime has some disadvantages, such as: (a) poor contact between the gas and liquid phases which reduces the efficiency of mass transfer; (b) radial variation of gas holdup, which results in liquid circulation and higher backmixing; and (c) wide residence time distribution of the bubbles due to a wide bubble size distribution (Fadavi & Chisti, 2007).

2.2.1.2 Prediction of gas holdup

Gas holdup, which is also termed "bubble to bed voidage", is defined as the ratio of gas volume and dispersed bed volume, as given by (Nedeltchev & Schumpe, 2008):

$$\bar{\varepsilon}_G = \frac{V_G}{V_G + V_L} \quad [2.4]$$

where $\bar{\varepsilon}_G$ is the average gas holdup, V_G is the gas volume and V_L is the liquid volume. For a bubble column with a constant cross-sectional area, Equation 2.4 is further simplified to:

$$\bar{\varepsilon}_G = \frac{H - H_0}{H} \quad [2.5]$$

where H is the gas–liquid dispersion height and H_0 is the gas-free liquid height. Gas holdup can also be calculated by measuring the static pressure drop across the column height (Kantarci et al., 2005b):

$$\Delta P = (\rho_G \bar{\varepsilon}_G + \rho_L \varepsilon_L) g \Delta H \quad [2.6]$$

where ΔP is the pressure drop, ΔH is the height difference between the two pressure transducers, ρ is the density of each phase, ε is the holdup of each phase, g is the gravitational acceleration, and subscripts G and L denote gas and liquid phases respectively. The sum of the holdup of individual phases is equal to one as given by:

$$\bar{\varepsilon}_G + \varepsilon_L = 1 \quad [2.7]$$

Substituting Equation 2.7 to Equation 2.6 gives:

$$\Delta P = \left[\rho_G \bar{\varepsilon}_G + \rho_L \left(1 - \bar{\varepsilon}_G\right)\right] g \Delta H \quad [2.8]$$

Since gas density is very small compared with liquid density, the first term of Equation 2.8 can be omitted.

$$\Delta P = \rho_L \left(1 - \bar{\varepsilon}_G\right) g \Delta H \quad [2.9]$$

Re-arranging Equation 2.9, average gas holdup can be calculated from:

$$\bar{\varepsilon}_G = 1 - \frac{\Delta P}{g \rho_L \Delta H} \quad [2.10]$$

Average gas holdup can also be determined from the ratio of the superficial gas velocity and the average bubble rise velocity, as shown in Equations 2.11 and 2.12 (Vandu, Koop & Krishna, 2004) In this case the value of the gas holdup denotes the gas residence time (Nedeltchev & Schumpe, 2008). Gas residence time decreases with an increase in bubble size since large bubbles have higher rising velocities. In the homogeneous flow regime, the gas holdup is given as:

$$\bar{\varepsilon}_G = \frac{u_G}{u_{Sb}} \quad [2.11]$$

where u_{Sb} is the rise velocity of small bubbles and u_G is the superficial gas velocity. In the heterogeneous flow regime, the gas holdup is given as:

$$\bar{\varepsilon}_G = \frac{(u_G - u_{trans)}}{u_{Lb}} + \bar{\varepsilon}_{trans}\left[1 - \frac{(u_G - u_{trans})}{u_{Lb}}\right] \quad [2.12]$$

where u_{Lb} is the rise velocity of large bubbles, u_{trans} is the transition velocity and ε_{trans} is the gas holdup at a transition velocity.

Gas holdup varies linearly with superficial gas velocity up to the transition velocity. The variation of the gas holdup with superficial gas velocity is of the form $\bar{\varepsilon}_G \propto u_G^n$ (Moshtari, Babakhani & Moghaddas, 2009; Christi & Moo-Young, 1988), where the value of the

constant 'n' depends on the flow regime. At superficial gas velocities above the transition velocity and below the heterogeneous flow regime (i.e. in the transition flow regime) gas holdup is the sum of small bubble holdup and large bubble holdup (Krishna et al., 1991). It is claimed that the former is constant above the transition velocity and is the same as that at the transition velocity. It varies with $u_G - u_{trans}$ and is independent of gas density or liquid properties (Krishna et al., 1991). Gas holdup will again increase with superficial gas velocity in the heterogeneous flow regime since there is a majority of large bubbles. The trend will, however, be non-linear, with a lower slope than that in the homogeneous flow regime.

2.2.3 Gas holdup correlations

Table 2.2: Summary of the gas holdup correlations investigated by researchers

Researcher	System	Height/Diameter ratio	Sparger	Range of u_G	Operating conditions	Correlation
Mouza et al. (2005)	Air–water/ butanol/gycerine	1.5 m × 0.1 × 0.1 m	Porous disk	0–1 cm/s	25 °C	$\bar{\varepsilon}_G = 0.001\left[Fr^{0.5}Ar^{0.1}Eo^{2.2}\left(\frac{d_S}{D_C}\right)\right]^{2/3}$
Yifeng et al. (2008)	Air–water/ paraffin/K_2CO_3 solution	1.5/0.1 m	Nozzles	0–0.15 m/s	ambient pressure and T = 20 °C	$\frac{\bar{\varepsilon}_G}{(1-\bar{\varepsilon}_G)^4} = 0.579\left(\frac{u_G\mu_L}{\sigma_L}\right)^{0.918}\left(\frac{\mu_L^4 g}{\rho_L\sigma_L^3}\right)^{-0.252}$
Mandal et al. (2003)	Air–water/ CMC solution	1.5/0.052 m	Nozzles	0–0.15 m/s	25 °C	$\bar{\varepsilon}_G = 0.365\,\mathrm{Re}^{-0.164}Mo^{-0.029}A_r^{0.032}H_r^{0.207}$
Moshtari et al. (2009)	Air–water homogeneous flow regime heterogeneous flow regime	2.8/0.15 m	Porous and perforated plate	0–0.15 m/s	25 °C	$\bar{\varepsilon}_G = 0.450u_G^{0.954}$ $\bar{\varepsilon}_G = 1.335u_G^{0.449}$
Zhang et al. (2003)	Air–water–quartz	Tapered column	Perforated plate	0.02–0.28 m/s	1 atm and 25 °C	$\frac{\bar{\varepsilon}_G}{(1-\bar{\varepsilon}_G)^4} = 3.611(1-C_{P,sl})^{3.37}U_G^{0.658}S_b^{-0.355}$

Jawad et al. (2009)	Air–water–silica	–	–	0.001–0.0462 m/s	25 °C	$\bar{\varepsilon}_G = 6.23 Fr_G^{0.38} \mathrm{Re}^{-0.175} H_r^{0.06} d_r^{0.088}$
Abdullah (2007)	Air–water/butanol/ ethanol/paraffin	1.5/0.1 m	Single-hole distributor	0–0.35 m/s	25 °C	$\bar{\varepsilon}_G = 0.0012 Fr^{0.38} Ar^{0.062} Eo^{1.5} (d_o / D_c)^{0.55}$
Yamagiwa et al. (1990)	Air–water	Various ratios	Nozzle	V_j = 3–5 m/s	20 °C	$\bar{\varepsilon}_G = 9.73 \times 10^{-2} V_j^{0.23} L_j^{0.35} D_n^{-0.66} D_C^{0.45}$
Ghosh & Upadhyay (2007)	Air–water/ propylene glycol/ carborymethyl cellulose	2.9/0.145 m	Single-hole distributor	0–0.015 m/s	25 °C	$\varepsilon_G (\mu_L)^{0.13} D_C^{0.15} (H_C / D_C)^{0.2} = U_G / (0.65 + 2.5 U_G^{0.666})$
Nikolic et al. (2005) for a two phase	Air–water	1.84/0.254 cm	Gas distributor with reciprocating plates	0–2 cm/s	20 °C	$\frac{\bar{\varepsilon}_G}{(\bar{\varepsilon}_G)_{I=0}} 1 + 48.9 U_G^{-0.668} I^{1.693} D_C^{0.751} \varepsilon_S^{0.238}$
for a three phase	Air–water– polypropylene sphere	and 0.86/0.092 m				
Urseanu et al. (2003)	Nitrogen–glucose/ Telluse oil	1.22/0.15 m 1.22/0.23 m	Perforated plate Ring sparger	0–0.5 m/s	0.1–1 MPa	$\bar{\varepsilon}_G = 0.21 U_G^{0.58} D_C^{-0.18} \sigma_L^{-0.12} \rho_G^{[(0.3 \exp(-9\sigma_L)]}$
Deckwer et al. (1980b)	–	0.6/0.041 m 1/0.1 m	Porous sparger	0–3.3 cm/s	143–270 °C 400–1 100 kPa	$\bar{\varepsilon}_G = 0.053 u_G^{1.1} \pm 0.015$

Sivasubramaniana & Naveen Prasad (2009)	Air–isolmy alcohol/ propanol/ polystyrene particles	2.6/0.084 m	Perforated plate	0–0.035 m/s	25 °C	$\varepsilon_{Gr} = 18.577 U_{Gr}^{(0.984+1.16\times10^{-4}C_s)} \sigma_L^{0.05} \rho_L^{-0.038} \mu_L^{0.996}$
Shirsat et al. (2003)	Air–water/ CMC solution	1.5/0.0516 m	Nozzle	gas/liquid flow ratio = 0–1	28 °C	$\bar{\varepsilon}_G = 1.5063 \mathrm{Re}_L^{-0.168} M_O^{-0.034} Su^{-0.048} \mu_r^{0.076} A_r^{-0.031} H_r^{0.215}$

The units of the symbols in the correlations are in SI units.

2.2.2 Measuring equipment and techniques

Many measuring techniques for gas holdup have been reported in the literature. This study will only review a few of them.

2.2.2.1 Overall gas holdup

Overall gas holdup can be measured by the level expansion or pressure difference methods. Zhang, Zhao & Zhang (2003) and Fransolet, Crine, L'Homme et al. (2001) compared the two measuring techniques. Zhang et al. (2003) reported a close agreement between the two techniques with a maximum percentage error of ±10%, as shown in Figure 2.5.

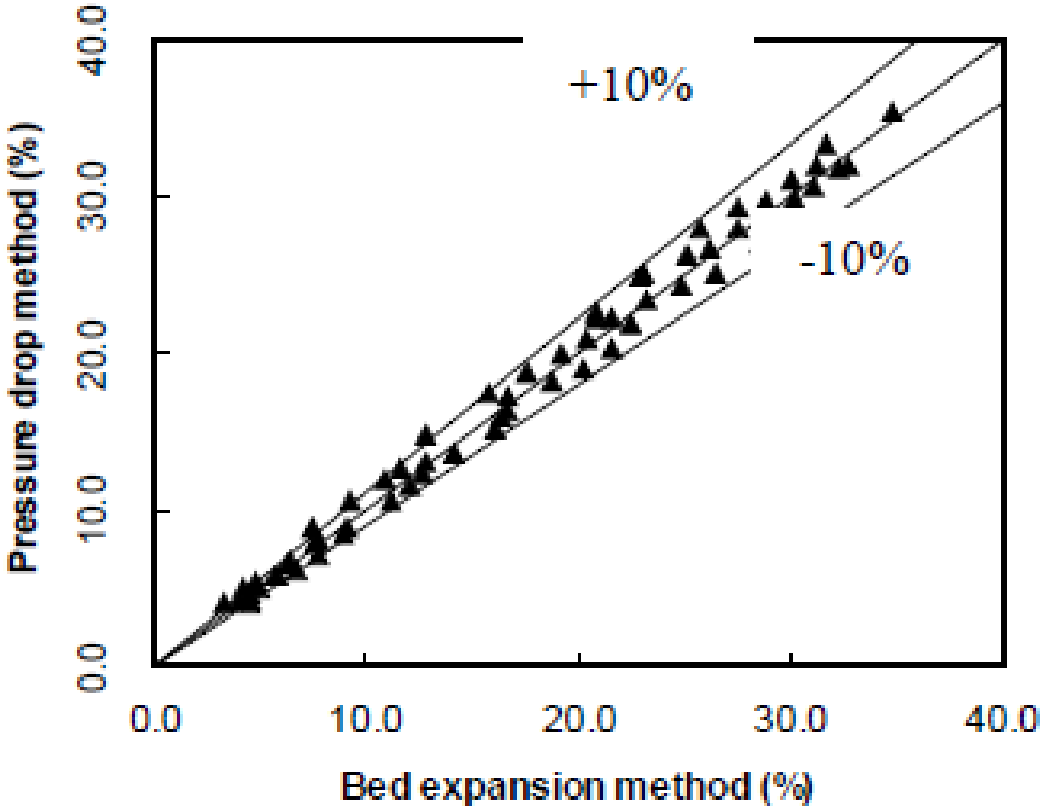

Figure 2.5: Comparison of the overall gas holdup measured by the pressure drop and the bed expansion method (Zhang et al.*, 2003)*

Fransolet et al. (2001) reported that the two techniques agree with each other at low superficial gas velocities but that a significant difference is observed at high superficial gas velocities, as shown in Figure 2.6. They explained that this deviation can be attributed to the fact that the volume of a column over which the gas holdup is determined is greater in the level expansion method than it is in the pressure difference method.

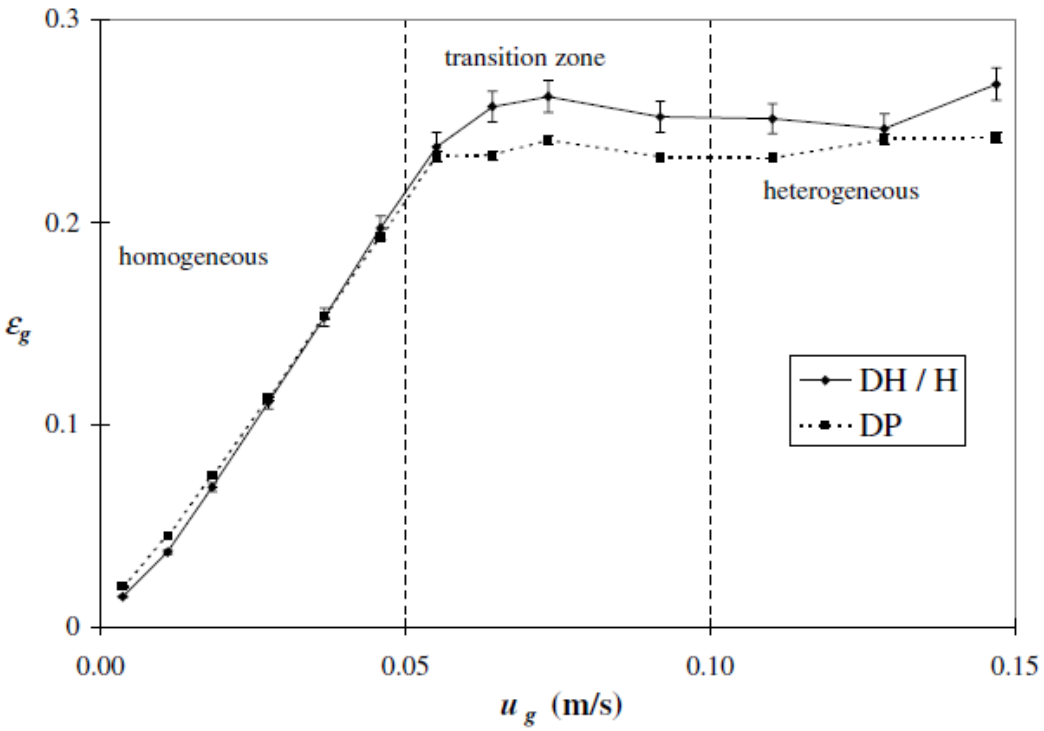

Figure 2.6: Gas holdup as a function of superficial gas velocity obtained by using the level expansion and pressure difference methods (Fransolet et al.*, 2001)*

2.2.2.2 Level expansion method

This technique is used to measure the level of gas–liquid dispersion and gas-free liquid for calculating the gas holdup. Different techniques can be employed for measuring the liquid level, such as visual observation, bubbler tube, floater/displacers, capacitance technique, etc.

- *Visual observation*: This is a simple technique in which the liquid level is measured by a ruler or by a scale attached to the column wall. It can be applied only for transparent columns. Orvalho, Ruzicka & Drahos (2009) reported the measurement of the liquid level using a ruler. They explained that this technique will give a better approximation in the homogeneous flow regime in which the liquid surface is well defined, steady and horizontal. In the heterogeneous flow regime, the liquid surface oscillates and the liquid level has to be measured by taking the mean of the lowest and highest liquid surface positions. The measurements done by the authors were taken from 10–20 oscillations, depending on the complexity of the motion. These oscillations develop gradually and their amplitude increases with the gas flowrate beyond the critical point. As the oscillation became intense, it became difficult to measure the level with the ruler.

- *Bubbler tube*: This is an inexpensive, simple and well-known technique. It does not have temperature restrictions and it is mostly employed in corrosive and slurry-type applications (Omega, 2001). It uses a dip tube installed with an open end. The system consists of a tube, a gas supply, a pressure transmitter and a differential pressure regulator. The regulator produces the constant gas flow required to prevent calibration changes (Bahner, 2013). When a gas, usually air or an inert gas, is flowing through the tube; bubbles escape from the open end. The air pressure in the tube corresponds to the hydraulic head of the liquid at the outlet of the dip tube. The air pressure in the bubble tube varies proportionally with the change in head pressure. This technique is affected by changes in gas flowrate and liquid density. The dip tube must be located far from the column bottom to prevent blockage of the tube opening by slurry particles. The dip tube should have a reasonably large diameter so that the pressure drop of gas flowing through the tube is negligible and prevents the clogging of the dip tube if the gas is not filtered (Omega, 2001).
- *Floater and displacers*: According to Archimedes Principle, the buoyancy force acting on an object is equal to the weight of the fluid displaced (Omega, 2001). As the level changes around the displacer float, which has a constant diameter and is stationary, the buoyancy force varies in proportion to the level and can be detected to give an indication of level (Omega, 2001).

Other level-measuring techniques are given in Table 2.2 (Omega, 2001). Many of these cannot be applied to molten salt bubble columns due to high operating temperatures and aggressive corrosion by molten salt in these systems.

Table 2.3: Level measuring techniques (Omega, 2001)

Type	Maximum temperature(°F)	Accuracy	Applications								Limitations
			Liquids					Solids			
			Clean	Viscous	Slurry/sludge	Interface	Foam	Powder	Chunky	Sticky	
Capacitance	2000	1–2% FS	G	F–G	F	G–L	P	F	F	P	Interface between conductive layers and detection of foam is a problem.
Conductivity switch	1800	1/8 in.	F	P	F	L	L	L	L	L	Can detect interface only between conductive and non-conductive liquids. Field effect design for solids.
Diaphragm	350	0.5% FS	G	F–G	F			F	F	P	Switches only for solid service.
Differential pressure	1200	0.1% AS	E	G–E	G	P					Only extended diaphragm seals or repeaters can eliminate plugging. Purging and sealing legs are also used.
Laser	UL	0.5 in.	L	G	G		F	F	F	F	Limited to cloudy liquids or bright solids in tanks with transparent vapour spaces.

Microwave switches	400	0.5 in.	G	G	F	G		G	G	F	Thick coating is a limitation.
Optical switches	260	0.25 in.	G	F	E	F–G	F	F	P	F	Refraction type for clean liquids only, reflection type requires clean vapour space.
Radar	450	0.12 in.	G	G	F	P		P	F	P	Interference from coating, agitator blades, spray, or excessive turbulence.
Radiation	UL	0.25 in.	G	E	E	G	F	G	E	E	Requires *nuclear regulator commission* licence.
Resistance tape	225	0.5 in.	G	G	G						Limited to liquids under near-atmospheric pressure and temperature conditions.
Rotating paddle switch	500	1 in.						G	F	P	Limited to detection of dry, non-corrosive, low-pressure solids.
Slip tube	200	0.5 in.	F	P	P						An unsafe manual device.
Tape-type level sensors	300	0.1 in.	E	F	P	G		G	F	F	Only the inductively coupled float is suited for interface measurement. Float hang-up is a potential problem with most designs.

Thermal	850	0.5 in.	G	F	F	P	F				Foam and interface detection is limited by the thermal conductive involved.
Ultrasonic	300	1%FS	F–G	G	G	F–G	F	F	F	G	Presence of dust, foam, dew in vapour space; sloping or fluffy process material interferes with performance.
Vibrating switches	300	0.2 in.	F	G	G	F		F	G	G	Excessive material build-up can prevent operation.

AS = in % of actual span, E = Excellent, FS = in % of full scale, F = Fair, G = Good, L = Limited, P = Poor and UL = unlimited.

2.2.4 Effect of operating parameters on gas holdup

Gas holdup depends on the rising velocities of the bubbles. High gas holdup is attained for low bubble rise velocities due to high bubble residence time. On the other hand, bubble rise velocity is dependent on bubble sizes. Also, gas holdup is affected by the number of bubbles in the column at a given superficial gas velocity.

2.2.4.1 Superficial gas velocity

Li & Prakash (2000) reported that gas holdup due to both small and large bubbles increases with superficial gas velocity. Gas holdup due to large bubbles was found to be lower than gas holdup due to small bubbles since large bubbles rise faster than small bubbles. The difference between the two gas holdups was found to decrease as the superficial gas velocity increases due to increased bubble coalescence.

Kumar et al. (1997) reported the effect of superficial gas velocity on the radial variation of gas holdup. They found an increase in local gas holdup with superficial gas velocity for all column radii, excluding the region close to the column wall. Gas holdup increased insignificantly for lower gas velocities, showing a flatter profile, which confirms a bubbly flow regime at the experimental conditions used. At higher gas velocities the gas holdup profile became parabolic.

2.2.4.2 Operating temperature

Malayeri, Muller–Steinhagen & Smith (2003) also reported the effect of temperature on gas holdup. They explained that an increase in temperature will result in the lowering of surface tension and liquid viscosity, and an increase in vapour pressure. These combined effects will result in an increase in the drainage and evaporation of the liquid film between the bubbles and will thus enhance bubble coalescence. The authors also observed that a variation in gas holdup becomes more significant near the boiling point.

Bukur, Petrovic & Daly (1987) reported the effect of temperature on gas holdup using Fischer–Tropsch-derived paraffinic wax as a liquid medium. Studies were done in a temperature range of 150–280 ^{o}C, where foamy and turbulent regimes were observed for the superficial gas velocities used. In the foamy regime, gas holdup increased with temperature, except for the gas holdups measured at 250 ^{o}C and 265 ^{o}C. In the turbulent bubbling regime, the effect of temperature on gas holdup was very small for the temperature range of 160–280 ^{o}C.

2.3 Axial dispersion coefficient

The modelling of bubble column reactors is often carried out assuming ideal plug flow patterns for both the gas and liquid phases. However, such ideal fluid flow does not exist in bubble columns and plug flow assumptions can result in deviations of design calculations from reality (Nikolic, Nikolic, Veljkovic et al., 2004). However, in the homogeneous regime, plug flow is normally assumed since the deviation from reality is minimal.

This non-ideal behaviour of fluid flow decreases the reactant conversion and affects the selectivity. The study of non-ideal flow is therefore of particular importance for the design and scale-up of bubble columns reactors and therefore it cannot be ignored (Nikolic et al., 2004). Neglecting non-ideal flow can lead to detrimental errors when modelling, designing and optimising bubble columns.

Two opposite magnitudes of axial dispersion may be desired when designing bubble columns depending on the application. Most frequently, it is desired to have as low an axial dispersion as possible to maintain the highest concentration driving force throughout the column and attain higher reactant conversion (Dhanasekaran & Karunanithiy, 2010). However, for the aerobic biological reactions operated in a semi-batch mode, it is desired to attain a high axial dispersion as possible to ensure homogeneity in the fermentation broths.

The liquid backmixing is a result of various mechanisms, namely liquid circulations due to non-uniform radial gas holdup, turbulent diffusion due to the eddies generated by rising bubbles and molecular diffusion (Degaleesan & Dudukovik, 1998). Non-ideal flow of gases is frequently encountered with wide bubble size distribution where gas bubbles travel with different velocities. The rising bubbles carry the liquid upwards and the liquid has to return downwards near the walls of the column, causing circulation patterns (Lakota, Jazbec & Levec, 2001). Backmixing of the phases is therefore dependent on the magnitude of liquid circulations.

2.3.1 Circulation patterns

Circulation cells occur in the heterogeneous flow regime. This is a high-interaction flow regime which is characterised by circulation cells and polydispersed bubbles. In this flow regime, gas holdup is non-uniformly distributed in the radial direction, as shown in Figure 2.7. The radial variation of gas holdup results in a variation of gravitational pressure in the radial direction, which increases from the column centre towards the column wall (Joshi et al., 2002). As a result, liquid circulation will develop because of gravitational pressure

variations. In a circulation cell, the liquid flows in the upwards direction in the column centre and downwards near the column wall. The liquid flow is zero at r_0 before flowing down near the wall. r_0 is the radius of the column in which the liquid velocity is zero.

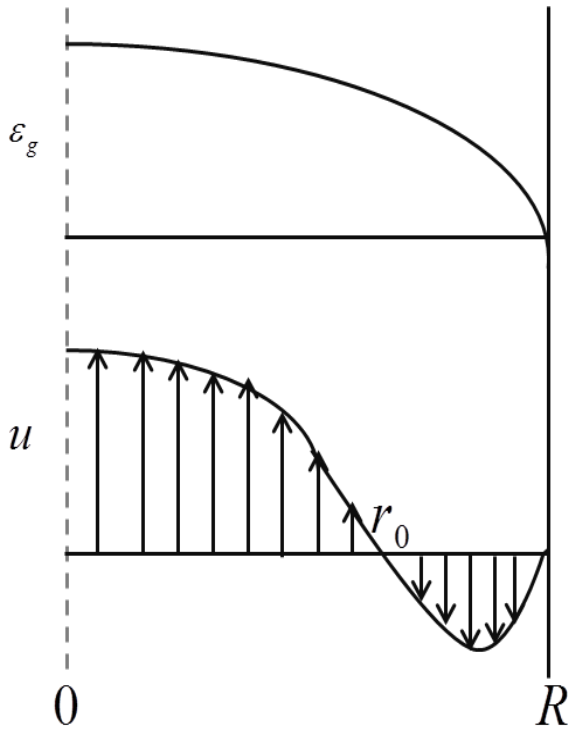

Figure 2.7: Schematic diagram of gas holdup and liquid velocity profile

One of the causes of backmixing of the phases is liquid circulation. The rising bubbles in a bubble column carry the liquid in their wakes and in between them in the case of higher gas loading (Groen, Oldeman, Mudde et al., 1996). The liquid carried by bubbles has to flow down and thus results in the liquid circulation.

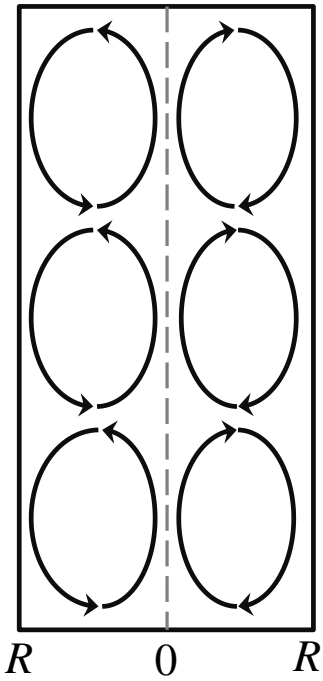

Figure 2.8: Liquid circulation patterns in bubble columns

In the circulation loop of the reactor, the liquid rises through the centre and flows downwards near the column walls, as shown in Figure 2.8. Most of the gas bubbles rise up the column centre and leave the reactor at the top surface. However, smaller gas bubbles will circulate along with the liquid since they do not have enough buoyancy to disengage and leave the column (Gupta, Ong, Al-Dahhan et al., 2001). The circulation mechanism is also facilitated by bubble–bubble interactions, bubble wakes and shear-induced turbulence. Phase circulation is therefore the main course of backmixing.

CHAPTER 3: EXPERIMENTAL SETUP AND PROCEDURE

3.1 Experimental setup

A schematic diagram and a photograph of the experimental setup used are shown in Figures 3.1 and 3.2 respectively (See Appendix 10 for a photograph of the insulated experimental setup). The experimental setup was designed to be operated with molten lithium chloride (LiCl) and potassium chloride (KCl) eutectic at 450 °C. Before the column was loaded with the salt, it was necessary to test its performance with liquids that are easy to handle. Tap water and heat transfer oil 32 were used for this purpose. Heat transfer oil was used to study the behaviour of the experimental setup as the temperature is ramped up.

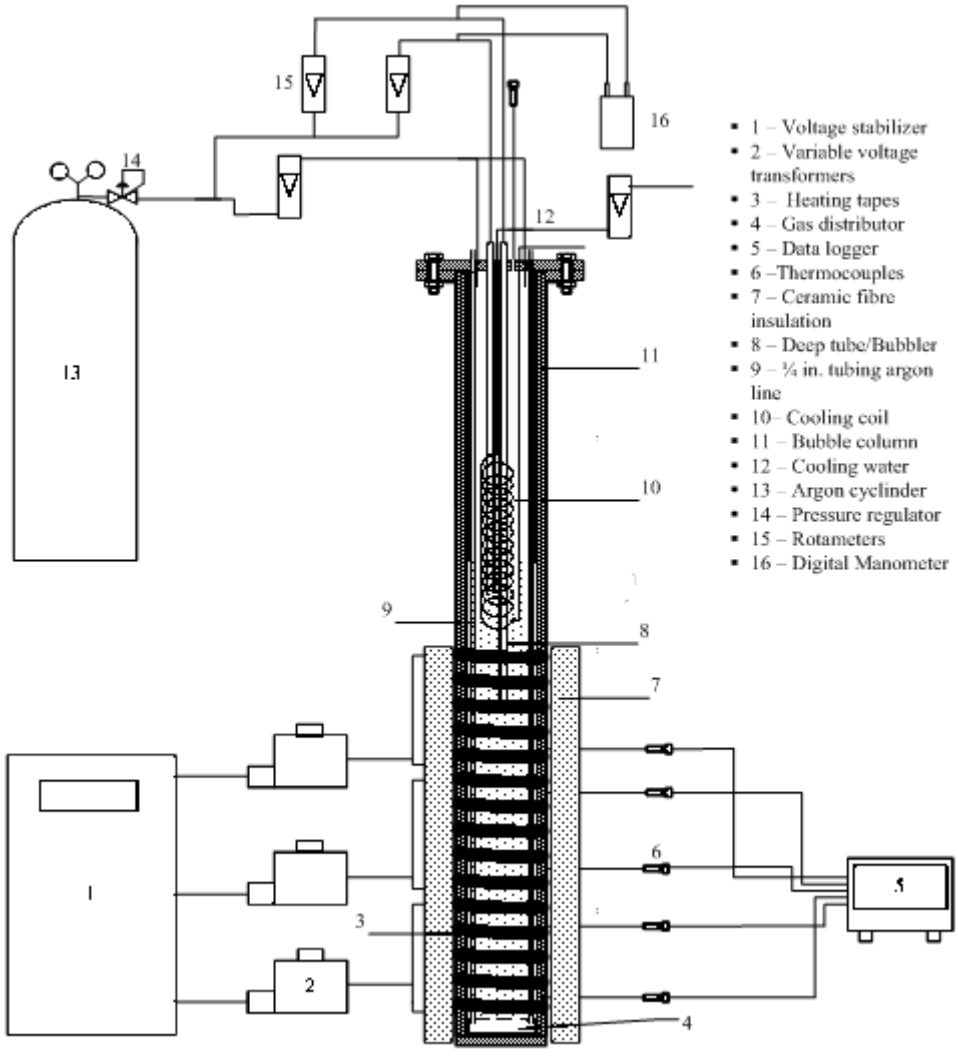

Figure 3.1: Schematic diagram of the experimental setup

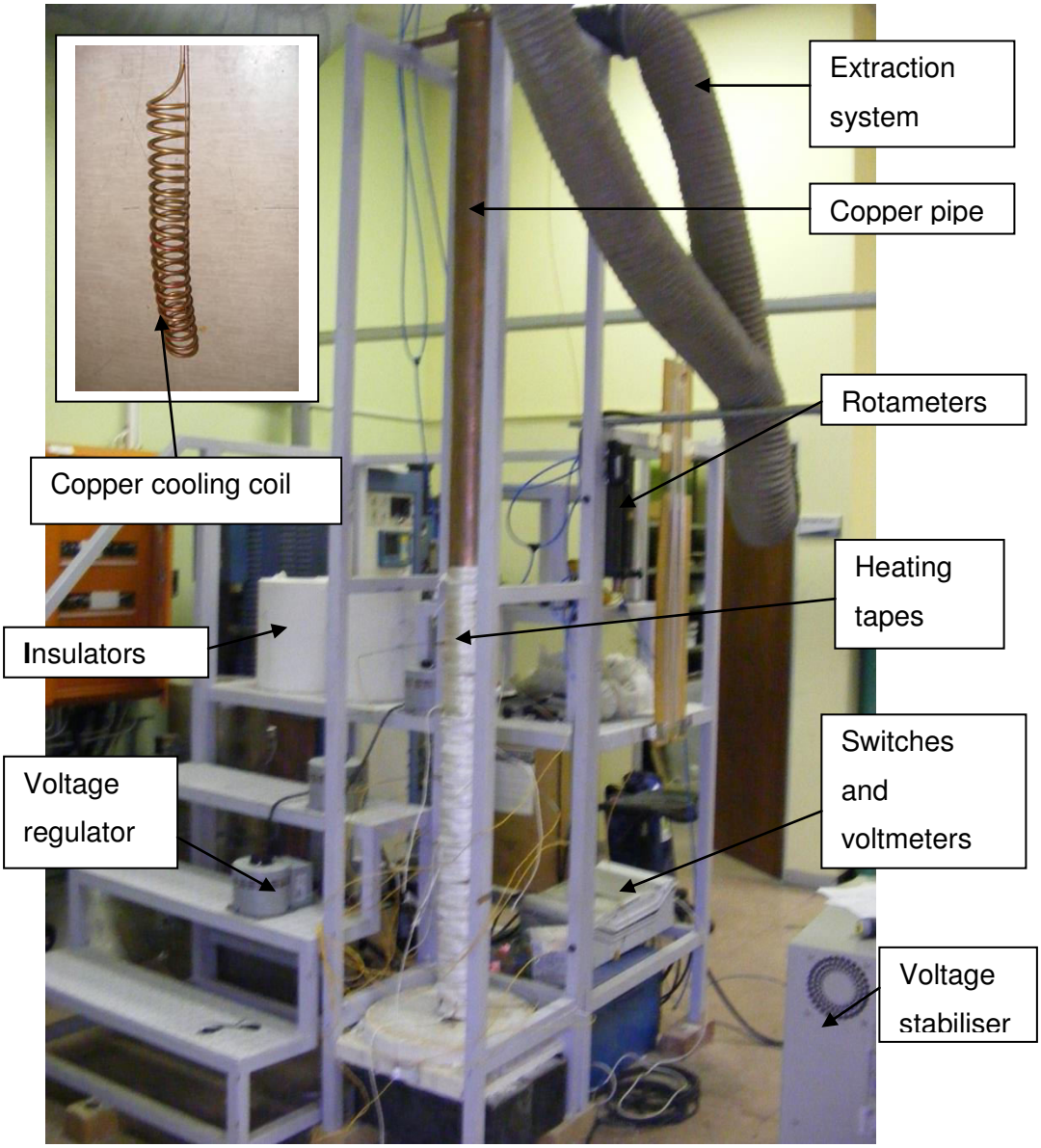

Figure 3.2: Photograph of the experimental setup

Experiments were carried out on the bubble column operated with water at 40 °C, heat transfer oil at 75, 103 and 170 °C, and molten LiCl–KCl eutectic at 450 °C. The physical properties of the liquids are given in Table 3.1. Argon gas was bubbled through the column via the perforated plate gas distributor. The experiments were operated batchwise with regard to the liquids and continuously with regard to argon. Heat was induced into the column with the aid of three heating tapes. The liquid level was measured with a short and a long bubbler tube. The height difference between the tip of the two bubbler tubes and the gas distributor was fixed to 1.306 and 1.118 m for the short and long bubbler tubes respectively.

Table 3.1: Physical properties of the liquids

T (°C)	μ_L (kg.m^{-1}.s^{-1})	k (W.m^{-1}.K^{-1})	ρ_L (kg.m^{-3})
Water			
40	0.000651	0.632	992.2
Heat transfer oil 32			
75	0.0112	0.13	828.9
103	0.00428	0.128	819.0
170	0.00154	0.123	775.2
Paratherm heat transfer fluid			
81	0.00857	0.126	820.0
LiCl–KCl eutectic mixture			
450	0.003441	0.00346	1628

3.1.1 Column

The bubble column was made from copper pipe and had an inside diameter, outside diameter and height of 108 mm, 118 mm and 2.5 m respectively. The liquid level was 1.3 m when the experiment was run with water and heat transfer oil. The copper pipe was manufactured by rolling and welding a copper plate to form the pipe. The welding on the pipe was X-rayed and tested for leakages using air at 6 bar. The bottom of the column was closed with a welded copper disc. After the tests had been completed, water was drained by siphoning using a hosepipe, whereas the heat transfer oil was drained by tilting the column. Four Swagelok fittings were welded onto the column lid to fit the column tubing. In addition, the lid had a hole through which to feed the salt and other liquids to the columns.

3.1.2 Gas supply

Argon gas was supplied to the system from a cylinder containing 17.5 kg gas and pressurised to 200 bar. The cylinder was fitted with a pressure regular to reduce the downstream pressure to the desired working conditions. Tubes of different material, 6.35 mm diameter, were used as gas lines. Plastic tubing was used for the gas line from the cylinder to the stainless steel tube with a length of 20 mm from the column lid. Stainless steel tubing was used inside the column to feed argon to the gas distributor. The argon was therefore pre-heated by heat exchange with the column media.

3.1.3 Gas distributor

Argon was bubbled through the column via a perforated plate gas distributor made of stainless steel. A perforated plate with a diameter of 96 mm, 15 mm pitch and holes with a diameter of 0.5 mm was used. The perforated plate had 17 small holes and two large holes

of 6.5 mm diameter, as shown in Figure 3.3 (Appendix 8 shows the design of the perforations). Two argon inlet tubes were fitted in the 6.5 mm holes.

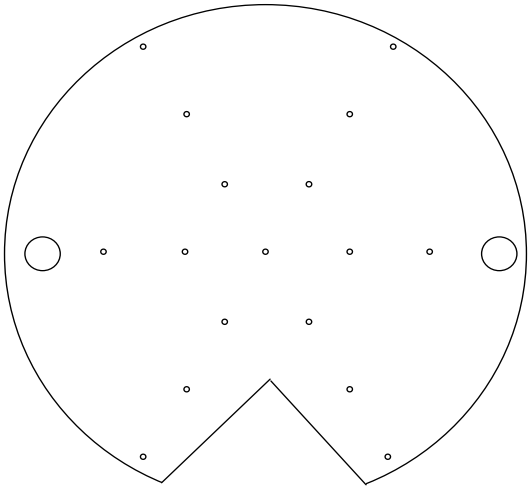

Figure 3.3: Perforated plate showing the arrangement of the orifices

As shown in Figure 3.4, the gas distributor was made from the perforated plate welded to the gas chamber below it. The gas distributor had a V-shaped gap to enable it to pass the thermowells inside the column when it was inserted through the top of the column during installation.

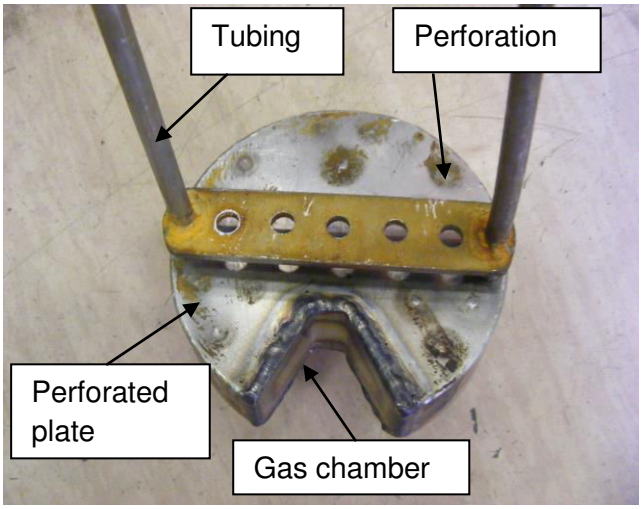

Figure 3.4: Gas distributor fitted with ¼ in. stainless steel tubing

3.1.4 Heat transfer section

Three heating tapes, each with dimensions of 3 000 mm × 44 mm and a power rating of 1 570 W, were used as the heat source. Each heating tape was wrapped around the copper pipe to form a heating zone of 350 mm in length. Thus the total length of the heating section was 1 050 mm. The top and bottom heaters were used as guard heaters to minimise the

axial heat conduction at the ends of the heater in the middle. The heat transfer flux from the middle heater could be measured accurately and hence by using the power input of the middle heater, the heat transfer coefficient could be calculated accurately. The heating tapes were insulated with ceramic fibre insulation which was vacuum-formed and moulded to a thickness of 75 mm and i.d. of 135 mm. Temperature differences were measured at five different points along the column using pairs of type K thermocouples with 2 mm diameter sheaths.

Each pair consisted of a thermocouple that measures the wall temperature and another that measures the liquid temperature. The spacing between the five pairs of thermocouples was 170 mm. Liquid temperatures were measured by inserting thermocouples through the thermowells which are welded to the copper pipe. The thermowells were made from ¼ in. stainless steel tubing welded to a copper rod and the total length of each thermowell was 30 mm. In order to measure the wall temperature accurately, the thermocouples were silver-soldered on the outside wall of the copper pipe, as shown in Figure 3.5.

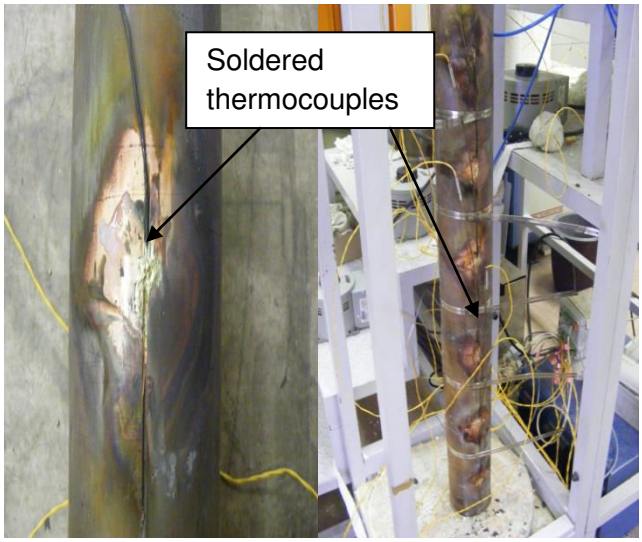

Figure 3.5: Thermocouples soldered to the wall of the copper pipe

The tips of the thermocouples in a pair were placed at the same axial position. This was done to account for the fact that a temperature gradient formed along the height of the column. The thermocouples were calibrated using a water bath with a uniform temperature and the average error in the calibration results was less than 0.35 ^{o}C (see Appendix 7).

The power of the heaters was controlled by the AC voltage controllers. A voltage stabiliser was also installed to supply the voltage controllers with a stable voltage. To balance the system, heat was removed by cooling water flowing through the copper tube on the inside of

the column. The removal of heat by the cooling water also increased the temperature difference and therefore improved the accuracy of the measurements. The coiled copper tube was positioned above the heating section so that it did not significantly change the hydrodynamics in the heating section. Above the heating section, the column was also insulated to maximise the absorption of heat by the cooling water.

The rate of heat transfer was obtained by measuring the voltage across an electric current flowing through the heating tapes. A multimeter was used to measure the voltage and a clamp current meter was used to measure the current. The measurements of the rate of heat transfer were confirmed by calculating the energy balance over the cooling water coil.

3.1.5 Modified experimental setup

Due to the column failing when it was operated with molten salt, it had to be modified. Figure 3.6 shows the modified experimental setup that was also used to measure the heat transfer coefficients. The column was modified by making the following changes:

- The height of the column was reduced from 2.5 m to 1.4 m.
- The liquid level was reduced from 1.3 m to 0.9 m.
- Heating tapes were replaced with heating cables.
- The liquid temperature was measured by long thermocouples inserted from the column lid.
- The thermowells were omitted.

Figure 3.6: Schematic diagram of the modified experimental setup

3.2 Experimental procedure

3.2.1 Heat transfer coefficient

The heat transfer coefficient was calculated from Equation 3.1:

$$h = \frac{Q}{A(T_W - T_B)} \qquad [3.1]$$

where Q is the rate of heat transfer, A is the heat transfer area, T_W is the wall temperature and T_B is the bulk liquid temperature. The rate of heat transfer is calculated from:

$$Q = P - Q_{loss} \quad [3.2]$$

where,

$$Q_{loss} = k_i A \frac{\Delta T}{\Delta L} \quad [3.3]$$

where P is the electrical power, Q_{loss} is the heat loss from the heating tapes to the surrounding environment, k_i is the thermal conductivity of the insulation material, ΔL is the distance between the measured temperature difference and ΔT_i is the temperature difference at ΔL (ΔL = 45 mm was used).

3.2.1.1 Column operated with water

The experiments were conducted as follows:

- The column was filled with water up to a level of 1.3 m.
- The heaters were switched on to increase the temperature of the water.
- The rotameter for the cooling water was turned on to remove heat from the column and increase the temperature difference between the column wall and the liquid.
- After the heaters had stabilised, the liquid temperature was controlled at 40 °C.
- Rotameters were used to control the argon flowrate to superficial gas velocities in the range of 0.006–0.05 m/s.
- Measurements and readings were taken after the system had reached steady state.
- Power and temperature readings were taken at each gas flowrate.
- The experimental procedure was repeated four times on different days for each superficial gas velocity.

3.2.1.2 Column operated with heat transfer oil

The experimental procedure for heat transfer oil at 75 °C and 103 °C was performed in a similar way to that for water, except that at 170 °C the system was operated without cooling water. The power of the heating tapes could not raise the oil temperature up to 170 °C while heat was being removed using the cooling water. Also, at 170 °C when the column was operated without cooling water, the temperature difference between the column wall and the liquid was high enough to be measured accurately. The insulation above the heating section was removed so that heat could be removed through the upper column wall. Furthermore, for the experiments at 103 °C, the heating tapes were at maximum power for higher superficial gas velocities and cooling water was used to control the liquid temperature.

3.2.1.3 Column operated with molten salt mixture

The salt used was a eutectic mixture of LiCl and KCl. Approximately 18 kg of the salt eutectic was weighed and melted. The masses of LiCl and KCl were 8 kg and 9.95 kg respectively. This was achieved by initially melting 13.6 kg of the salt eutectic at 450 °C and filling the heating zone with the salt in a molten state. The remaining 4.35 kg was then added and quickly melted as it settled in the pool of molten salt. See Appendix 9 for a detailed calculation of the amount of each salt in the eutectic mixture.

3.2.2 Gas holdup

Appendix 6 shows the derivation of the equations needed to calculate the gas holdup. The procedure for measuring the gas holdup was the same for all the liquids used.

- The argon flowrate was controlled with the aid of rotameters.
- The argon flow was switched on and the flowrate varied to give a superficial gas velocity in the range of 0.006 m/s to 0.05 m/s.
- The flowrate in the bubbler tubes was kept at 2–3 l/h for all level measurements.
- Bubbler tubes were used to measure the change in the liquid level due to an increase in the superficial gas velocity.
- Manometer readings were taken at each argon flowrate.
- This procedure was done three times.

3.3 Experimental understanding

3.3 1 Impact of cooling water

The heat transfer area of the bubble column was very large. Therefore for the operating temperatures of 40 °C, 75 °C and 103 °C a low heat was needed in order for the system to reach steady state at the desired operating temperature. Heat loss from the column contents to the surroundings was therefore very low and that could have reduced the temperature difference between the column wall and the liquid to below 1 °C, which could be difficult to measure accurately. More heat was therefore removed to increase the temperature difference to a value that could be measured accurately. Heat was removed by using cooling water flowing through a ¼ in. coiled copper tube. In order to keep the system at steady state at the desired temperature, more heat was added to compensate the heat absorbed by the cooling water. Additionally, the use of cooling water was useful in the verification of the measurements of electrical power.

3.3.2 Comparison between stainless steel and copper bubble column

Since bubble columns have high values of heat transfer coefficients, a copper pipe was considered for measuring the heat transfer coefficient because of its higher thermal conductivity. This higher thermal conductivity ensures that the resistance to conductive heat transfer is higher than the resistance to convective heat transfer, so that the radial and axial temperatures in the pipe wall can be distributed faster and attain uniformity. For an aggressive medium such as molten salt, stainless steel is a good material of construction. However, the thermal conductivity of stainless steel is 25 $W.m^{-2}.K^{-1}$ which is very low compared with the 300 $W.m^{-2}.K^{-1}$ of copper. As a result, the temperature might not be uniform when a stainless steel pipe is used.

The temperature profile for a copper pipe as heated in the experimental column was compared with that of a stainless steel pipe by modelling the two-dimensional heat conduction in the pipe wall using the software package Abaqus Version 6.12. The modelling was done on a pipe wall 8 mm thick and with a spacing of 20 mm between two heating elements that are at the same temperature. The boundary conditions were as follows:

- It was assumed that the two heating elements are at the same temperature of 72 °C. Therefore the top and bottom boundary conditions were that the temperature is 72 °C.
- On the inner side of the pipe, there is a gas-liquid dispersion with a heat transfer coefficient of 2 000 $W.m^{-2}.K^{-1}$.
- On the outer side of the pipe, there is natural convection by air with a heat transfer coefficient of 10 $W.m^{-2}.K^{-1}$.

Figure 3.7 shows the calculated two-dimensional temperature profile in the wall of a stainless steel pipe. The temperature was not uniform since there was a temperature difference of about 5 °C between the maximum and minimum temperatures. It would therefore be difficult to measure the temperature difference between the wall and the liquid in the column accurately when using stainless steel. The average inner wall temperature would not be estimated accurately due significant non-uniformity of the temperature in both the axial and radial directions. It could also be difficult to position the thermocouple in the column wall in such a way that it measures the inner wall temperature accurately. This is because the distance between the bi-metallic coupling of the thermocouple and the tip of the thermocouple sheath is not known, thus making it difficult to compensate for the heat conduction through the column wall when estimating the inner wall temperature.

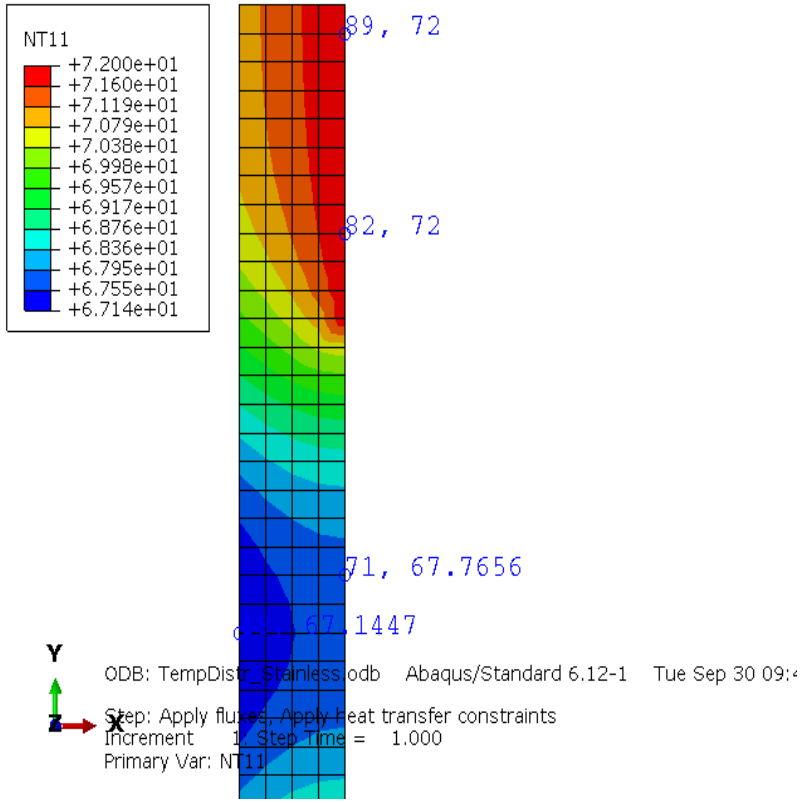

Figure 3.7: Temperature profile between spacing of heating elements for a stainless steel pipe

Figure 3.8 shows the predicted two-dimensional temperature profile of the wall of a copper pipe. As shown in the figure, the temperature is uniform in both the axial and radial directions, with a temperature difference of about 0.8 ^{o}C between the maximum and minimum temperatures. The high thermal conductivity of a copper pipe ensures a nearly uniform temperature in the wall. Such temperature uniformity is important due to the fact that the thermocouple at the wall could be positioned almost anywhere in the axial or radial directions and still give a good measurement of the inner wall temperature of the pipe. The temperature difference would therefore be measured accurately when a copper pipe was used and that was the main reason for choosing a copper pipe for the experiments.

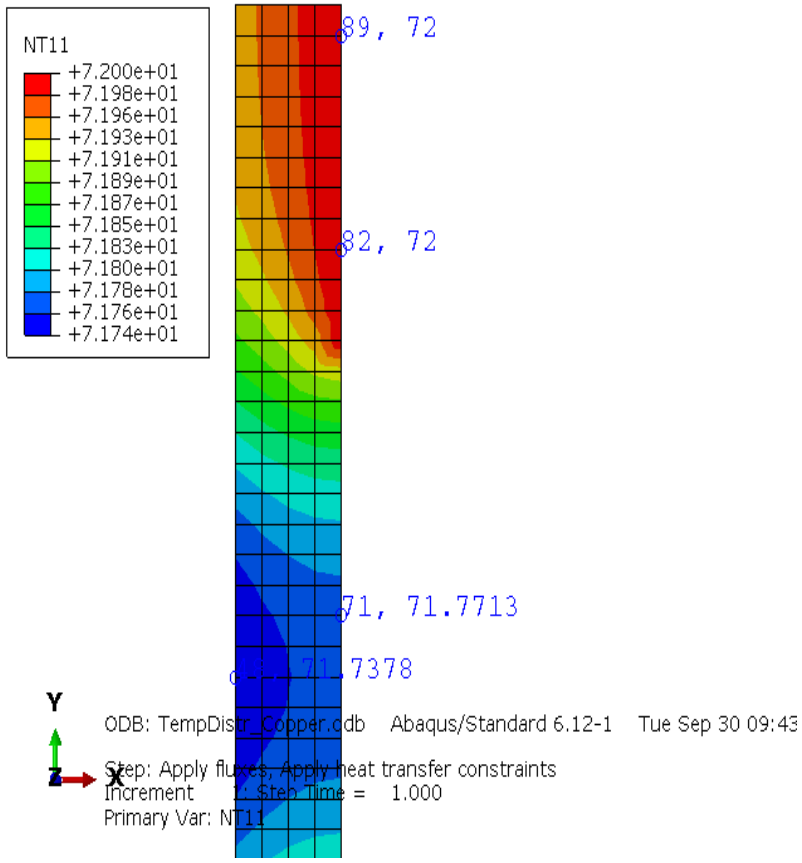

Figure 3.8: Temperature profile between spacing of heating elements for a copper pipe

3.3.3 Modelling of the temperature profile in the thermowell

Thermowells were welded to the bubble column wall. Figure 3.9 shows a photograph of one of the thermowells that were used to measure the liquid temperature. The copper part of the thermowell was threaded to allow it to be fitted to the threaded hole in the column wall. The fitted thermowell was then welded onto the column wall for proper sealing. Stainless steel extensions were welded onto the copper thermowells. Stainless steel was included in the thermowell because there is a large temperature gradient on the heated stainless steel which ensures a good representation of the liquid temperature to be measured. When the column wall is being heated, the thermowell conducts heat and that poses challenges with regard to isolating the heat conducted by the thermowell and the sensitivity of the thermocouple that measures the liquid temperature. The thermowell should therefore be a poor conductor of heat in order for the thermocouple to measure only the liquid temperature without sensing any heat from the wall.

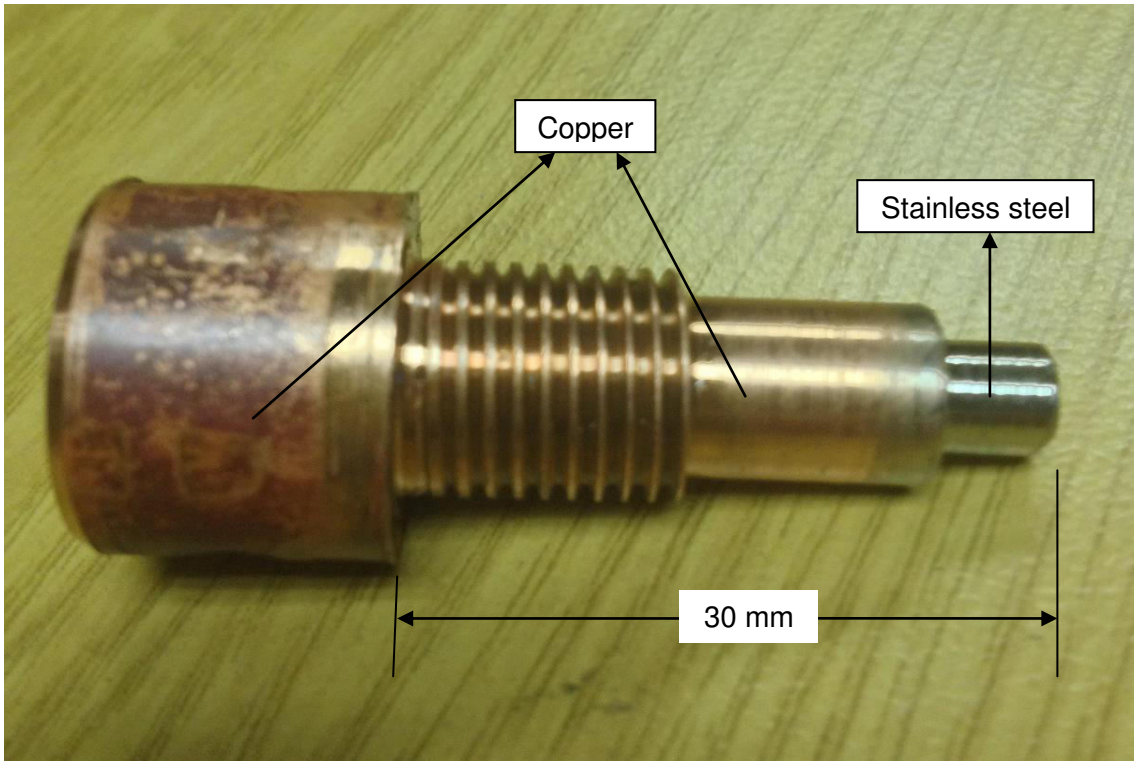

Figure 3.9: Thermowell used for temperature measurements

The purpose of this modelling was to determine whether the temperature measured at the tip of the well would be representative of the liquid surrounding the tip, thus confirming the reason for the inclusion of stainless steel in the thermowell for measuring a liquid temperature correctly. Assuming that there is no temperature gradient in the radial direction of the wall of the thermowell, the energy balance for a small element of Δx is given by:

$$q_x = q_{x+\Delta x} + h2\pi\Delta x(T - T_B) \quad [3.4]$$

Rearranging Equation 3.4 and dividing the equation by Δx gives:

$$\lim_{\Delta x \to 0} \frac{q_{x+\Delta x} - q_x}{\Delta x} = \frac{-h2\pi r\Delta x(T - T_B)}{\Delta x} \quad [3.5]$$

$$\frac{dq}{dx} = -h2\pi r(T - T_B) \quad [3.6]$$

$$\frac{d}{dx}\left(-kA\frac{dT}{dx}\right) = -h2\pi r(T - T_B) \quad [3.7]$$

Differentiating and rearranging Equation 3.7 gives:

$$\frac{d^2T}{dx^2} = \frac{h2\pi r}{kA}\left(T - T_B\right) \qquad [3.8]$$

Let $T - T_B = y$ and $\frac{h2\pi r}{kA} = b^2$

Differentiating $T - T_B = y$ twice gives:

$$\frac{d^2T}{dx^2} = \frac{d^2y}{dx^2} \qquad [3.9]$$

Substituting Equation 3.9, y and b into Equation 3.8 gives:

$$\frac{d^2y}{dx^2} - b^2y = 0 \qquad [3.10]$$

The general solution to Equation 3.10 is given by:

$$y = C_1e^{-bx} + C_2e^{bx} \qquad [3.11]$$

Substituting Equation 3.11 into $T - T_B = y$ gives:

$$T - T_B = C_1e^{-bx} + C_2e^{bx} \qquad [3.12]$$

Differentiating Equation 3.12 gives:

$$\frac{dT}{dx} = b\left(-C_1e^{-bx} + C_2e^{bx}\right) \qquad [3.13]$$

The boundary condition at beginning of the thermowell is:

$T = T_W$ at $x = 0$

Substituting the above boundary condition into Equation 3.12 therefore gives:

$$T_W - T_B = C_1 + C_2 \qquad [3.14$$

The boundary condition of the tip of the thermowell is:

$$-k\left(\frac{dT}{dx}\right) = h_t(T - T_B) \text{ at } x = L$$

Substituting the above boundary conditions into Equation 3.13 gives:

$$-\frac{h_t}{k}(T - T_B) = b\left(-C_1 e^{-bx} + C_2 e^{bx}\right) \qquad [3.15]$$

Substituting Equation 3.12 into Equation 3.15 yields:

$$b\left(-C_1 e^{-bL} + C_2 e^{bL}\right) = -\frac{h_t}{k}\left(C_1 e^{-bL} + C_2 e^{bL}\right) \qquad [3.16]$$

Substituting Equation 3.14 into Equation 3.16 and making C_1 the subject of the equation gives:

$$C_1 = \frac{(T_W - T_B)e^{bL}\left(1 + \frac{h_t}{kb}\right)}{\left(e^{-bL} + e^{bL}\right) + \frac{h_t}{kb}\left(e^{bL} - e^{-bL}\right)} \qquad [3.17]$$

For L = 0.03 m, T_B = 40 °C, T_W = 45 °C, k_{steel} = 25 W.m^{-2}.K^{-1}, k_{copper} = 300 W.m^{-2}.K^{-1}, h_t = 3 000 W.m^{-2}.K^{-1}, r = 3.175 mm, Equation 3.12 is plotted in Figure 3.10. The temperature gradients for copper and stainless steel thermowells are plotted and compared. As shown in Figure 3.10, the stainless steel thermowell gives a better representation of the liquid temperature in a bubble column due to the large temperature difference between the beginning and the tip of the thermowell. It was concluded that a stainless steel tip of 12 mm would be adequate.

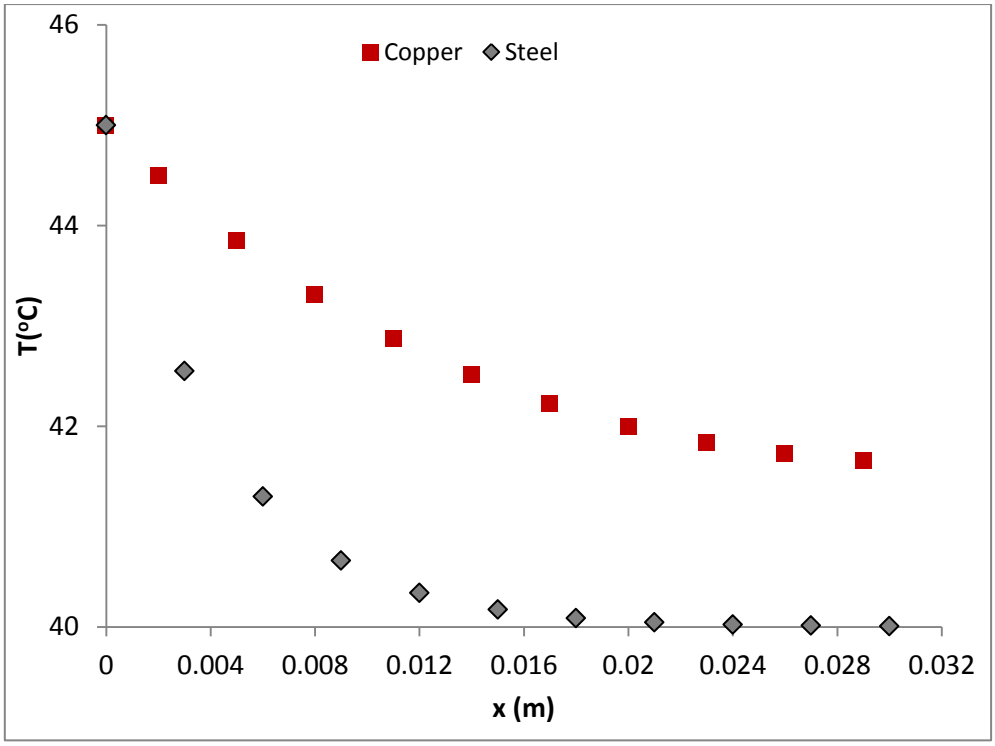

Figure 3.10: Temperature profile for stainless steel and copper thermowells

CHAPTER 4: RESULTS AND DISCUSSION

4.1 Heat transfer coefficient

4.1.1 Column operated with water

Table 4.1 shows the values of heat input, which is the rate of heat generated by the heaters and transferred to the column; and heat output, which is calculated from the energy balance of the cooling water.

Table 4.1: Comparison of heat input and heat output

u_G [m/s]	Total power [W]	Heat loss [W]	Heat input [W]	Heat output [W]	% error
0.006	1 543.8	52.1	1 491.7	1 510.3	1.3
0.015	2 031.0	69.8	1 961.2	1 936.5	1.3
0.023	2 386.9	79.5	2 307.4	2 248.1	2.6
0.031	2 795.0	91.8	2 703.2	2 546.1	5.8
0.039	3 222.0	102.4	3 119.5	2 897.8	7.1
0.046	3 665.9	118.5	3 547.4	3 367.3	5.1

When the system reaches steady state, heat input must equal to heat output. It was found that the values of heat input and heat output are close to one another, with some small errors that were regarded as acceptable. Therefore, the rate of heat transfer was measured accurately. Table 4.2 shows the values of the temperature difference at different axial positions of the copper pipe. The second difference pair, ΔV_2, was omitted from the calculations of average temperature difference because, according to Dixon's test of outliers, there is more that 95% confidence that it is an outlier (Grubbs, 1969).

Table 4.2: Temperature difference measured at different axial positions of the heating zone for u_G = 0.031 m/s

	ΔV_1 [mV]	ΔV_2 [mV]	ΔV_3 [mV]	ΔV_4 [mV]	ΔV_5 [mV]	$\Delta V_{average}$ [mV]	$\Delta T_{average}$ [°C]	s
ΔV	0.085	0.133	0.080	0.085	0.101	0.097		
ΔT	2.1	3.3	2.0	2.1	2.5		2.2	0.192

It was expected that the temperature difference between the wall and the liquid would be uniform as a result of the high thermal conductivity of the copper metal. The values of the

temperature difference are close to one another with the standard deviation, s, of 0.192 and this confirms the uniformity of the wall temperature.

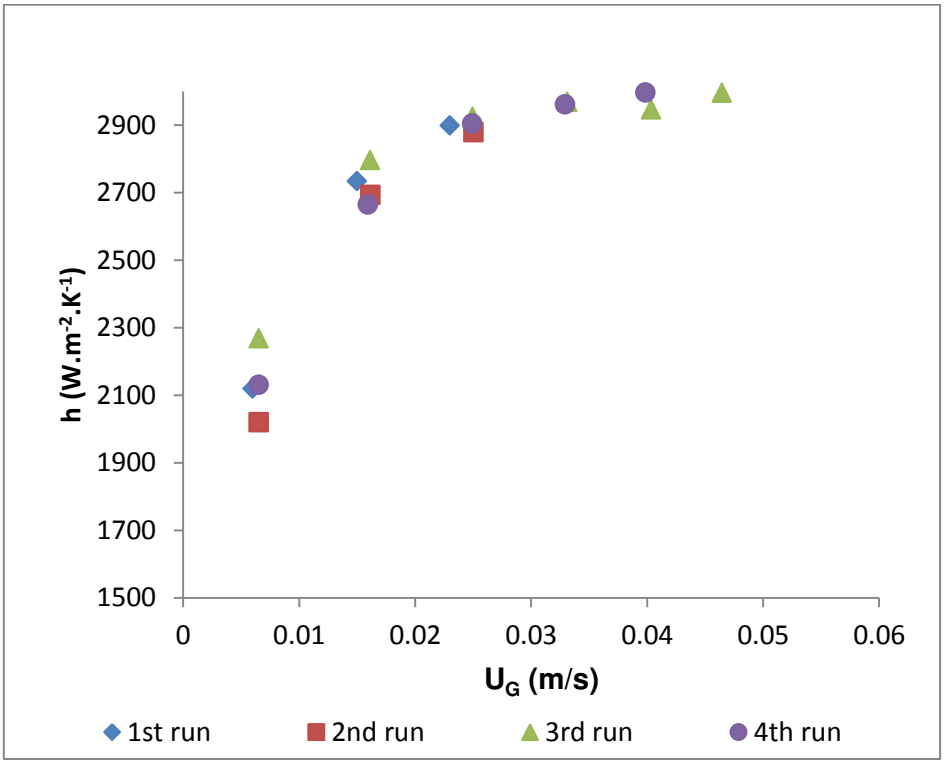

Figure 4.1: Different runs for measuring the heat transfer coefficient

The experiments for measuring the heat transfer coefficient were repeated several times on different days to check the repeatability of the experimental setup. The results of different runs in Figure 4.1 show that the experiment was repeatable, with an experimental error ranging from 0.5 to 4% (Appendix 1 and 4 shows the values of experimental error and how was it calculated, respectively). The heat transfer coefficient increases with superficial gas velocity. As the superficial gas velocity increases, the number of bubbles increases and this reduces the surface film thickness. The heat transfer coefficient will thus be lowered as a result of the reduced surface film thickness.

The measured heat transfer coefficients were compared with those in the literature, as shown in Figure 4.2. Recent developments regarding work on the wall heat transfer coefficient are very rare and the comparison was therefore made with the old research work.

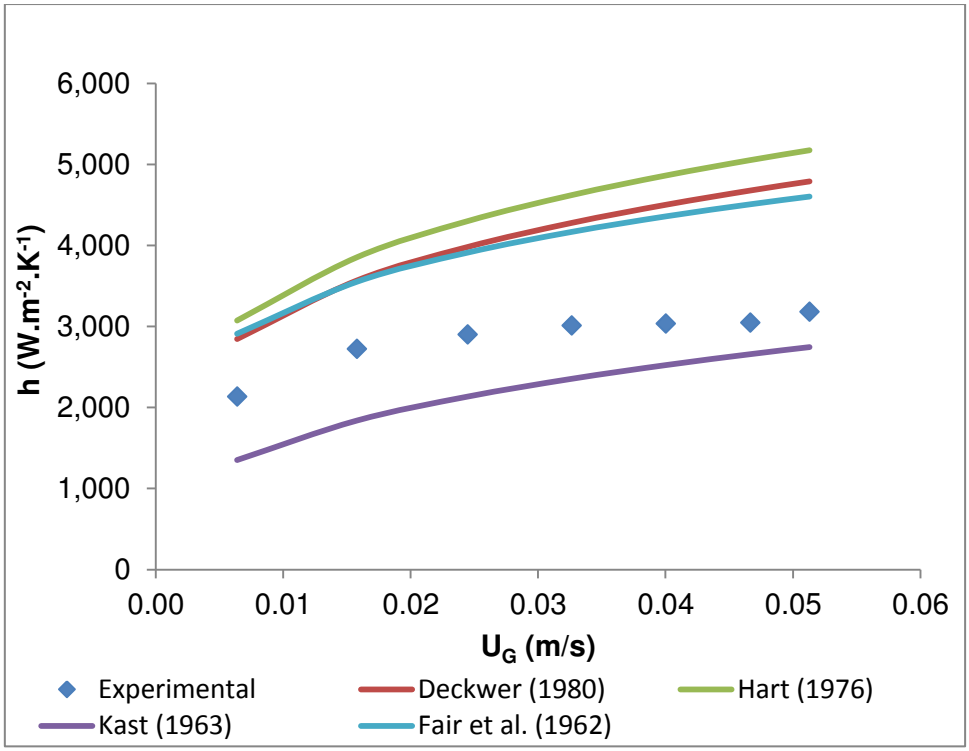

Figure 4.2: Comparison of experimental heat transfer coefficient with the literature for measurements in water medium

The experimental values for the heat transfer coefficient are in good agreement with those of Kast (1963), and in somewhat less good agreement with those of Deckwer (1980a), Hart (1976) and Fair et al. (1962). However, the results of Kast (1963) might have deviated from the other literature results because of uncertainties in the way the correlation of Kast (1963) is written. In Table 2.1 (Chapter 2) the gas viscosity is included in the correlation of Kast (1963) which is peculiar.

The experimental results for the heat transfer coefficients that were measured in the modified experimental setup in Figure 3.6 (Chapter 3) are shown in Figure 4.3. These results show better agreement with the literature compared with those in Figure 4.2. The difference in the results obtained for these two systems could be attributed to the difference in the way the liquid temperature was measured in the two systems. In the modified setup, the thermocouples that were inserted from the column lid were closer to the inner surface of the bubble column. In Figure 3.2 (Chapter 3) the liquid temperature was measured by using thermowells that were 30 mm long and they measured the liquid temperature near the column centre. Therefore, the thermowells contributed to a slightly larger temperature difference compared with the thermocouples in the modified system.

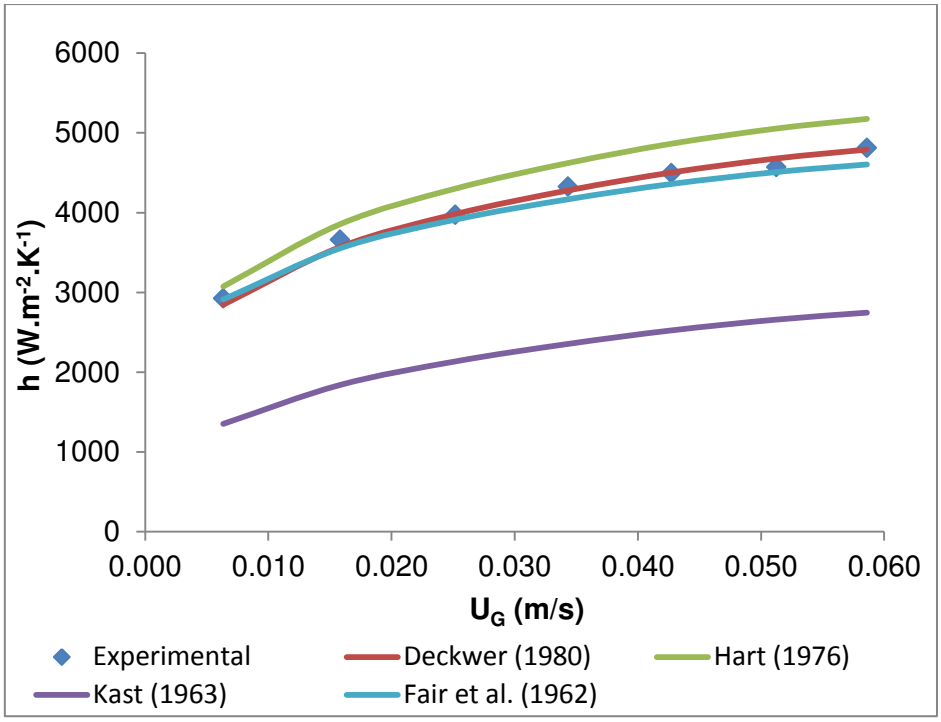

Figure 4.3: Comparison of experimental heat transfer coefficient with the literature for measurements in water medium in the modified experimental setup[1]

It is normally assumed that there is no radial temperature profile between the column centre and a liquid–film interface. However, there is a temperature gradient from the column centre towards the wall and the assumption of no temperature gradient can result in disparities between the measurements of the temperature between the wall and the fluid. In Appendix 5 it is shown that the temperature difference between the column centre and a liquid–film interface could be 0.4 °C or more. For the temperature differences that were measured in the system shown in Figure 3.2 (Chapter 3), as shown in Table 4.2 above, the radial temperature profile could have affected the measurements by about 20%.

4.1.2 Column operated with heat transfer oil

Heat transfer coefficients for the argon–heat transfer oil system are shown in Figure 4.4. Similar to the argon–water system, the heat transfer coefficient increases with superficial gas velocity due to an increased number of bubbles and turbulence in the system. For the operating temperatures of 75 °C and 103 °C, the heat transfer coefficient flattened out above a superficial gas velocity of 0.035 m/s. At the operating temperature of 170 °C, the heat

1. *Results for the modified setup are shown only in Figure 4.3, all the other results are for the setup in Figure 3.2.*

transfer coefficient increased significantly. At u_G = 0.05 m/s, the heat transfer coefficient of the second graph was lower than that at u_G = 0.045 m/s. At u_G = 0.05 m/s, the operating temperature was controlled to 98 °C instead of 103 °C because the heating tapes were already at their maximum power and the cooling water could not control the temperature effectively. Since the measurements at 103 °C were not done at constant temperature, the slight differences in physical properties affected the results.

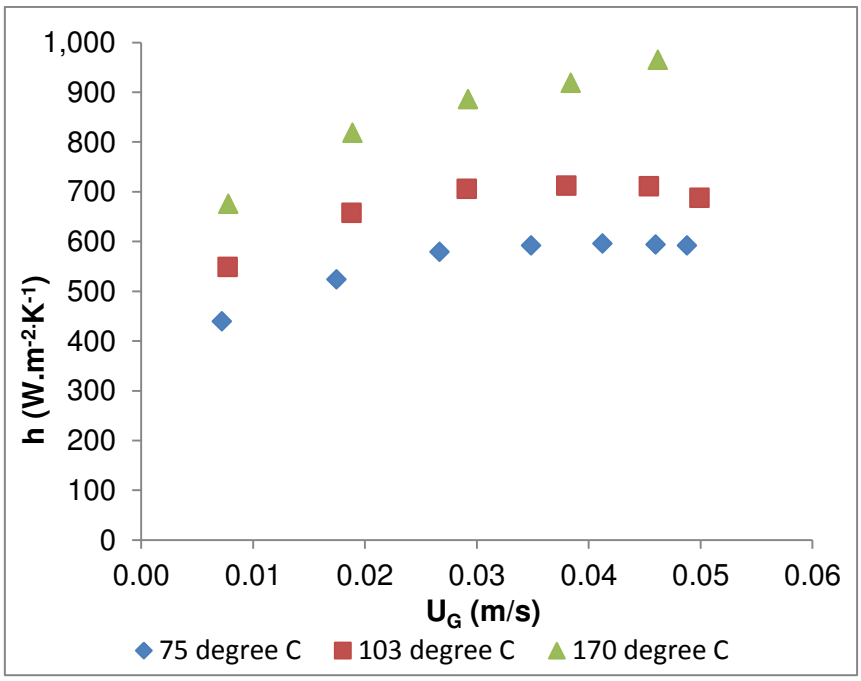

Figure 4.4: Heat transfer coefficient at different temperatures

The heat transfer coefficients for the argon–heat transfer oil system are lower than those obtained for the argon–water system. The viscosity of heat transfer oil is higher than that of water. The bubble sizes increase with an increase in liquid viscosity. Large bubbles rise at the core of the bubble column with little turbulence at the column wall. Therefore, the wall heat transfer coefficient of the oil compare to that of water is significantly affected by the liquid thermal conductivity than the viscosity. The high heat transfer coefficient of the argon–water system is therefore attributed to the higher thermal conductivity of water compared to heat transfer oil. On the other hand, as shown in Figure 4.4, the heat transfer coefficient increases with an increase in temperature.

There are no data available in the literature for heat transfer coefficients in a bubble column operated with heat transfer oil 32. The experimental values at 75 °C were compared with those of another heat transfer fluid. Yang, Luo, Lau et al. (2000) measured the heat transfer

coefficient in a bubble column operated with air and Paratherm NF heat transfer fluid at 81 °C and 4.2 MPa.

Differences between the experimental results and the literature are attributed to different physical properties of the two oils. It can also be observed in Figure 4.5 that the heat transfer coefficient for the heat transfer fluid is lower than that when the system is operated with water; this confirms that an increase in liquid viscosity decreases the heat transfer coefficient.

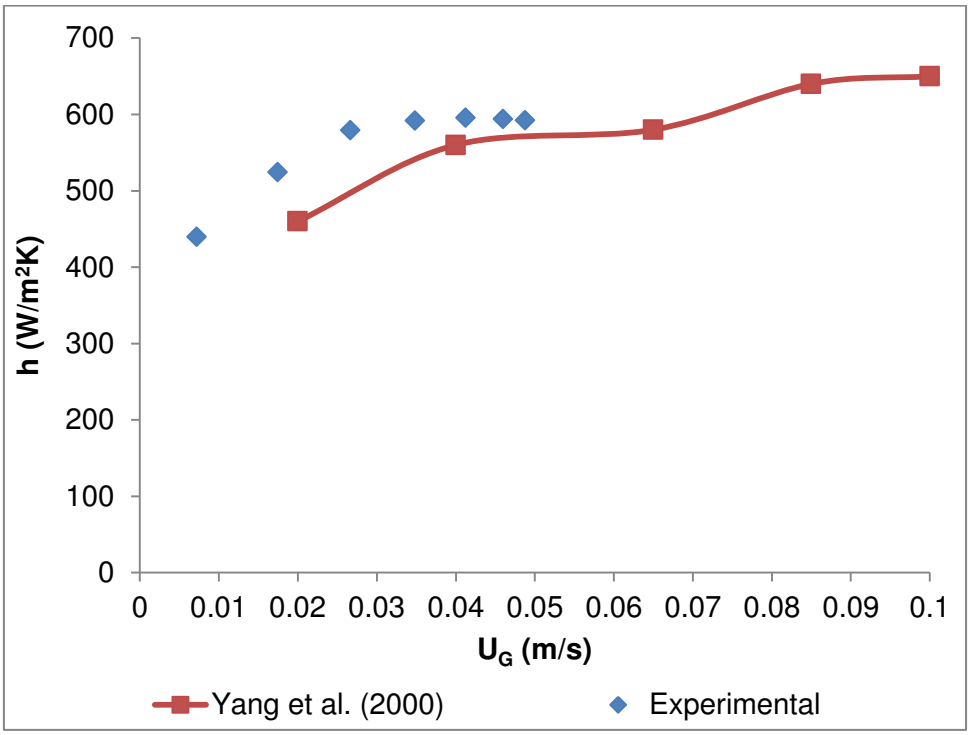

Figure 4.5: Comparison of heat transfer coefficients with the literature for measurements in heat transfer oil medium

4.1.3 Column operated with molten salt mixture

The photographs in Figure 4.6 show the mechanical failure of the experimental setup after it had been operated with molten salt. The weld of the thermowells failed and caused the salt to leak. The molten salt was then exposed to oxygen and caused an aggressive corrosion of the pipe within hours. All three heating tapes were also damaged beyond repair by the molten salt.

Figure 4.6: Copper pipe damaged by leakage of molten salt

After the salt had leaked through the welds of the thermowells and the column, it was decided to cut the 2.5 m copper pipe into a 1.4 m length and heat it with ceramic band heaters. A ceramic band heater with three heating zones was used because the heating cables shown in Figure 3.6 (Chapter 3) were damaged and they could not be used again. The new test rig did not have any thermowells, although there were some other welds since the pipe was a welded copper plate. Figure 4.7 show the experimental setup before the salt was loaded.

Figure 4.7: Experimental setup before salt leakage (new test rig)

After the column in the new test rig had been operated with molten salt, it was also found to have leaked at the welds. Figure 4.8 shows the experimental setup after the salt had leaked out of the column.

Figure 4.8: Experimental setup after salt leakage

4.2 Gas holdup

4.2.1 Column operated with water

As shown in Figure 4.9, gas holdup increases with superficial gas velocity (experimental data for gas holdup can be obtained in Appendix 2). As the superficial gas velocity increases, the number of bubbles increases, thus increasing the gas holdup. The experimental results were in good agreement with the literature.

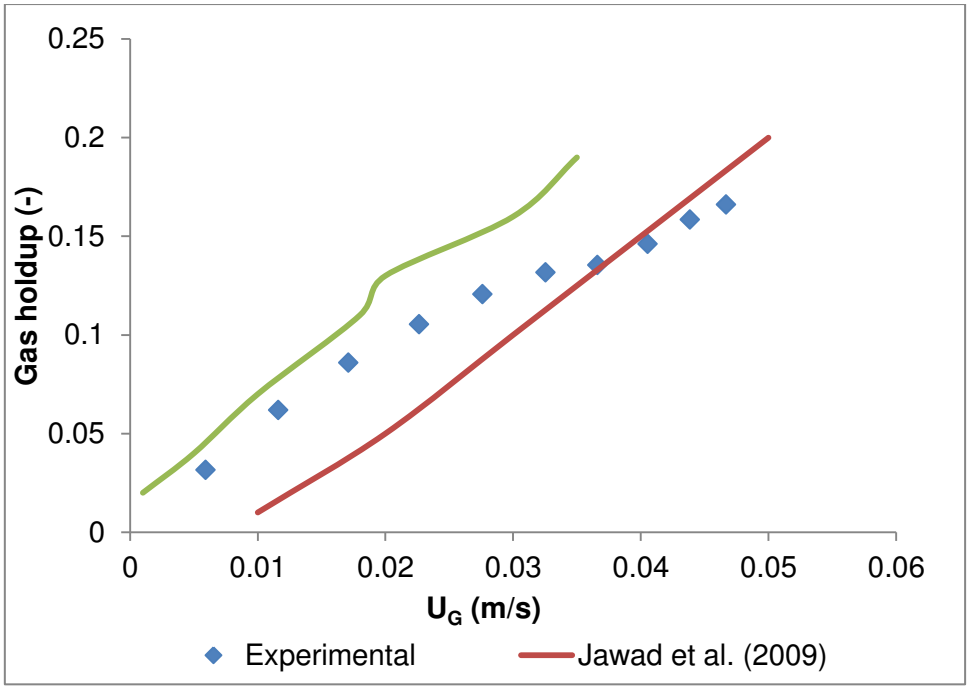

Figure 4.9: Comparison of experimental results for gas holdup with the literature

4.2.2 Column operated with heat transfer oil

The gas holdup for the heat transfer oil also increased with superficial gas velocity and temperature, and was greater than that of the argon–water system. This can be attributed to the higher operating temperature.

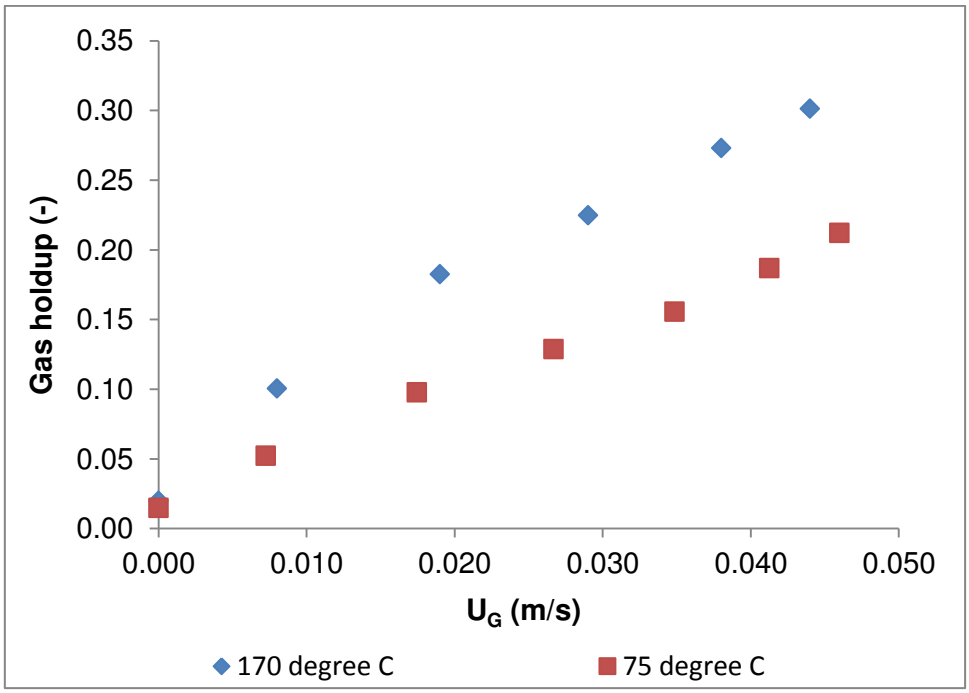

Figure 4.10: Experimental gas holdup at heat transfer oil

4.3 Mechanistic model for dispersion coefficients

4.3.1 Liquid flow model

Ueyama & Miyauchi (1970) applied a force balance equation to develop a theoretical model for predicting a liquid velocity profile. Equation 4.1 is basically the sum of forces acting on liquid in a bubble column.

$$-\frac{1}{r}\frac{d}{dr}(r\tau)=\frac{dP}{dZ}+(1-\varepsilon_G)\rho_L g \qquad [4.1]$$

where r is a radial coordinate, τ is the shear stress, P is the pressure and Z is the axial coordinate.

The shear stress is given by:

$$\tau=-(\upsilon_M+\upsilon_t)\rho_L\left(\frac{du}{dr}\right) \qquad [4.2]$$

where is u the interstitial liquid velocity, υ_M is the molecular viscosity (whose contribution is due to the random movement of molecules) and υ_t is the turbulent kinematic viscosity (whose contribution to momentum exchange is due to circulation cells). Integrating Equation 4.1 between $r=0$ and $r=R$ gives:

$$-\frac{dP}{dZ}=\left(\frac{2}{R}\right)\tau_w+(1-\bar{\varepsilon}_G)\rho_L g \qquad [4.3]$$

where τ_W is the shear stress at the wall. Substituting Equations 4.3 and 4.2 into Equation 4.1 (neglecting υ_M in the turbulent core), one obtains the modified basic equation for axial liquid flow in the turbulent core:

$$-\frac{1}{r}\frac{d}{dr}\left(\upsilon_t r\frac{du}{dr}\right)=\frac{2}{R\rho_l}\tau_w-(\bar{\varepsilon}_G-\varepsilon_G)g \qquad [4.4]$$

Equation 4.4 can be solved by applying the following simplifying assumptions: (a) υ_t is constant throughout the turbulent core region of the column, and (b) the profile of the gas holdup is approximated by Equation 4.5:

$$\frac{\varepsilon_G}{\bar{\varepsilon}_G} = \left[\frac{(n+2)}{n}\right]\left(1-\phi^n\right) \qquad [4.5]$$

Boundary conditions:

$$\frac{du}{dr} = 0 \text{ at } r = 0$$

Ueyama & Miyauchi (1979) used the universal velocity profile to model the laminar sublayer at the wall, assuming that both the laminar sublayer and the buffer layer consist of only liquid. The liquid velocity at the wall was found to be equal to:

$$u_W = 11.63\sqrt{|\tau_w|/\rho_L} \text{ at } r = R$$

The solution that satisfies the above boundary conditions is given by:

$$u + |u_w| = \frac{R^2}{\upsilon_t}\left[\left(\frac{\tau_w}{2R\rho_l} + \frac{\bar{\varepsilon}_G g}{2n}\right)\left(1-\phi^2\right) - \frac{\bar{\varepsilon}_G g}{n(n+2)}\left(1-\phi^{n+2}\right)\right] \qquad [4.6]$$

Let

$$N = \frac{R^2}{\upsilon_t} \times \frac{\bar{\varepsilon}_G g}{n(n+2)} \qquad [4.7]$$

and

$$P = \frac{R^2}{\upsilon_t}\left(\frac{\tau_W}{2R\rho_L} + \frac{\bar{\varepsilon}_G g}{2n}\right) \qquad [4.8]$$

From the boundary condition at $r = R$, the shear stress at the wall is given by:

$$\tau_W = -\rho_L \left(\frac{|u_W|}{11.63} \right)^2 \quad [4.9]$$

Substituting Equation 4.9 into Equation 4.8 yields:

$$P = \frac{R^2}{\upsilon_t} \left(\frac{-|u_W|^2}{11.63^2 2R} + \frac{\bar{\varepsilon}_G g}{2n} \right) \quad [4.10]$$

Substituting Equations 4.7 and 4.8 into Equation 4.6 gives:

$$u + |u_W| = P\left(1 - \phi^2\right) - N\left(1 - \phi^{n+2}\right) \quad [4.11]$$

From Equation 4.5, let

$$M = \bar{\varepsilon}_G \left(\frac{n+2}{n} \right) \quad [4.12]$$

Equation 4.5 then becomes:

$$\varepsilon_G = M\left(1 - \phi^n\right) \quad [4.13]$$

However, there are four unknowns in Equation 4.6, namely: an interstitial liquid velocity, the liquid velocity at the wall, the shear stress at the wall and the turbulent kinematic viscosity. These unknowns can be estimated by substituting Equation 4.6 or Equation 4.11 and Equation 4.9 into a liquid mass balance expression inside the column, as given by:

$$\int_0^R \rho_L 2\pi r u \left(1 - \varepsilon_G\right) dr = 0 \quad [4.14]$$

Equation 4.14 implies that the sum of the liquid mass flowrates in the circulation patterns is equal to zero for a semi-batch column.

In Equation 4.14, by substituting $r = R\phi$, one obtains:

$$\int_0^1 2\pi\phi R^2 u(1-\varepsilon_G)d\phi = 0 \qquad [4.15]$$

Substituting Equations 4.11 and 4.13 into Equation 4.15 gives:

$$\int_0^1 2\pi\phi R^2 \left[-|u_w| + P(1-\phi^2) - N(1-\phi^{n+2})\right]\left[1 - M(1-\phi^n)\right]d\phi = 0 \qquad [4.16]$$

Integrating Equation 4.16 yields:

$$\left[-2\pi R^2 \frac{\phi^2}{2}|u_W| + 2\pi R^2 P\left(\frac{\phi^2}{2} - \frac{\phi^4}{4}\right) - 2\pi R^2 N\left(\frac{\phi^2}{2} - \frac{\phi^{n+4}}{n+4}\right) + 2\pi R^2 |u_W| M\left(\frac{\phi^2}{2} - \frac{\phi^{n+2}}{n+2}\right)\right.$$

$$\left. - 2\pi R^2 PM\left(\frac{\phi^2}{2} - \frac{\phi^4}{4} - \frac{\phi^{n+2}}{n+2} + \frac{\phi^{n+4}}{n+4}\right) + 2\pi R^2 NM\left(\frac{\phi^2}{2} - \frac{\phi^{n+2}}{n+2} - \frac{\phi^{n+4}}{n+4} + \frac{\phi^{2n+4}}{2n+4}\right)\right]_0^1 = 0$$

[4.17]

Simplifying Equation 4.17 yields:

$$-\pi R^2|u_W| + \frac{1}{2}\pi R^2 P - 2\pi R^2 N\left(\frac{1}{2} - \frac{1}{n+4}\right) + 2\pi R^2|u_W|M\left(\frac{1}{2} - \frac{1}{n+2}\right) - 2\pi R^2 PM\left(\frac{1}{4} - \frac{1}{n+2} + \frac{1}{n+4}\right)$$
$$+ 2\pi R^2 NM\left(\frac{1}{2} - \frac{1}{n+2} - \frac{1}{n+4} + \frac{1}{2n+4}\right) = 0 \qquad [4.18]$$

Substituting Equation 4.10 into Equation 4.18 gives:

$$-\pi R^2|u_W| + \frac{1}{2}\pi\frac{R^4}{\upsilon_t}\left(\frac{-|u_W|^2}{11.63^2 2R} + \frac{\bar{\varepsilon}_G g}{2n}\right) - 2\pi R^2 N\left(\frac{1}{2} - \frac{1}{n+4}\right) + 2\pi R^2|u_W|M\left(\frac{1}{2} - \frac{1}{n+2}\right)$$

$$-2\pi M\frac{R^4}{\upsilon_t}\left(\frac{-|u_W|^2}{11.63^2 2R} + \frac{\bar{\varepsilon}_G g}{2n}\right)\left(\frac{1}{4} - \frac{1}{n+2} + \frac{1}{n+4}\right)$$

$$+ 2\pi R^2 NM\left(\frac{1}{2} - \frac{1}{n+2} - \frac{1}{n+4} + \frac{1}{2n+4}\right) = 0 \qquad [4.19]$$

Simplifying Equation 4.19 gives:

$$-\frac{1}{4}\pi\frac{R^3}{\upsilon_t}\frac{|u_W|^2}{11.63^2}+\frac{\pi R^3 M|u_W|^2}{\upsilon_t 11.63^2}\left(\frac{1}{4}-\frac{1}{n+2}+\frac{1}{n+4}\right)-\pi R^2|u_W|+2\pi R^2|u_W|M\left(\frac{1}{2}-\frac{1}{n+2}\right)$$

$$+\frac{1}{4}\pi\frac{R^4}{\upsilon_t}\frac{\bar{\varepsilon}_G g}{n}-2\pi R^2 N\left(\frac{1}{2}-\frac{1}{n+4}\right)-\frac{\pi R^4 M\bar{\varepsilon}_G}{\upsilon_t n}\left(\frac{1}{4}-\frac{1}{n+2}+\frac{1}{n+4}\right)$$

$$+2\pi R^2 NM\left(\frac{1}{2}-\frac{1}{n+2}-\frac{1}{n+4}+\frac{1}{2n+4}\right)=0 \qquad [4.20]$$

u_W can be calculated by solving the quadratic formula provided that the values of v_t, R, n, g and $\bar{\varepsilon}_G$ are known. u will therefore be calculated for any radial position. The correlations to calculate exponential factor, n, are not generally available. However, in the churn turbulent flow regime, the exponential levels off to a value of approximately 2 as the superfial gas velocity increases (Shaikh & Al-Dahhan, 2005).

4.3.2 Model for turbulent viscosity and dispersion coefficients

In this section, a mechanistic model for estimating the kinematic turbulent viscosity and dispersion coefficient was developed. A similar approach to that of Ueyama & Miyauchi (1979) was used in developing the model. The major difference is that, whereas Ueyama & Michauchi (1979) determined the turbulent viscosities by fitting their model to liquid velocities, this work describes a way of estimating kinematic turbulent viscosity using a mechanistic model for the momentum exchange in bubble columns.

The turbulent viscosity is a function of the liquid flow patterns that cause momentum exchange between circulation cells. For ordinary molecular viscosity, the mechanism of momentum exchange is the random movement of molecules between different layers of flow which exchange momentum. In the case of turbulent flow on a larger scale, liquid eddies exchange momentum in a similar way to that of the molecules in viscous flow. In a bubble column, it is assumed that the circulation cells cause exchange of momentum.

Analogous to the kinetic gas theory for molecular viscosity or to the Prandtl mixing length theory for turbulent flow, the turbulent viscosity is defined as the product of the mass flux

across the surface of a differential control volume and a penetration depth which is the distance that liquid in a circulation cell has to travel before it acquires the same momentum as that of the liquid in its new environment.

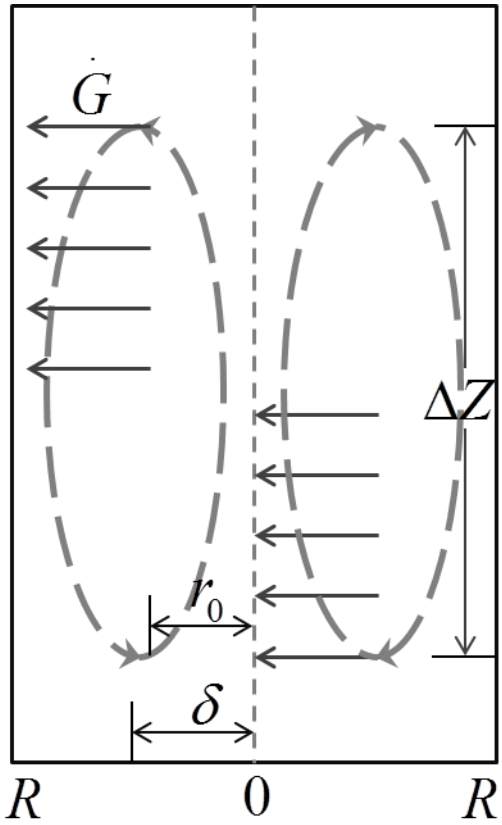

Figure 4.11: Schematic diagram depicting the momentum exchange between circulation cells

Figure 4.11 shows the mechanism of momentum exchange in bubble columns. In order to estimate the turbulent viscosity, the mass flux, $\dot{G}$, across the curved surface where the liquid velocity is zero is used. The turbulent viscosity is the product of this mass flux and the distance that has to be travelled by a lump of fluid for it to change momentum, δ, as given by:

$$\mu_t = \delta \dot{G} \qquad [4.21]$$

The kinematic turbulent viscosity will therefore be calculated from:

$$\upsilon_t = \frac{\delta m_{upwards}}{2\pi r_0 \Delta Z \rho_L} \qquad [4.22]$$

where $m_{upwards}$ is the liquid mass flowrate in the upward direction in the circulation cell, r_0 is the radius of the column in which the liquid velocity is zero and ΔZ is the height of the circulation cell. The curved surface at r_0 is used to calculate $\dot{G}$ since the liquid flowing upwards with the flowrate $m_{upwards}$ has to cross this curved surface area before flowing down. Joshi & Sharma (1979) used an energy balance technique to show that the energy of a recirculation cell is at a minimum when the height of the cell is equal to the diameter of the column. However in this work, after comparing the model to data published in the literature when assuming that the exponential factor n equals 2, the height of the circulation cells was found to be approximately equal to 1.4 times the column diameter. The penetration depth is expected to be dependent on the column radius because the column wall confines the movement of the liquid and, therefore, the liquid is forced to change its momentum. The circulation cells are often symmetrical about the column centre; therefore, it was assumed that the penetration depth is approximately equal to half of the column radius.

The upwards mass flowrate is calculated from:

$$m_{upwards} = \int_0^{r_0} 2\pi r \rho_L u(1-\varepsilon_G) dr \qquad [4.23]$$

Substituting $r_0 = R\phi_0$ yields:

$$m_{upwards} = \int_0^{\phi_0} 2\pi\phi\rho_L R^2 u(1-\varepsilon_G) d\phi \qquad [4.24]$$

Substituting Equation 4.11 into Equation 4.24 and integrating gives:

$$m_{upwards} = \rho_L \left[-2\pi R^2 \frac{\phi^2}{2} |u_W| + 2\pi R^2 P\left(\frac{\phi^2}{2} - \frac{\phi^4}{4}\right) - 2\pi R^2 N\left(\frac{\phi^2}{2} - \frac{\phi^{n+4}}{n+4}\right) + 2\pi R^2 |u_W| M\left(\frac{\phi^2}{2} - \frac{\phi^{n+2}}{n+2}\right) \right.$$
$$\left. - 2\pi R^2 PM\left(\frac{\phi^2}{2} - \frac{\phi^4}{4} - \frac{\phi^{n+2}}{n+2} + \frac{\phi^{n+4}}{n+4}\right) + 2\pi R^2 NM\left(\frac{\phi^2}{2} - \frac{\phi^{n+2}}{n+2} - \frac{\phi^{n+4}}{n+4} + \frac{\phi^{2n+4}}{2n+4}\right) \right]_0^{\phi_0} \qquad [4.25]$$

Simplifying Equation 4.25 yields:

$$m_{upwards} = -\pi R^2 \rho_L \phi_0^2 |u_W| + 2\pi R^2 \rho_L P\left(\frac{\phi_0^2}{2} - \frac{\phi_0^4}{4}\right) - 2\pi R^2 \rho_L N\left(\frac{\phi_0^2}{2} - \frac{\phi_0^{n+2}}{n+4}\right) + 2\pi R^2 \rho_L |u_W| M\left(\frac{\phi_0^2}{2} - \frac{\phi_0^{n+2}}{n+2}\right)$$
$$- 2\pi R^2 \rho_L PM\left(\frac{\phi_0^2}{2} - \frac{\phi_0^4}{4} - \frac{\phi_0^{n+2}}{n+2} + \frac{\phi_0^{n+4}}{n+4}\right) + 2\pi R^2 \rho_L NM\left(\frac{\phi_0^2}{2} - \frac{\phi_0^{n+2}}{n+2} - \frac{\phi_0^{n+4}}{n+4} + \frac{\phi_0^{2n+4}}{2n+4}\right) = 0$$

[4.26]

$m_{upwards}$ is dependent on v_t and therefore v_t is firstly guessed in Equation 4.26 and then recalculated using Equation 4.22 until both the guessed value and the calculated value are the same. This was done using a Microsoft spreadsheet.

To calculate the value of ϕ_0, Equation 4.11 becomes:

$$0 + |u_W| = P\left(1 - \phi_0^2\right) - N\left(1 - \phi_0^{n+2}\right) \quad [4.27]$$

For $n = 2$ as used by Ueyama & Miyauchi (1979), let $\phi_0^2 = B$

$$-|u_W| + P(1 - B) - N\left(1 - B^2\right) = 0 \quad [4.28]$$

$$NB^2 - PB + P - N - |u_W| = 0 \quad [4.29]$$

B can be calculated by solving the quadratic formula.

The axial dispersion coefficient can be defined by Fick's law of diffusion:

$$\dot{N}_B = -E_Z A \frac{dC_B}{dZ} \quad [4.30]$$

where $\dot{N}_B$ is the molar flow of substance B, E_Z is the axial dispersion coefficient and C_B is the concentration of substance *B*. The molar flux can also be obtained from a molar balance in the upwards direction:

$$\dot{N}_B = \frac{m_{upwards}}{\rho_L}\left(C_{B2} - C_{B1}\right) \quad [4.31]$$

In differential form, Equation 4.31 is equivalent to Equation 4.32:

$$\dot{N}_B = \frac{m_{upwards}}{\rho_L}\left(-\frac{dC_B}{dZ}\Delta Z\right) \quad [4.32]$$

As the height of a circulation cell is equal 1.4 times the column diameter, Equation 4.32 is simplified to:

$$\dot{N}_B = -\frac{m_{upwards}}{\rho_L}1.4D_C\frac{dC_B}{dZ} \quad [4.33]$$

Comparing Equation 4.30 with Equation 4.33, the axial dispersion coefficient is given by:

$$E_Z = \frac{1.4D_C m_{upwards}}{\rho_L A} \quad [4.34]$$

Similarly, the radial dispersion coefficient can be estimated from Equation 4.35:

$$E_r = \frac{m_{upwards}}{2\pi r_o D_C \rho_L} \times \delta \quad [4.35]$$

4.3.3 Model verification

Figure 4.12 shows a comparison between the estimated kinematic turbulent viscosity and the experimental kinematic turbulent viscosity from the literature. The experimental kinematic viscosities were measured at different column diameters from 10 to 25 cm. The predicted kinematic turbulent viscosity is comparable to the experimental values from the literature. The percentage error when comparing the estimated kinematic turbulent viscosity with the literature values is as follows: the error was in the range of 35.4–52.6% when comparing the estimated values with those of Miyauchi & Shyu (1970); 0.9–29% for those of Hills (1974); 18.4% for those of Yashitome (1967); 2.2–33% for those of Pavlov (1965) and 35.2% for those of Yamagoshi (1969).

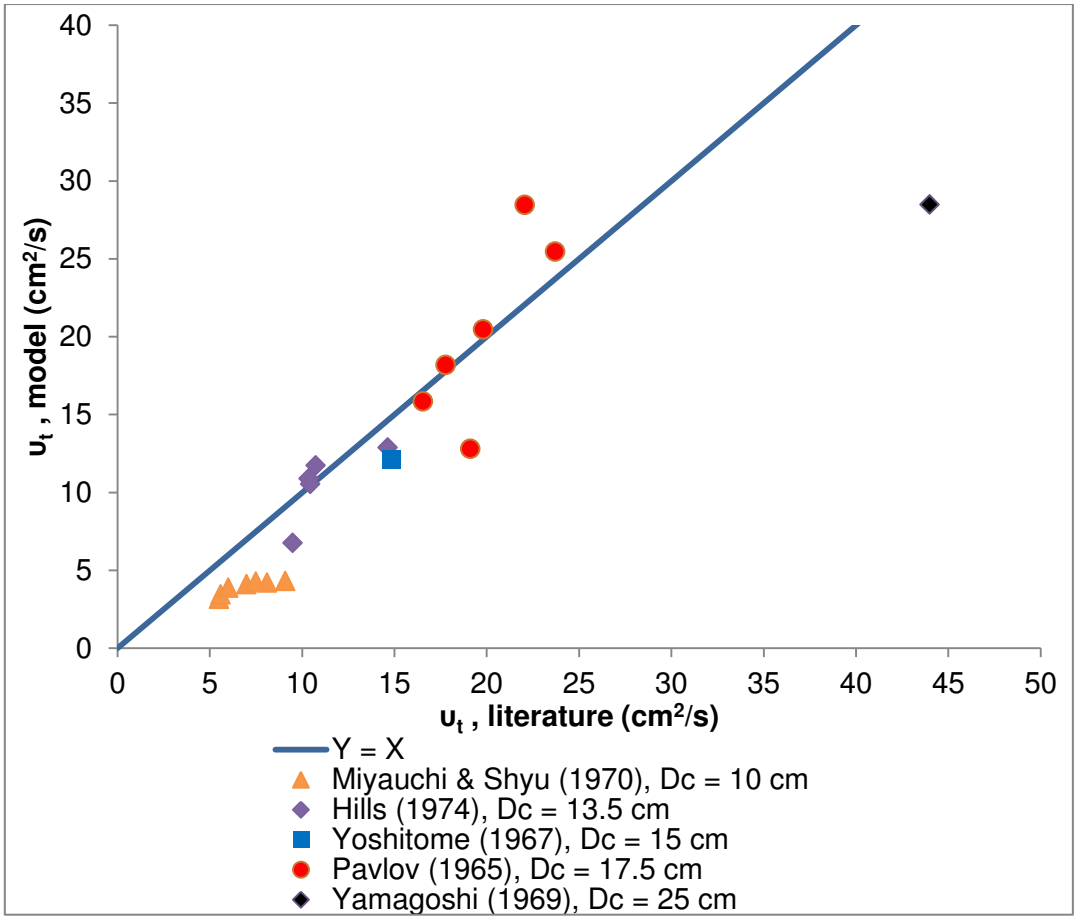

Figure 4.12: Comparison of predicted and experimental kinematic turbulent viscosity

Figure 4.13 shows the axial dispersion values estimated by the model. It was found that at a fixed average gas holdup, the axial dispersion coefficient is directly proportional to a column diameter to the power 1.5.

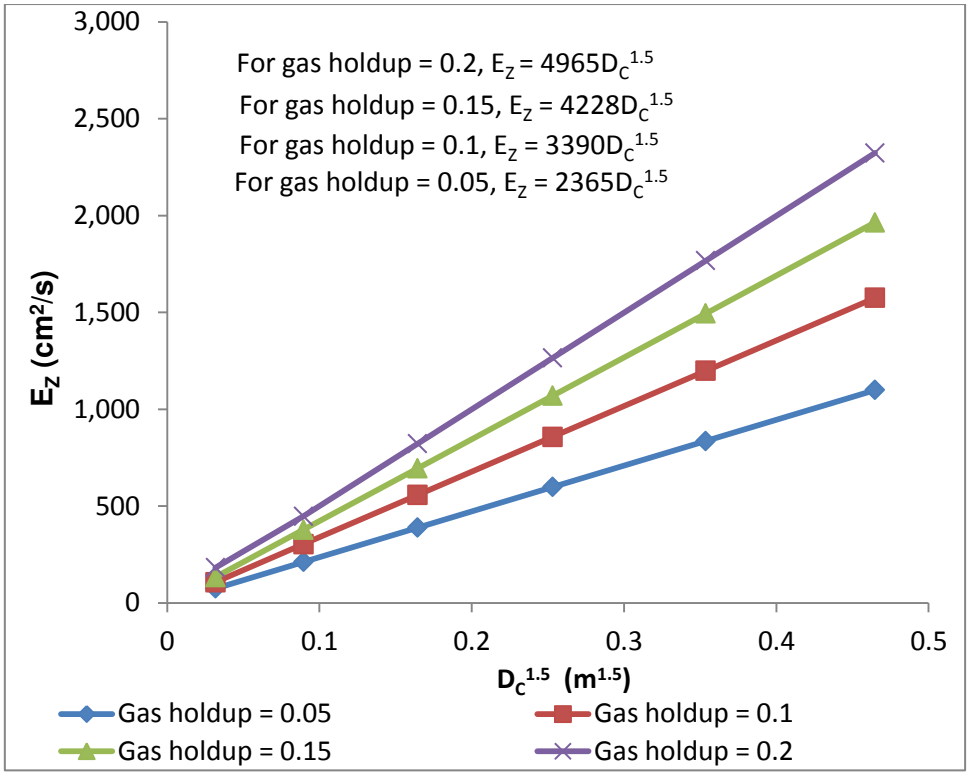

Figure 4.13: Variation of axial dispersion coefficient with the column diameter

Figure 4.14 shows the calculated axial dispersion coefficients as function of the specific energy dissipation rate and column diameter using the same form of correlation as Baird & Rice (1975). The model fits the experimental data reasonably when the height of the circulation cell is slightly greater than the column diameter. The estimated results are correlated with the dash line correlation. The height of the circulation cell was assumed to be 1.4 times the column diameter. The axial dispersion coefficient was modelled for column diameters from 10 to 60 cm and superficial gas velocities of 3 to 12 cm/s (detailed information on the data used for the model can be found in Appendix 3). It was found that the axial dispersion coefficients are within the range of those reported in the literature as given by Baird & Rice (1975) which shows data up to 3500 cm^2/s.

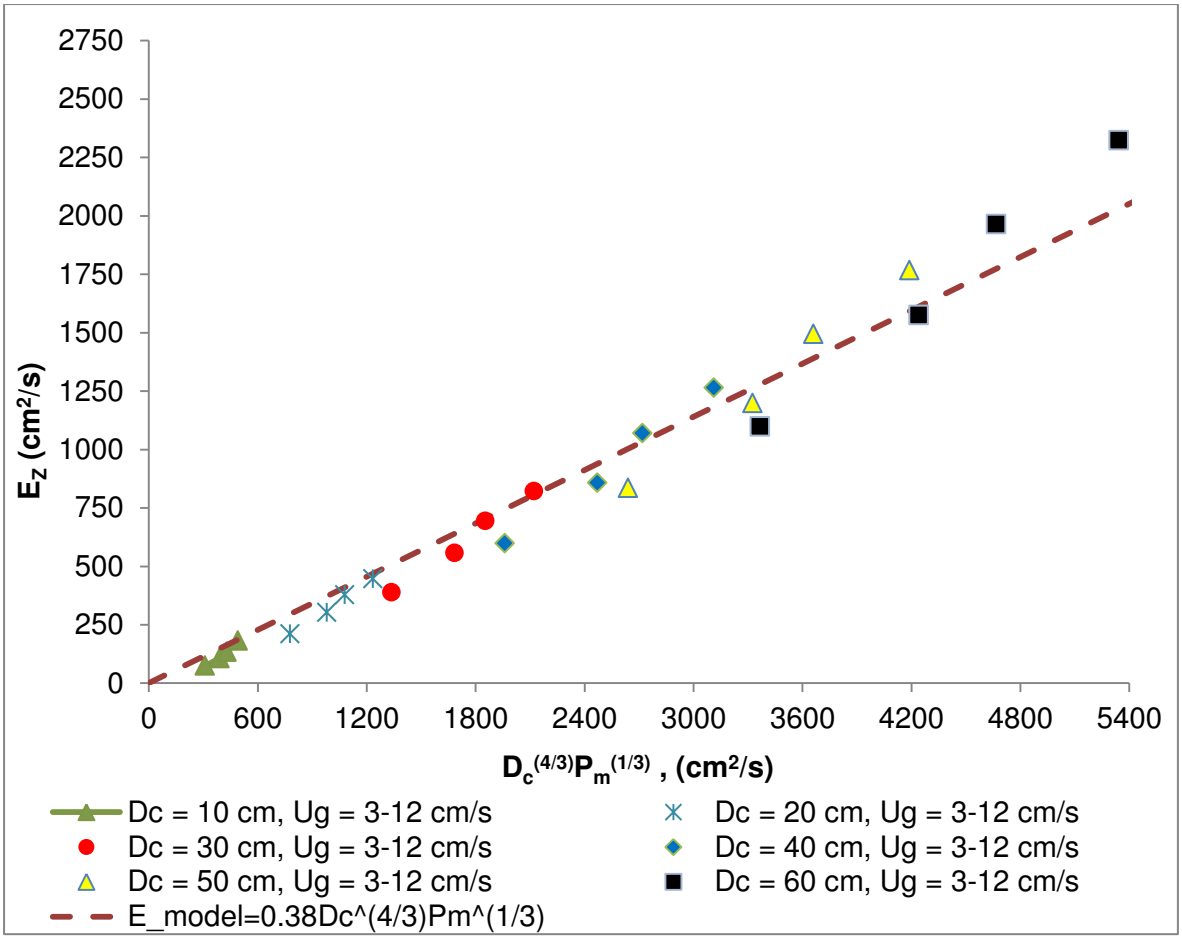

Figure 4.14: Predicted axial dispersion coefficient

Figure 4.15 shows the linearized correlation for the axial dispersion coefficient with experimental data as reported by Baird & Rice (1975). The linearized correlation is similar to the correlation of Baird & Rice (the solid line) but has a slightly higher slope. This figure was prepared in order to compare the estimated axial dispersion coefficients derived from Figure 4.14 (the dashed lined) with the reported experimental data which unfortunately did not include any information on gas holdup. It can be seen that the estimated results fit the experimental data reasonably well compare to the solid line correlation which slightly under predict the experimental data. The axial dispersion coefficient was measured for column diameters of 10 to 107 cm and superficial gas velocities in the range of 2.3 to 45 cm/s. The correlated axial dispersion coefficient ranges from 40 to 3500 cm^2/s. Baird & Rice (1975) reported up to higher values because of higher superficial gas velocities and column diameters.

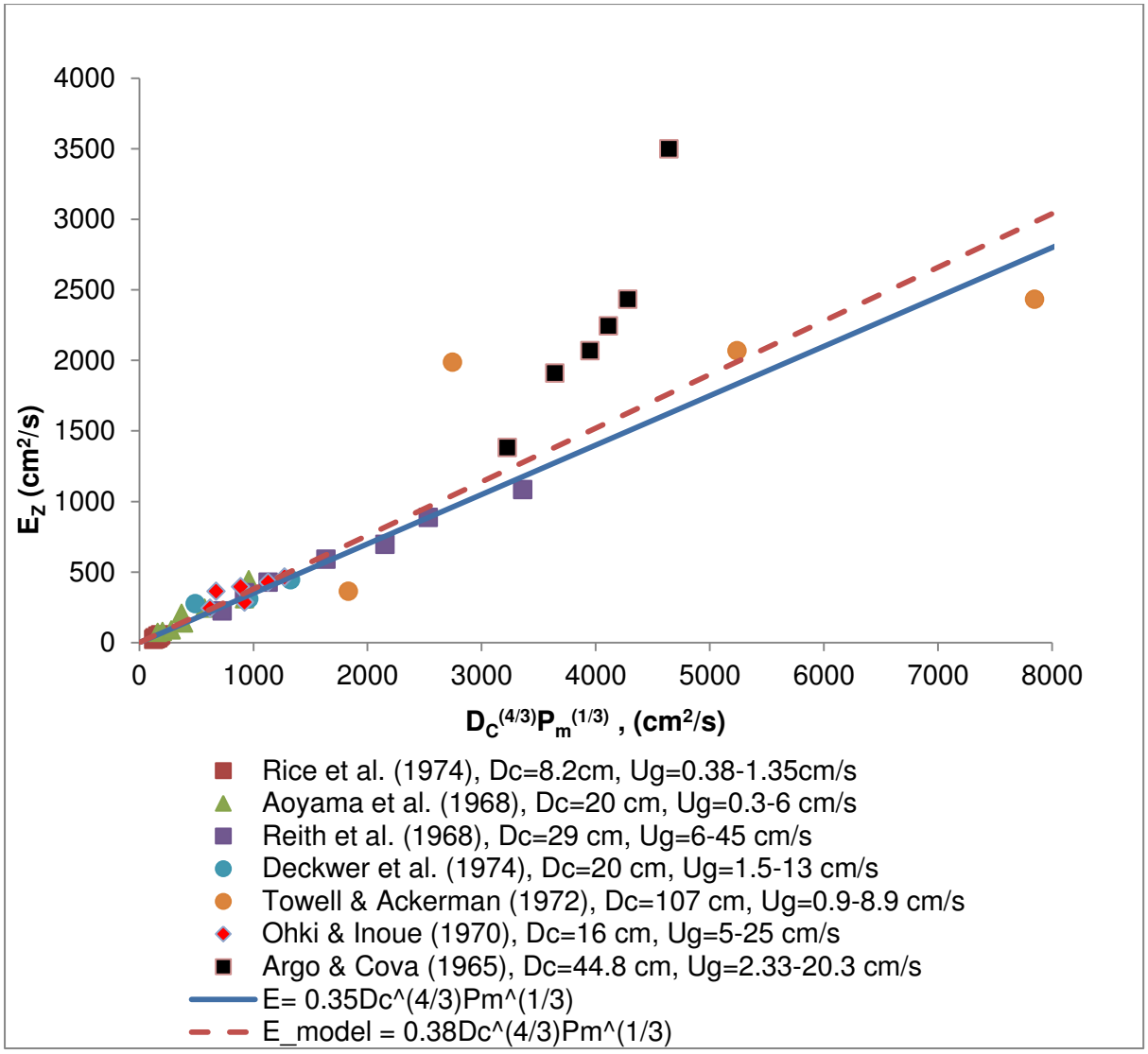

Figure 4.15: Experimental axial dispersion coefficients from the literature (Baird & Rice, 1975)

Table 4.3 compares the ratios of the axial to radial dispersion coefficient obtained from the model with those reported in the literature. The ratios obtained are in the range of 23.6 to 24.7 and are of the same order of magnitude than the values reported in the literature.

Table 4.3: Ratios of axial to radial dispersion coefficient

Model $0.03 \leq u_G \leq 0.12\,m$	**Deckwer (1992)**	**Abdulrazzaq (2010)**	**Camacho Rubio et al (2004)**
23.6–24.7	10	50–100	100

CHAPTER 5: CONCLUSIONS AND RECOMENDATIONS

An experimental method and setup for measuring the heat transfer coefficient for a molten salt bubble column were developed and tested. The system worked with water and heat transfer oil, and the results obtained are comparable with those in the literature. The system was also tested with molten salt but failed at the welds, resulting in severe corrosion. It is believed that the setup can work for molten salts, provided that the problems of mechanical failure are solved.

The heat transfer coefficient increases with superficial gas velocity as a result of an increase in the number of bubbles and lowering of the surface film thickness by turbulence. The heat transfer coefficients for the argon–heat transfer oil system are lower than those obtained for the argon–water system due to heat transfer oil having a higher viscosity and higher thermal conductivity than those of water. The heat transfer coefficient increases with an increase in temperature due to a decrease in the liquid viscosity.

Gas holdup increased with superficial gas velocity. The experimental gas holdup values were in good agreement with the literature. The gas holdup for heat transfer oil was higher than that for the argon–water system.

Mechanistic models were developed for estimating kinematic turbulent viscosity and dispersion coefficients. The predicted kinematic turbulent viscosities agreed with the experimental values in most of the literature. It was found that the estimated axial dispersion coefficients are within the range of those reported in the literature. The model estimated the ratios of axial to radial dispersion coefficients within the values reported in the literature

The following recommendations should be taken into consideration when measuring the wall heat transfer coefficient in bubble columns.

- The temperature difference should be high enough for it to be measured accurately.
- Column wall temperatures can be measured accurately by soldering the thermocouples to the column wall. Any air gap between a thermocouple and the column wall should be avoided.
- Liquid temperature can be measured accurately by inserting thermocouples from the lid of the column since when using a thermowell installed through the column wall, it could be difficult to measure the liquid temperature closer to the inner wall temperature.

- The radial positioning of the thermocouple used to measure the liquid temperature can affect the determination of the heat transfer coefficient by about 20%.
- A material with a high thermal conductivity must be used for the construction of a bubble column when the column is used to measure wall heat transfer coefficients in order to measure the inner wall temperature accurately.
- When working with molten salt, the welding on a pipe should be minimised as much as possible due to the fact that molten salt is very aggressive to the welding on a metal such as copper.

REFERENCES

Abdullah, AN (2007) Characteristic of bubbles and gas holdup in a two-phase column for different liquid phases. *Engineering & Technology*, 25(2), 282–290.

Abdulrazzaq, BS (2010) Investigation measurement of dispersion coefficient and mixing times in bubble column. *Diyala Journal of Engineering Sciences*, 3(2), 97–112.

Al-Hemiri, AA and Ahmedzeki, NS (2008) Prediction of the heat transfer coefficient in a bubble column using an artificial neural network. *International Journal of Chemical Reactor Engineering*, 6, 1–18.

Bahner, MA (2013) A practical overview of level measurement technologies. Available at: *http://www.gilsoneng.com/reference/Levelpap.pdf* [accessed on 14 April 2013].

Baird, MHI and Rice, RG (1975) Axial dispersion in large unbaffle columns. *The Chemical Engineering Journal*, 9, 171–174.

Bukur, DB, Petrovic, D and Daly, JG (1987) Flow regime transitions in a bubble column with a paraffin wax as the liquid medium. *Industrial and Engineering Chemical Research*, 26(6), 1087–1092.

Camacho Rubio, F, Sánchez Mirón, A, Cerón García, MC, García Camacho, F, Molina Grima, E and Chisti, Y (2004) Mixing in bubble columns: a new approach for characterizing dispersion coefficients *Chemical Engineering Science*, 59, 4369–4376.

Cartland Glover, GM, Generalis, SC and Thomas, NH (2000) CFD and bubble column reactors: Simulation and experiment. *Chemical Papers*, 54(6a), 361–369.

Cengel, YA (2003) Heat transfer, 2nd ed. New York: McGraw–Hill, pp 17–26, 755–756.

Chen, W, Hasegawa, T, Tsutsumi, A, Otawara, K and Shigaki, Y (2003) Generalized dynamic modelling of local heat transfer in bubble columns. *Chemical Engineering Journal,* 96, 37–44.

Cho, YJ, Woo, KJ, Kang, Y and Kim, SD (2002) Dynamic characteristics of heat transfer coefficient in pressurized bubble columns with viscous liquid medium. *Chemical Engineering and Processing*, 41, 699–706.

Cho, YJ, Yang, HC, Eun, HC, Yoo, JH and Kim, JH (2005) Hydrodynamic and gas phase axial dispersion in an air-molten salt two-phase system (molten salt oxidation reactor). *Chemical Engineering and Processing*, 44, 1054–1062.

Christi, MY and Moo-Young, M (1988) Gas hold-up in pneumatic reactors. *The Chemical Engineering Journal*, 38, 149–152.

Daous, M and Al-Zahrani, A (2006) A simple approach to measuring the gas phase heat and mass transfer coefficients in a bubble column. *Chemical Engineering Technology*, 29(12), 1438–1443.

Deckwer, WD (1992) Bubble column reactors. Wiley, Chichester, 113–156.

Deckwer, WD (1980a) On mechanism of heat transfer in bubble column reactors. *Chemical Engineering Science*, 35(6), 1341 – 1346.

Deckwer, WD, Loulsl, Y, Zaldl, A and Ralek, M (1980b) Hydrodynamic properties of the Fischer–Tropsch slurry process. *Industrial and Engineering Chemistry Process Design and Development*, 19, 699–708.

Degaleesan, S and Dudukovik, MP (1998) Liquid backmixing in bubble columns and the axial dispersion coefficient. *AIChE Journal*, 44(11), 2369–2378.

Degaleesan, S, Dudukovic, M and Pan, Y (2001) Experimental study of gas-induced liquid-flow structures in bubble columns. *AIChE Journal*, 47(9), 1913–1931.

Delnoij, E, Kuipers, JAM and Van Swaaij, WPM (1997) Computational fluid dynamics applied to gas–liquid contactors. *Chemical Engineering Science*, 52(21.22), 3623–3638.

Dhanasekaran, S and Karunanithiy, T (2010) Axial mixing in a novel perforated plate bubble column. *International Journal of Chemical Reactor Engineering*, 8(A118), 1–22.

Dhotre, MT, Ekambara, K and Joshi, JB (2004) CFD simulation of sparger design and height to diameter ratio on gas holdup profiles in bubble column reactors. *Experimental Thermal and Fluid Science*, 28, 407–421.

Dhotre, MT, Vitankar, VS and Joshi, JB (2005) CFD simulation of steady state heat transfer in bubble columns. *Chemical Engineering Journal*, 108, 117–125.

Fadavi, A and Chisti, Y (2007) Gas holdup and mixing characteristics of a novel forced circulation loop reactor. *Chemical Engineering Journal*, 131, 105–111.

Fair, JR, Lambright, AJ and Andersen, JW (1962) Heat transfer and gas holdup in sparged contactors. *I & EC Process Design and Development*, 1, 33–36.

Fazeli, A, Fatemi, S, Ganji, E and Khakdaman, HR (2008) A statistical approach of heat transfer coefficient analysis in the slurry bubble column. *Chemical Engineering Research and Design*, 86, 508–516.

Fransolet, E, Crine, M, L'Homme, G, Toye, D and Marchot, P (2001) Analysis of electrical resistance tomography measurements obtained on a bubble column. *Measurement Science and Technology*, 12, 1055–1060.

Gandhi, AB and Joshi, JB (2010) Estimation of heat transfer coefficient in bubble column reactors using support vector regression. *Chemical Engineering Journal*, 160, 302–310.

Gandhi, B, Prakash, A and Bergougnou, MA (1999) Hydrodynamic behaviour of slurry bubble column at high solids concentrations. *Powder Technology*, 103, 80–94.

Ghosh, UK and Upadhyay, SN (2007) Gas holdup and solid–liquid mass transfer in Newtonian and non–Newtonian fluids in bubble columns. *Canadian Journal of Chemical Engineering*, 85, 825–835.

Groen, JS, Oldeman, RGC, Mudde, RF and Van den Akker, HEA (1996) Coherent structures and axial dispersion in bubble column reactors. *Chemical Engineering Science*, 51(10), 2511–2520.

Grubbs, FE (1969) Procedures for detecting outlying observations in samples. *Technometrics* 11(1), 1–21.

Gupta, P, Ong, B, Al-Dahhan, MH, Dudukovic, MP and Toseland, BA (2001) Hydrodynamics of churn turbulent bubble columns: Gas–liquid recirculation and mechanistic modelling. *Catalysis Today*, 64, 253–269.

Hart, WF (1976) Heat transfer in bubble-agitated systems. A general correlation. *Industrial and Engineering Chemical Process Design and Development*, 15(1), 109–114.

Hikita, H, Asai, S, Kikukawa, H, Zaike, T and Ohue, M (1981) Heat transfer coefficient in bubble columns. *Industrial and Engineering Chemical Process Design and Development,* 20(3), 540–545.

Hills, JH (1974) Radial non-uniformity of velocity and voidage in a bubble column. *Transactions of the Institution of Chemical Engineers*, 52, 1.

Hulet, C, Clementy, P, Tochonz, P, Schweich, D, Dromardy, N and Anfrayzz, J (2009) Literature review on heat transfer in two- and three-phase bubble columns. *International Journal of Chemical Reactor Engineering*, 7, 1–94.

Janz, GJ (1988) Thermodynamic and transport properties for molten salts: Correlation equations for critically evaluated density, surface tension, electrical conductance and viscosity data. *Journal of Physical and Chemical Reference Data*, 17(2), 44.

Jawad, AH, Ibrahim, RI and Abdulrahman, AA (2009) CFD modelling and gas holdup measurement in three-phase slurry bubble column. *Journal of Engineering and Technology*, 27(16), 3012–3022.

Jhawar, AK and Prakash, A (2007) Analysis of local heat transfer and hydrodynamics in a bubble column using fast response probes. *Chemical Engineering Science*, 62, 7274–7281.

Joshi, JB and Sharma, MM (1979) A circulation cell model for bubble columns. *Transactions of the Institution of Chemical Engineers*, 57, 244–251.

Joshi, JB, Sharma, MM, Shah YT, Singh CPP, Moonis, A and Klinzing GE (1980) Heat transfer in multiphase contactors. *Chemical Engineering Communications*, 6, 257–271.

Joshi, JB, Vitankar, VS, Kulkarni, AA, Dhotre, MT and Ekambara, K (2002) Coherent flow structures in bubble column reactors (Review papers). *Chemical Engineering Science*, 57, 3157–3183.

Kantarci, N, Borak, F and Ulgen, KO (2005a) Bubble column reactors (Review). *Process Biochemistry*, 40, 2263–2283.

Kantarci, N, Ulgen, KO and Borak, F (2005b) A study on hydrodynamics and heat transfer in a bubble column reactor with yeast and bacterial cell suspensions. *Canadian Journal of Chemical Engineering*, 83, 764–773.

Kast, W (1963) Investigations into heat transfer in bubble columns. (Untersuchungen zum Wärmeübergang in Blasensäulen, in German). *Chemie Ingenieur Technik*, 35.11, 785–788.

Kim, SJ, Cho, YJ, Lee, CG, Kang, Y and Kim, SD (2002) Diagnosis of bubble distribution in a three-phase bubble column reactor for dehydration of ortho-boric acid. *Korean Journal of Chemical Engineering*, 19(1), 175–182.

Krishna, R, Wilkinson, PM and Van Dierendonck, LL (1991) A model for gas holdup in bubble columns incorporating the influence of gas density on flow regime transitions. *Chemical Engineering Science*, 46(10), 2491–2496.

Kulkarni, A V (2010) Design of a pipe/ring type of sparger for a bubble column reactor. *Chemical Engineering Technology,* 33(6), 1015–1022.

Kumar, SB, Moslemian, D and Dudukovic, MP (1997) Gas holdup measurements in bubble columns using computed tomography. *AIChE Journal*, 43(6), 1414–1425.

Lakota, A, Jazbec, M and Levec, J (2001) Impact of structured packing on bubble column mass transfer characteristics. Part 1. Back mixing in the liquid phase. *Acta Chimica Slovaka*, 48, 453–468.

Li, H and Prakash, A (2002) Analysis of flow patterns in bubble and slurry bubble columns based on local heat transfer measurements. *Chemical Engineering Journal*, 86, 269–276.

Li, H and Prakash, A (2001) Survey of heat transfer mechanisms in a slurry bubble column. *Canadian Journal of Chemical Engineering*, 79, 717–725.

Li, H and Prakash, A (2000) Influence of slurry concentrations on bubble population and their rise velocities in a three-phase slurry bubble column. *Powder Technology*, 113, 158–167.

Li, H and Prakash, A (1997) Heat transfer and hydrodynamics in a three–phase slurry bubble column. *Industrial and Engineering Chemical Process Design and Development*, 36, 4688–4694.

Malayeri, MR, Muller-Steinhagen, H and Smith, JM (2003) Neural network analysis of void fraction in air/water two-phase flows at elevated temperatures. *Chemical Engineering and Processing*, 42, 587–597.

Mandal, A, Kundu, G and Mukherjee, D (2003) Gas holdup and entrainment characteristics in a modified downflow bubble column with Newtonian and non-Newtonian liquid. *Chemical Engineering and Processing*, 42, 777–787.

Mena, PC, Ruzicka, MC, Rocha, FA, Teixeira, JA and Drahoš, J (2005) Effect of solids on homogeneous-heterogeneous flow regime transition in bubble columns. *Chemical Engineering Science*, 60, 6013–6026.

Miyauchi, T and Shyu, CN (1970) Flow of fluid in a gas bubble column. *Kagaku Kogaku*, 34, 958.

Moshtari, B, Babakhani, EG and Moghaddas, JS (2009) Experimental study of gas hold-up and bubble behaviour in gas–liquid bubble column. *Petroleum & Coal*, 51(1), 22–28.

Mouza, AA, Dalakoglou, GK and Paras, SV (2005) Effect of liquid properties on the performance of bubble column reactors with fine pore spargers. *Chemical Engineering Science*, 60, 1465–1475.

Mudde, RF and Saito, T (2001) Hydrodynamical similarities between bubble column and bubbly pipe flow. *Journal of Fluid Mechanics*, 437, 203–228.

Nedeltchev, S and Schumpe, A (2008) A new approach for the prediction of gas holdup in bubble column operated under various pressure in homogeneous regime. *Journal of Chemical Engineering of Japan*, 41(8), 744–755.

Nikolic, LB, Nikolic, VD, Veljkovic, VB, Lazic, ML and Skala, DU (2004) Axial dispersion of the liquid phase in a three-phase Karr reciprocating plate column. *Journal of the Serbian Chemical Society*, 69(7), 581–599.

Nikolic, LB, Nikolic, VD, Veljkovic, VB and Skala, DU (2005) Gas hold-up in a three-phase reciprocating plate column. *Journal of the Serbian Chemical Society*, 70(11), 1363–1371.

Omega (2001) Transactions in measurements and control. Volume IV. Available at: http://www.omega.com/literature/transaction/Transactions_Vol IV.pdf [accessed on 14 April 2011].

Orvalho, S, Ruzicka, MC and Drahos, J (2009) Bubble column with electrolytes: Gas holdup and flow regimes. *Industrial and Engineering Chemistry Research*, 48, 8237–8243.

Pavlov, VP (1965) Tsirkulyatsiya Zhidkosti v Barbotazhnom Apparate Periodichesko deistviya" *Khim. Prom*, 9, 698.

Rampure, MR, Mahajani, SM and Ranade VV (2009) CFD simulation of bubble columns: Modeling of nonuniform gas distribution at sparger. *Industrial and Engineering Chemistry Research*, 48, 8186–8192.

Ruthiya, KC (2005) Mass transfer and hydrodynamics in catalytic slurry reactors PhD thesis, Eindhoven Netherlands: Eindhoven University of Technology.

Ruzicka, MC, Zahradnik, J, Drahos, J and Thomas, NH (2001) Homogeneous–heterogeneous regime transition in bubble columns. *Chemical Engineering Science*, 56, 4609–4626.

Sada, E, Katoh, S, Yoshil, H, Yamanishi, T and Nakanishi, A (1984) Performance of the gas bubble column in molten salt systems. *Industrial and Engineering Chemistry Process Design and Development*, 23, 151–154.

Shaikh, A and Al-Dahhan, MH (2007) A review on flow regime transition in bubble columns. *International Journal of Chemical Reactor Engineering*, 5, 1–70.

Shaikh, A and Al-Dahhan, M (2005) Characterization of the hydrodynamic flow regime in bubble columns via computed tomography. *Flow Measurement and Instrumentation*, 16, 91-98.

Shirsat, S, Mandal, A, Kundu, G and Mukherjee, D (2003) Hydrodynamic studies on gas–liquid downflow bubble column with non–Newtonian liquids. *Journal of the Institution of Engineers (India)*, 84, 38–43.

Singh, MK and Majumder, KS (2010) Theoretical study on effect of operating parameters on mass transfer in bubbly flow. *Journal of Engineering and Applied Science*, 5(2), 163–170.

Sivasubramanian, V and Naveen Prasad, BS (2009) Effects of superficial gas velocity and fluid property on the hydrodynamic performance of an airlift column with alcohol. *International Journal of Engineering, Science and Technology*, 1(1), 245–253.

Soong, Y, Harke, FW, Gamwo, IK, Schehl RR and Zarochak MF (1997) Hydrodynamic study in a slurry-bubble-column reactor. *Catalysis Today*, 35, 427–434.

Takeda, O and Okabe, TH (2006) High-speed titanium production by magnesiothermic reduction of titanium trichloride. *Materials Transactions*, 47(4), 1145–1154.

Terasaka, K, Suyama, Y, Nakagawa, K, Kato, M and Essaki, K (2006) Absorption and stripping of CO_2 with a molten salt slurry in a bubble column at high temperature. *Chemical Engineering Technology*, 29(9), 1118–1121.

Tiefeng, W, Jinfu, W and Yong, J (2007) Slurry reactors for gas-to-liquid processes: A review. *Industrial and Engineering Chemistry Research*, 46, 5824–5847.

Todt, J, Lucke, J, Schugerl, K and Kenken, A (1977) Gas holdup and longitudinal dispersion in different types of multiphase reactors and their possible application for microbial processes. *Chemical Engineering Science*, 32, 369–375.

Ueyama, K and Miyauchi, T (1979) Properties of recirculation turbulent two phase flow in gas bubble columns. *AIChE Journal*, 25(2), 258–266.

Urseanu, MI, Guit, RPM, Stankiewicz, A, Van Kranenburg, G and Lommen, JHGM (2003) Influence of operating pressure on the gas hold-up in bubble columns for high viscous media. *Chemical Engineering Science*, 58, 697–704.

Van Baten, JM, Ellenberger, J and Krishna, R (2003) Scale-up strategy for bubble column slurry reactors using CFD simulations. *Catalysis Today*, 79(80), 259–265.

Van Vuuren, DS, Oosthuizen, SJ and Heydenrych, MD (2011) Titanium production via metallothermic reduction of $TiCl_4$ in molten salt: Problems and products. *Journal of South Africa Institute of Mining and Metallurgy*, 111, 141–148.

Vandu, CO, Koop, K and Krishna, R (2004) Large bubble sizes and rise velocities in bubble column slurry reactor. *Chemical Engineering Technology*, 27(11), 1195–1199.

Vinit, PC (2007) Hydrodynamics and mass transfer in slurry bubble columns: Scale and pressure effects. PhD thesis, Eindhoven, Netherlands: Eindhoven University of Technology.

Wu, C and Al-Dahhan, M. (2012) Heat transfer coefficients in mimicked Fischer–Tropsch slurry bubble columns. *Industrial and Engineering Chemistry Research*, 51, 1543–1548

Wu, C, Al-Dahhan, MH and Prakash, A (2007) Heat transfer coefficients in a high-pressure bubble column. *Chemical Engineering Science*, 62, 140–147.

Yamagiwa, K, Kusabiraki, D and Ohkawa, A (1990) Gas holdup and gas entrainment rate in downflow bubble column with gas entrainment by a liquid jet operating at high liquid throughput. *Journal of Chemical Engineering of Japan*, 23(3), 343–348.

Yamagoshi,T (1969) BSc thesis. Japan: University of Tokyo, Department of Chemical Engineering.

Yang, GQ, Luo, X, Lau, R and Fan, LS (2000) Heat-transfer characteristics in slurry bubble columns at elevated pressures and temperature. *Industrial and Engineering Chemistry Research*, 39, 2568–2577.

Yashitome, H (1967) Dr. Eng. dissertation. Japan: Tokyo Institute of Technology.

Yifeng, S, Yifei, W, Qinghua, Z, Jian–hui, L, Guangsua, Y, Xin, G and Zunhong, Y (2008) Influence of liquid properties on flow regime and back mixing in a special bubble column. *Chemical Engineering and Processing*, 47, 2296–2302.

Zhang, K, Zhao, Y and Zhang, B (2003) Gas holdup characteristics in a tapered bubble column. *International Journal of Chemical Reactor Engineering*, 1, 1–9.

APPENDICES

Appendix 1: Experimental data for heat transfer coefficient measurements

Tables A1.1 to A1.14 show the experimental data for the heat transfer measurements.

Table A1.1: Data for the column operated with water at 40 °C and u_G = 0.006 m/s

Run	ΔT_1 (°C)	ΔT_2 (°C)	ΔT_3 (°C)	ΔT_4 (°C)	ΔT_5 (°C)	$\Delta T_{average}$ (°C)	ΔT_{loss} (°C)	Q_{loss} (W)	P_e (W)	Q_{input} (W)	h (W.m^{-2}.K^{-1})	Experimental error
1	1.88	2.46	1.76	1.71	1.73	1.77	74.73	18.95	517.52	498.57	2 119.58	4.0
2	1.93	2.63	1.98	1.93	2.08	1.98	76.63	19.43	554.42	534.99	2 020.23	
3	1.93	2.46	1.63	1.58	1.73	1.72	75.59	19.17	543.00	523.83	2 267.99	
4	2.08	2.66	1.93	1.73	1.68	1.86	84.53	21.44	551.12	529.69	2 130.96	

Table A1.2: Data for the column operated with water at 40 °C and u_G = 0.016 m/s

Run	ΔT_1 (°C)	ΔT_2 (°C)	ΔT_3 (°C)	ΔT_4 (°C)	ΔT_5 (°C)	$\Delta T_{average}$ (°C)	ΔT_{loss} (°C)	Q_{loss} (W)	P_e (W)	Q_{input} (W)	h (W.m^{-2}.K^{-1})	Experimental error
1	1.91	2.76	1.78	1.71	1.88	1.82	91.71	23.26	681.76	658.50	2 734.17	1.8
2	2.03	1.91	1.91	1.93	2.18	2.01	94.53	23.97	744.60	720.63	2 693.62	
3	1.91	2.66	1.66	1.68	1.83	1.77	86.94	22.05	684.18	662.13	2 796.84	
4	2.08	2.89	1.86	1.93	2.03	1.98	93.61	23.74	726.19	702.45	2 664.92	

Table A1.3: Data for the column operated with water at 40 °C and u_G = 0.024 m/s

Run	ΔT_1 (°C)	ΔT_2 (°C)	ΔT_3 (°C)	ΔT_4 (°C)	ΔT_5 (°C)	$\Delta T_{average}$ (°C)	ΔT_{loss} (°C)	Q_{loss} (W)	P_e (W)	Q_{input} (W)	h (W.m^{-2}.K^{-1})	Experimental error
1	1.98	3.04	1.83	1.91	2.28	2.00	104.47	26.49	800.90	774.41	2 898.91	0.5
2	2.08	3.06	1.93	2.11	2.43	2.14	111.34	28.24	843.51	815.27	2 879.54	
3	2.08	3.09	1.98	1.98	2.18	2.06	100.64	25.52	826.16	800.64	2 924.89	
4	2.08	2.99	1.93	1.93	2.13	2.02	107.43	27.24	803.17	775.92	2 904.70	

Table A1.4: Data for the column operated with water at 40 °C and u_G = 0.033 m/s

Run	ΔT_1 (°C)	ΔT_2 (°C)	ΔT_3 (°C)	ΔT_4 (°C)	ΔT_5 (°C)	$\Delta T_{average}$ (°C)	ΔT_{loss} (°C)	Q_{loss} (W)	P_e (W)	Q_{input} (W)	h (W.m^{-2}.K^{-1})	Experimental error
1	2.13	3.34	2.01	2.13	2.53	2.20	120.63	30.59	937.86	907.27	3 093.19	1.7
2	2.21	3.36	2.08	2.23	2.61	2.28	129.14	32.75	947.10	914.35	3 020.05	
3	1.98	3.01	1.88	2.03	2.23	2.03	112.77	28.60	829.34	800.74	2 969.44	
4	2.11	3.26	2.06	2.11	2.51	2.20	118.99	30.18	895.73	865.55	2 961.60	

Table A1.5: Data for the column operated with water at 40 °C and u_G = 0.040 m/s

Run	ΔT_1 (°C)	ΔT_2 (°C)	ΔT_3 (°C)	ΔT_4 (°C)	ΔT_5 (°C)	$\Delta T_{average}$ (°C)	ΔT_{loss} (°C)	Q_{loss} (W)	P_e (W)	Q_{input} (W)	h (W.m^{-2}.K^{-1})	Experimental error
1	2.36	3.84	2.33	2.48	3.04	2.55	134.65	34.15	1 084.16	1 050.01	3 090.34	2.1
2	2.28	3.61	2.28	2.41	2.86	2.46	138.45	35.11	1 047.44	1 012.33	3 100.80	
3	2.06	3.21	2.03	2.16	2.51	2.19	120.75	30.62	884.06	853.43	2 946.60	
4	2.06	3.11	2.03	2.11	2.43	2.16	125.70	31.88	891.47	859.59	2 996.41	

Table A1.6: Data for the column operated with water at 40 °C and u_G = 0.047 m/s

Run	ΔT_1 (°C)	ΔT_2 (°C)	ΔT_3 (°C)	ΔT_4 (°C)	ΔT_5 (°C)	$\Delta T_{average}$ (°C)	ΔT_{loss} (°C)	Q_{loss} (W)	P_e (W)	Q_{input} (W)	h (W.m^{-2}.K^{-1})	Experimental error
1	2.56	4.29	2.63	2.71	3.54	2.86	155.69	39.48	1 232.04	1 192.55	3 109.52	1.5
2	2.26	3.59	2.28	2.33	2.86	2.43	145.36	36.86	1 017.06	980.20	3 038.08	
3	2.03	3.16	2.06	2.13	2.48	2.18	126.95	32.19	899.56	867.37	2 995.76	
4												

Table A1.7: Data for the column operated with water at 40 °C and u_G = 0.051 m/s

Run	ΔT_1 (°C)	ΔT_2 (°C)	ΔT_3 (°C)	ΔT_4 (°C)	ΔT_5 (°C)	$\Delta T_{average}$ (°C)	ΔT_{loss} (°C)	Q_{loss} (W)	P_e (W)	Q_{input} (W)	h (W.m^{-2}.K^{-1})	Experimental error
1												
2	2.18	3.51	2.26	2.38	2.78	2.40	148.75	37.72	1 045.42	1 007.69	3 272.58	4.0
3	1.96	3.09	1.98	2.08	2.43	2.11	130.10	32.99	897.60	864.61	3 087.31	
4												

Table A1.8: Data for the column operated with heat transfer oil at $T = 75\,^{o}C$ (u_G = 0.007 m/s) and $103\,^{o}C$ (u_G = 0.009 m/s)

Run	ΔT_1 (°C)	ΔT_2 (°C)	ΔT_3 (°C)	ΔT_4 (°C)	ΔT_5 (°C)	$\Delta T_{average}$ (°C)	ΔT_{loss} (°C)	Q_{loss} (W)	P_e (W)	Q_{input} (W)	h (W.m^{-2}.K^{-1})
					T = **75 °C**						
1	7.4	7.4	7.4	7.4	7.4	7.4	83.4	21.16	493.73	472.57	440.77
2	7.5	6.8	8.9	7.4	8.9	7.9	90.4	22.93	472.15	449.22	438.41
					T = **103 °C**						
1	9.3	9.1	12.0	10.2	12.0	10.5	136.0	34.48	817.21	782.73	547.71
2	9.9	9.2	11.8	9.9	11.6	10.5	130.3	33.05	814.95	781.90	549.74

Table A1.9: Data for the column operated with heat transfer oil at $T = 75\,^{o}C$ (u_G = 0.017 m/s) and $103\,^{o}C$ (u_G = 0.019 m/s)

Run	ΔT_1 (°C)	ΔT_2 (°C)	ΔT_3 (°C)	ΔT_4 (°C)	ΔT_5 (°C)	$\Delta T_{average}$ (°C)	ΔT_{loss} (°C)	Q_{loss} (W)	P_e (W)	Q_{input} (W)	h (W.m^{-2}.K^{-1})
					T = **75 °C**						
1	6.9	6.9	6.9	6.9	6.9	6.9	98.5	24.98	553.10	528.11	525.85
2	8.0	7.2	9.3	7.8	9.7	8.4	94.1	23.87	552.31	528.44	522.64
					T = **103 °C**						
1	10.4	8.7	11.4	9.0	10.9	10.1	145.6	36.92	933.58	896.65	653.49
2	9.8	8.4	11.4	9.1	10.4	9.8	144.4	36.62	918.23	881.61	662.17

Table A1.10: Data for the column operated with heat transfer oil at $T = 75\,^{o}C$ (u_G = 0.027 m/s) and $103\,^{o}C$ (u_G = 0.029 m/s)

Run	ΔT_1 (°C)	ΔT_2 (°C)	ΔT_3 (°C)	ΔT_4 (°C)	ΔT_5 (°C)	$\Delta T_{average}$ (°C)	ΔT_{loss} (°C)	Q_{loss} (W)	P_e (W)	Q_{input} (W)	h (W.m^{-2}.K^{-1})
T = **75 °C**											
1	7.5	6.8	8.9	7.4	8.9	7.9	102.4	25.98	649.54	623.56	583.07
2	8.7	7.9	10.3	8.5	10.3	9.1	101.6	25.77	630.74	604.97	575.17
T = **103 °C**											
1	11.1	9.1	12.0	9.6	11.5	10.7	159.9	40.54	1 056.72	1 016.18	701.08
2	10.8	9.1	12.0	9.7	11.7	10.7	155.6	39.46	1 067.53	1 028.07	710.61

Table A1.11: Data for the column operated with heat transfer oil at $T = 75\,^{o}C$ (u_G = 0.0035 m/s) and $103\,^{o}C$ (u_G = 0.038 m/s)

Run	ΔT_1 (°C)	ΔT_2 (°C)	ΔT_3 (°C)	ΔT_4 (°C)	ΔT_5 (°C)	$\Delta T_{average}$ (°C)	ΔT_{loss} (°C)	Q_{loss} (W)	P_e (W)	Q_{input} (W)	h (W.m^{-2}.K^{-1})
T = **75 °C**											
1	8.0	7.2	9.3	7.8	9.7	8.4	108.8	27.59	689.67	662.08	580.76
2	9.3	8.8	11.2	9.4	11.0	9.9	109.6	27.80	695.10	667.30	603.30
T = **103 °C**											
1	12.0	10.2	13.4	11.2	14.0	12.2	175.31	44.5	1 209.45	1 164.99	705.92
2	11.8	10.2	13.5	11.0	13.7	12.0	174.88	44.3	1 224.87	1 180.52	719.47

Table A1.12: Data for the column operated with heat transfer oil at $T = 75\,^{o}C$ (u_G = 0.041 m/s) and $103\,^{o}C$ (u_G = 0.045 m/s)

Run	ΔT_1 (°C)	ΔT_2 (°C)	ΔT_3 (°C)	ΔT_4 (°C)	ΔT_5 (°C)	$\Delta T_{average}$ (°C)	ΔT_{loss} (°C)	Q_{loss} (W)	P_e (W)	Q_{input} (W)	h (W.m^{-2}.K^{-1})
T = 75 °C											
1	8.7	7.9	10.3	8.5	10.3	9.1	119.1	30.21	762.05	731.84	591.92
2	10.0	9.7	12.2	10.0	11.8	10.7	125.7	31.87	758.56	726.69	599.60
T = 103 °C											
1	12.3	10.7	13.9	11.8	14.1	12.6	182.2	46.22	1 243.74	1 197.52	702.52
2	12.4	10.7	13.7	11.5	14.0	12.5	178.9	45.38	1 262.80	1 217.42	719.93

Table A1.13: Data for the column operated with heat transfer oil at $T = 75\,^{o}C$ (u_G = 0.046 m/s) and 98 °C (u_G = 0.05 m/s)

Run	ΔT_1 (°C)	ΔT_2 (°C)	ΔT_3 (°C)	ΔT_4 (°C)	ΔT_5 (°C)	$\Delta T_{average}$ (°C)	ΔT_{loss} (°C)	Q_{loss} (W)	P_e (W)	Q_{input} (W)	h (W.m^{-2}.K^{-1})
T = 75 °C											
1	9.3	8.8	11.2	9.4	11.0	9.9	129.6	32.86	832.99	800.12	593.71
2	10.0	9.7	12.2	10.0	11.8	10.7	130.9	33.20	826.20	793.00	594.41
T = 98 °C											
1	13.7	12.0	14.9	12.5	14.9	13.6	181.9	46.13	1 309.82	1 263.69	685.15
2	13.5	11.5	14.5	12.3	15.0	13.3	185.0	46.93	1 298.44	1 251.51	691.27

Table A1.14: Data for the column operated with heat transfer oil at u_G = 0.049 m/s

Run	ΔT_1 (°C)	ΔT_2 (°C)	ΔT_3 (°C)	ΔT_4 (°C)	ΔT_5 (°C)	$\Delta T_{average}$ (°C)	ΔT_{loss} (°C)	Q_{loss} (W)	P_e (W)	Q_{input} (W)	h (W.m^{-2}.K^{-1})
T = 75 °C											
1	10.0	9.7	12.2	10.0	11.8	10.7	134.7	34.16	888.25	854.09	586.50
2	10.0	9.7	12.2	10.0	11.8	10.7	135.4	34.34	884.93	850.58	598.03
1											
2											

Appendix 2: Experimental data for gas holdup measurements

Tables A2.1 to A2.4 show the experimental data for the gas holdup measurements.

Table A2.1: First run for the column operated with water at 40 °C

	Small bubbler			Large bubbler			
u_G (m)	H_{mano} (mm)	H (m)	$\bar{\varepsilon}_G$ (–)	H_{mano} (mm)	H (m)	$\bar{\varepsilon}_G$ (–)	$\bar{\varepsilon}_G^{average}$ (–)
0.000	136.10	0.136	0.000	287.14	0.287	0.000	0.000
0.006	178.30	0.184	0.032	322.83	0.333	0.032	0.032
0.012	217.20	0.232	0.062	355.62	0.379	0.061	0.062
0.017	243.58	0.265	0.082	379.42	0.414	0.083	0.082
0.023	267.60	0.298	0.101	403.33	0.450	0.104	0.102
0.028	285.73	0.323	0.115	419.79	0.476	0.119	0.117
0.033	308.41	0.355	0.132	435.85	0.503	0.133	0.132
0.037	307.83	0.354	0.131	439.61	0.509	0.136	0.134
0.040	322.32	0.376	0.143	452.58	0.531	0.148	0.145
0.044	339.26	0.402	0.156	457.79	0.540	0.153	0.154
0.046	348.42	0.416	0.163	479.78	0.580	0.172	0.167

Table A2.2: Second run for the column operated with water at 40 °C

	Small bubbler			Large bubbler			
u_G (m)	H_{mano} (mm)	H (m)	$\bar{\varepsilon}_G$ (–)	H_{mano} (mm)	H (m)	$\bar{\varepsilon}_G$ (–)	$\bar{\varepsilon}_G^{average}$ (–)
0.000	145.08	0.145	0.000	312.43	0.312	0.000	0.000
0.006	185.34	0.191	0.031	347.44	0.359	0.031	0.031
0.012	229.75	0.246	0.065	382.50	0.408	0.063	0.064
0.017	262.45	0.288	0.090	412.56	0.453	0.090	0.090
0.023	290.50	0.327	0.111	433.81	0.487	0.109	0.110
0.028	309.31	0.354	0.126	447.93	0.510	0.121	0.123
0.033	321.00	0.371	0.135	453.97	0.520	0.127	0.131
0.037	331.86	0.387	0.143	459.57	0.529	0.132	0.137
0.041	340.13	0.400	0.149	473.81	0.554	0.144	0.147
0.044	363.32	0.436	0.167	485.64	0.575	0.155	0.161
0.047	367.33	0.443	0.170	493.88	0.590	0.162	0.166

Table A2.3: Third run for the column operated with water at 40 °C

	Small bubbler			Large bubbler			
u_G (m)	H_{mano} (mm)	H (m)	$\bar{\varepsilon}_G$ (–)	H_{mano} (mm)	H (m)	$\bar{\varepsilon}_G$ (–)	$\bar{\varepsilon}_G^{average}$ (–)
0.000	149.78	0.150	0.000	302.50	0.303	0.000	0.000
0.006	190.62	0.197	0.031	337.50	0.348	0.031	0.031
0.012	227.70	0.242	0.060	370.73	0.395	0.061	0.060
0.017	260.84	0.285	0.085	398.82	0.436	0.086	0.086
0.023	283.21	0.315	0.102	420.54	0.470	0.106	0.104
0.028	306.62	0.348	0.120	440.17	0.502	0.123	0.122
0.033	318.07	0.365	0.129	453.64	0.525	0.135	0.132
0.037	324.11	0.374	0.133	455.14	0.527	0.137	0.135
0.041	344.71	0.405	0.149	462.30	0.539	0.143	0.146
0.044	357.58	0.425	0.159	482.38	0.575	0.161	0.160
0.047	362.44	0.433	0.163	488.79	0.587	0.167	0.165

Table A2.4: Data for the column operated with heat transfer oil at 170 °C

	First run			Second run			Third run		
u_G (m)	H_{mano} (mm)	H (m)	$\bar{\varepsilon}_G$ (–)	H_{mano} (mm)	H (m)	$\bar{\varepsilon}_G$ (–)	H_{mano} (mm)	H (m)	$\bar{\varepsilon}_G$ (–)
0	173.59	0.233	0.039	111.71	0.148	0.025	102.91	0.136	0.023
0.008	289.20	0.440	0.153	161.27	0.225	0.074	156.02	0.218	0.075
0.019	369.71	0.621	0.232	246.38	0.377	0.158	239.08	0.366	0.157
0.029	409.78	0.726	0.272	295.39	0.480	0.206	278.33	0.447	0.196
0.038	458.67	0.870	0.320	341.83	0.590	0.252	330.15	0.566	0.247
0.046				384.39	0.702	0.294	392.00	0.731	0.308

Appendix 3: Data for mathematical modelling of dispersion coefficients

Tables A3.1 to A3.5 show the data used to model turbulent viscosities. The values of D_C, n and $\bar{\varepsilon}_G$ were obtained from the relevant literature that was compared with the model.

Table A3.1: Comparison of the estimated turbulent viscosity and that reported by Yamagoshi (1969)

D_C (m)	g (m/s^2)	n	ρ_L (kg/m^3)	$\bar{\varepsilon}_G$ (–)	$\upsilon_t^{guessed}$ (m^2/s)	u_W (m/s)	τ_W (N/m)	r_o (m)	ϕ_o (–)	$m_{upwards}$ (kg/s)	δ (m)	ΔZ (m)	υ_t^{model} (cm^2/s)	$\upsilon_t^{literature}$ (cm^2/s)	% Error
0.25	9.8	1.6	1000	0.15	0.002849	0.317	-0.744	0.080	0.638	7.99	0.0625	0.35	28.49	44.00	35.2

Table A3.2: Comparison of the estimated turbulent viscosity and that reported by Pavlov (1965)

D_C (m)	g (m/s^2)	n	ρ_L (kg/m^3)	$\bar{\varepsilon}_G$ (–)	$\upsilon_t^{guessed}$ (m^2/s)	u_W (m/s)	τ_W (N/m)	r_o (m)	ϕ_o (–)	$m_{upwards}$ (kg/s)	δ (m)	ΔZ (m)	υ_t^{model} (cm^2/s)	$\upsilon_t^{literature}$ (cm^2/s)	% Error
0.172	9.8	2	1000	0.12	0.001280	0.256	-0.486	0.057	0.664	2.57	0.043	0.241	12.80	19.11	33.0
0.172	9.8	2	1000	0.18	0.001585	0.297	-0.654	0.058	0.674	3.23	0.043	0.241	15.85	16.55	4.2
0.172	9.8	2	1000	0.23	0.001818	0.317	-0.745	0.059	0.683	3.76	0.043	0.241	18.18	17.78	2.2
0.172	9.8	2	1000	0.28	0.002047	0.326	-0.785	0.060	0.693	4.29	0.043	0.241	20.47	19.81	3.3
0.172	9.8	2	1000	0.38	0.002547	0.308	-0.702	0.062	0.720	5.55	0.043	0.241	25.47	23.71	7.4
0.172	9.8	2	1000	0.43	0.002847	0.281	-0.584	0.063	0.737	6.35	0.043	0.241	28.47	22.07	29.0

Table A3.3: Comparison of the estimated turbulent viscosity and that reported by Yoshitome (1967)

D_C (m)	g (m/s^2)	n	ρ_L (kg/m^3)	$\bar{\varepsilon}_G$ (–)	$\upsilon_t^{guessed}$ (m^2/s)	u_W (m/s)	τ_W (N/m)	r_o (m)	ϕ_o (–)	$m_{upwards}$ (kg/s)	δ (m)	ΔZ (m)	υ_t^{model} (cm^2/s)	$\upsilon_t^{literature}$ (cm^2/s)	% Error
0.15	9.8	2	1000	0.16	0.001212	0.267	-0.527	0.050	0.670	2.14	0.0375	0.21	12.12	14.86	18.4

Table A3.4: Comparison of the estimated turbulent viscosity and that reported by Hills (1974)

D_C (m)	g (m/s^2)	n	ρ_L (kg/m^3)	$\bar{\varepsilon}_G$ (–)	$\upsilon_t^{guessed}$ (m^2/s)	u_W (m/s)	τ_W (N/m)	r_o (m)	ϕ_o (–)	$m_{upwards}$ (kg/s)	δ (m)	ΔZ (m)	υ_t^{model} (cm^2/s)	$\upsilon_t^{literature}$ (cm^2/s)	% Error
0.138	9.8	1.8	1000	0.06	0.000675	0.168	-0.208	0.044	0.642	1.05	0.0345	0.193	6.75	9.50	29.0
0.138	9.8	1.3	1000	0.11	0.001089	0.201	-0.300	0.041	0.597	1.58	0.0345	0.193	10.89	10.37	5.1
0.138	9.8	1.8	1000	0.14	0.001054	0.238	-0.419	0.045	0.653	1.67	0.0345	0.193	10.54	10.44	0.9
0.138	9.8	1.8	1000	0.17	0.001173	0.254	-0.476	0.045	0.658	1.88	0.0345	0.193	11.73	10.75	9.2
0.138	9.8	1.8	1000	0.2	0.001288	0.265	-0.519	0.046	0.663	2.08	0.0345	0.193	12.88	14.64	12.0
0.138	9.8	1.6	1000	0.23	0.001519	0.258	-0.493	0.045	0.652	2.40	0.0345	0.193	15.19		

Table A3.5: Comparison of the estimated turbulent viscosity and that reported by Miyauchi & Shyu (1970)

D_C (m)	g (m/s^2)	n	ρ_L (kg/m^3)	$\bar{\varepsilon}_G$ (–)	$\upsilon_t^{guessed}$ (m^2/s)	u_W (m/s)	τ_W (N/m)	r_o (m)	ϕ_o (–)	$m_{upwards}$ (kg/s)	δ (m)	ΔZ (m)	υ_t^{model} (cm^2/s)	$\upsilon_t^{literature}$ (cm^2/s)	% Error
0.1	9.8	8	1000	0.12	0.000316	0.179	-0.238	0.037	0.730	0.41	0.025	0.14	3.16	5.50	42.5
0.1	9.8	8	1000	0.15	0.000345	0.203	-0.306	0.037	0.733	0.45	0.025	0.14	3.45	5.60	38.4
0.1	9.8	8	1000	0.21	0.000388	0.248	-0.454	0.037	0.738	0.50	0.025	0.14	3.88	6.00	35.4
0.1	9.8	8	1000	0.26	0.000411	0.283	-0.593	0.037	0.743	0.54	0.025	0.14	4.11	7.00	41.2
0.1	9.8	8	1000	0.29	0.000421	0.304	-0.684	0.037	0.746	0.55	0.025	0.14	4.21	8.10	48.0
0.1	9.8	8	1000	0.31	0.000426	0.318	-0.748	0.037	0.749	0.56	0.025	0.14	4.26	7.50	43.2
0.1	9.8	8	1000	0.34	0.000431	0.339	-0.850	0.038	0.752	0.57	0.025	0.14	4.31	9.10	52.6

Tables A3.6 to A3.11 show the data used to model dispersion coefficients. The value of n = 2 was used, similar to the work of Ueyama & Miyauchi (1979) and low $\bar{\varepsilon}_G$ values were chosen.

Table A3.6: Modelling of dispersion coefficients for D_C = 100 mm

D_C (m)	g (m/s^2)	n	ρ_L (kg/m^3)	$\bar{\varepsilon}_G$ (–)	$\upsilon_t^{guessed}$ (m^2/s)	u_W (m/s)	τ_W (N/m)	r_o (m)	ϕ_o (–)	$m_{upwards}$ (kg/s)	δ (m)	ΔZ (m)	υ_t^{model} (m^2/s)	E_Z (m^2/s)	$D_C^{(4/3)} P_m^{(1/3)}$ (m^2/s)	E_Z / E_r (–)
0.1	9.8	2	1000	0.05	0.00036	0.132	-0.129	0.033	0.655	0.420	0.025	0.14	0.00036	74.78	308.74	20.54
0.1	9.8	2	1000	0.1	0.00052	0.181	-0.242	0.033	0.661	0.601	0.025	0.14	0.00052	107.20	388.99	20.74
0.1	9.8	2	1000	0.15	0.00064	0.213	-0.336	0.033	0.669	0.750	0.025	0.14	0.00064	133.70	428.14	20.97
0.1	9.8	2	1000	0.2	0.00085	0.246	-0.446	0.034	0.687	1.023	0.025	0.14	0.00085	182.29	490.10	21.54

Table A3.7: Modelling of dispersion coefficients for D_C = 200 mm

D_C (m)	g (m/s^2)	n	ρ_L (kg/m^3)	$\bar{\varepsilon}_G$ (–)	$\upsilon_t^{guessed}$ (m^2/s)	u_W (m/s)	τ_W (N/m)	r_o (m)	ϕ_o (–)	$m_{upwards}$ (kg/s)	δ (m)	ΔZ (m)	υ_t^{model} (cm^2/s)	E_Z (m^2/s)	$D_C^{(4/3)} P_m^{(1/3)}$ (m^2/s)	E_Z / E_r (–)
0.2	9.8	2	1000	0.05	0.00103	0.187	-0.259	0.065	0.655	2.37	0.05	0.28	0.00103	211.52	777.98	20.54
0.2	9.8	2	1000	0.1	0.00146	0.256	-0.485	0.066	0.661	3.40	0.05	0.28	0.00146	303.21	980.20	20.74
0.2	9.8	2	1000	0.15	0.00180	0.301	-0.671	0.067	0.669	4.24	0.05	0.28	0.00180	378.15	1 078.85	20.98
0.2	9.8	2	1000	0.2	0.00211	0.331	-0.810	0.068	0.677	5.02	0.05	0.28	0.00211	447.18	1 234.97	21.24

Table A3.8: Modelling of dispersion coefficients for $D_C = 300$ mm

D_C (m)	g (m/s²)	n	ρ_L (kg/m³)	$\bar{\varepsilon}_G$ (–)	$\upsilon_t^{guessed}$ (m²/s)	u_W (m/s)	τ_W (N/m)	r_o (m)	ϕ_o (–)	$m_{upwards}$ (kg/s)	δ (m)	ΔZ (m)	υ_t^{model} (cm²/s)	E_Z (m²/s)	$D_C^{(4/3)} P_m^{(1/3)}$ (m²/s)	E_Z / E_r (–)
0.3	9.8	2	1000	0.05	0.00189	0.229	-0.388	0.098	0.655	6.54	0.075	0.42	0.00189	388.59	1 335.85	20.54
0.3	9.8	2	1000	0.1	0.00269	0.314	-0.727	0.099	0.661	9.37	0.075	0.42	0.00269	557.03	1 683.07	20.74
0.3	9.8	2	1000	0.15	0.00331	0.369	-1.007	0.100	0.669	11.69	0.075	0.42	0.00331	694.71	1 852.46	20.98
0.3	9.8	2	1000	0.2	0.00387	0.405	-1.214	0.102	0.677	13.83	0.075	0.42	0.00387	821.52	2 120.53	21.24

Table A3.9: Modelling of dispersion coefficients for $D_C = 400$ mm

D_C (m)	g (m/s²)	n	ρ_L (kg/m³)	$\bar{\varepsilon}_G$ (–)	$\upsilon_t^{guessed}$ (m²/s)	u_W (m/s)	τ_W (N/m)	r_o (m)	ϕ_o (–)	$m_{upwards}$ (kg/s)	δ (m)	ΔZ (m)	υ_t^{model} (cm²/s)	E_Z (m²/s)	$D_C^{(4/3)} P_m^{(1/3)}$ (m²/s)	E_Z / E_r (–)
0.4	9.8	2	1000	0.05	0.00291	0.265	-0.517	0.131	0.655	13.43	0.1	0.56	0.00291	598.27	1 960.39	20.54
0.4	9.8	2	1000	0.1	0.00413	0.362	-0.970	0.132	0.661	19.24	0.1	0.56	0.00413	857.60	2 469.94	20.74
0.4	9.8	2	1000	0.15	0.00510	0.426	-1.342	0.134	0.669	24.00	0.1	0.56	0.00510	1 069.57	2 718.52	20.98
0.4	9.8	2	1000	0.2	0.00596	0.468	-1.619	0.135	0.677	28.38	0.1	0.56	0.00596	1 264.81	3 111.93	21.24

Table A3.10: Modelling of dispersion coefficients for $D_C = 500$ mm

D_C (m)	g (m/s^2)	n	ρ_L (kg/m^3)	$\bar{\varepsilon}_G$ (–)	$\upsilon_t^{guessed}$ (m^2/s)	u_W (m/s)	τ_W (N/m)	r_o (m)	ϕ_o (–)	$m_{upwards}$ (kg/s)	δ (m)	ΔZ (m)	υ_t^{model} (cm^2/s)	E_Z (m^2/s)	$D_C^{(4/3)} P_m^{(1/3)}$ (m^2/s)	E_Z / E_r (–)
0.5	9.8	2	1000	0.05	0.00407	0.296	-0.647	0.164	0.655	23.45	0.125	0.7	0.00407	836.11	2 639.71	20.54
0.5	9.8	2	1000	0.1	0.00578	0.405	-1.212	0.165	0.661	33.62	0.125	0.7	0.00578	1 198.53	3 325.83	20.74
0.5	9.8	2	1000	0.15	0.00713	0.476	-1.678	0.167	0.669	41.93	0.125	0.7	0.00713	1 494.77	3 660.55	20.98
0.5	9.8	2	1000	0.2	0.00832	0.523	-2.024	0.169	0.677	49.58	0.125	0.7	0.00832	1 767.62	4 190.28	21.24

Table A3.11: Modelling of dispersion coefficients for $D_C = 600$ mm

D_C (m)	g (m/s^2)	n	ρ_L (kg/m^3)	$\bar{\varepsilon}_G$ (–)	$\upsilon_t^{guessed}$ (m^2/s)	u_W (m/s)	τ_W (N/m)	r_o (m)	ϕ_o (–)	$m_{upwards}$ (kg/s)	δ (m)	ΔZ (m)	υ_t^{model} (cm^2/s)	E_Z (m^2/s)	$D_C^{(4/3)} P_m^{(1/3)}$ (m^2/s)	E_Z / E_r (–)
0.6	9.8	2	1000	0.05	0.00535	0.324	-0.776	0.196	0.655	37.00	0.15	0.84	0.00535	1 099.10	3 366.14	20.54
0.6	9.8	2	1000	0.1	0.00760	0.444	-1.455	0.198	0.661	53.03	0.15	0.84	0.00760	1 575.51	4 241.07	20.74
0.6	9.8	2	1000	0.15	0.00937	0.522	-2.014	0.201	0.669	66.14	0.15	0.84	0.00937	1 964.93	4 667.90	20.98
0.6	9.8	2	1000	0.2	0.01094	0.573	-2.429	0.203	0.677	78.21	0.15	0.84	0.01094	2 323.60	5 343.41	21.24

Appendix 4: Calculation of experimental and percentage error

The experimental error was calculated as follows:

Calculate the mean, $\bar{x}$ for the data as given by:

$$\bar{x} = \frac{1}{N}\sum_{i=1}^{N} x_i \qquad [A4.1]$$

where N is the number of data points and x_i is the individual data point.

Calculate the standard deviation of the data as follows:

$$s = \sqrt{\frac{\sum_{i=1}^{N}(x_i - \bar{x})^2}{N}} \qquad [A4.2]$$

Calculate the standard error (SE) of the mean of the data as given by:

$$SE = \frac{s}{\sqrt{N}} \qquad [A4.3]$$

Calculate the critical value, z, for a 95% confidence level as given by:

$$z = \frac{(\bar{x} - \mu)\sqrt{N}}{s} \qquad [A4.4]$$

where μ is the mean value for the continuous variable x.

Calculate the confidence interval with the form:

$$Confidence\ interval\ (CI) = \bar{x} \pm (SE \times z) \qquad [A4.5]$$

Calculate the experimental error from the following equation:

$$Experimental\ \ error = \frac{SE \times z}{\bar{x}} \times 100 \qquad [A4.6]$$

The percentage error was calculated from Equation A4.7 below:

$$Percent\ \ error = \frac{Model\ \ value - Literature\ \ value}{Model\ \ value} \times 100 \qquad [A4.7]$$

Appendix 5: Temperature difference between the column centre and the liquid–film interface

The following mathematical modelling was done to estimate the radial temperature profile inside the bubble column. Assuming that the axial and radial thermal dispersion coefficients in a bubble column are constants, the steady-state temperature profile in a bubble column can be described by the following partial differential equation:

$$\frac{d^2T_{z,r}}{dr^2}+\frac{1}{r}\frac{dT_{z,r}}{dr}+\frac{E_Z}{E_r}\frac{d^2T_{z,r}}{dZ^2}=0 \qquad \text{[A5.1]}$$

Multiplying Equation A5.1 by r yields:

$$r\frac{d^2T_{z,r}}{dr^2}+\frac{dT_{z,r}}{dr}+\frac{rE_Z}{E_r}\frac{d^2T_{z,r}}{dZ^2}=0 \qquad \text{[A5.2]}$$

If the axial temperature profile is constant in the radial direction, the term $\frac{d^2T_{z,r}}{dZ^2}$ is constant in the radial direction. Let $\frac{d^2T_{z,r}}{dZ^2}=K$, where K is a constant. Equation A5.2 therefore becomes:

$$r\frac{d^2T_{z,r}}{dr^2}+\frac{dT_{z,r}}{dr}+\frac{rE_Z}{E_r}K=0 \qquad \text{[A5.3]}$$

Equation A5.3 can be written as:

$$\frac{d}{dr}\left(r\frac{dT_{z,r}}{dr^2}\right)+\frac{rE_Z}{E_r}K=0 \qquad \text{[A5.4]}$$

Integrating Equation A5.4 gives:

$$\int d\left(r\frac{dT_{z,r}}{dr^2}\right)=-\int\frac{rE_Z}{E_r}Kdr \qquad \text{[A5.5]}$$

$$r\frac{dT_{z,r}}{dr} = -\frac{E_Z}{E_r}K\frac{r^2}{2} + C_1 \qquad [A5.6]$$

In the centre of the column, the radial gradient of the temperature profile must be zero or else the temperature at the centre of the column will increase. Therefore, at $r = 0$, $\frac{dT_{z,r}}{dr} = 0$ and by substituting the above boundary condition into Equation A5.6, $C_1 = 0$. Thus Equation A5.6 becomes:

$$r\frac{dT_{z,r}}{dr} = -\frac{E_Z}{E_r}K\frac{r^2}{2} \qquad [A5.7]$$

If heat is supplied uniformly along the height of the column through the column wall, it is the same for all axial positions along the heated section. Therefore at $r = R$, $\frac{dT_{z,r}}{dZ} = F$ and applying this boundary condition to Equation A5.7 gives:

$$K = -\frac{2FE_r}{RE_Z} \qquad [A5.8]$$

Substituting Equation A5.8 into Equation A5.7 gives:

$$r\frac{dT_{z,r}}{dr} = \frac{F}{R}r^2 \qquad [A5.9]$$

Integrating Equation A5.9 gives:

$$\int dT_{z,r} = \int \frac{F}{R} r dr \qquad [A5.10]$$

$$T_{z,r} = \frac{F}{R}\frac{r^2}{2} + C_2 \qquad [A5.11]$$

C_2 is a constant in the radial direction but it not constant in an axial direction. Therefore at $r = 0$, $T_{z,r} = T_{z,0}$ and applying this boundary condition to Equation A5.11 one obtain $C_2 = T_{z,0}$.

Therefore Equation A5.11 becomes:

$$T_{z,r} = \frac{F}{R}\frac{r^2}{2} + T_{z,0} \qquad [A5.12]$$

Integrating $\frac{d^2T_{z,r}}{dZ^2} = K$ and substituting Equation 5.8 gives:

$$\int d\left(\frac{dT_{z,r}}{dZ}\right) = \int K dZ \qquad [A5.13]$$

$$\frac{dT_{z,r}}{dZ} = -\frac{2FE_rZ}{RE_Z} + C_3 \qquad [A5.14]$$

The boundary condition for perfect insulation of the bottom of the column is that at $Z = 0$, $\frac{dT_{z,r}}{dZ} = 0$. Applying this boundary condition to Equation A5.14 yields $C_3 = 0$. Equation A5.14 therefore becomes:

$$\frac{dT_{z,r}}{dZ} = -\frac{2FE_rZ}{RE_Z} \qquad [A5.15]$$

Integrating Equation A5.15 gives

$$\int dT_{z,r} = \int -\frac{2FE_rZ}{RE_Z} dZ \qquad [A5.16]$$

$$T_{z,r} = -\frac{FE_rZ^2}{RE_Z} + C_4 \qquad [A5.17]$$

C_4 is a constant in an axial direction but it not constant in a radial direction. Heat is supplied and removed from the column in such a way to ensure that the temperature in the centre at the bottom of the column is constant. Therefore; at $Z = 0$ and $r = 0$, $T_{z,r} = T_{0,0}$. Applying this boundary condition to Equation A5.17 yields $C_4 = T_{0,0}$. Equation A5.17 therefore becomes:

$$T_{z,0} = -\frac{FE_rZ^2}{RE_Z} + T_{0,0} \qquad [A5.18]$$

Substituting Equation A5.18 into Equation A5.12 yield

$$T_{z,r} = \frac{F}{R}\frac{r^2}{2} - \frac{FE_r Z^2}{RE_Z} + T_{0,0} \qquad [A5.19]$$

Checking the differential equation:

From Equation A5.19, differentiating with respect to r and Z, respectively gives:

$$\frac{dT_{z,r}}{dr} = \frac{F}{R}r \qquad [A5.20]$$

$$\frac{d^2T_{z,r}}{dr^2} = \frac{F}{R} \qquad [A5.21]$$

$$\frac{dT_{z,r}}{dZ} = -\frac{2FE_r}{RE_Z}Z \qquad [A5.22]$$

$$\frac{d^2T_{z,r}}{dZ^2} = -\frac{2FE_r}{RE_Z} \qquad [A5.23]$$

The differential equation in Equation 5.1 is checked by substituting Equations A5.20, A5.21, A5.22 and A5.23 into Equation A5.1:

$$\frac{d^2T_{z,r}}{dr^2} + \frac{1}{r}\frac{dT_{z,r}}{dr} + \frac{E_Z}{E_r}\frac{d^2T_{z,r}}{dZ^2} = \frac{F}{R} + \frac{F}{R} + \frac{E_Z}{E_r}\left(\frac{-2FE_r}{RE_Z}\right) = 0 \qquad [A5.24]$$

The conclusion from checking the differential equation is that the assumption made in Equation A5.3, that the term $\frac{d^2T_{z,r}}{dZ^2}$ is constant in the radial direction, is correct. However, it is only correct for the chosen boundary conditions.

The temperature difference between the centre of a column and liquid–film interface is calculated as follows:

The temperature at the centre of the column is given by:

$$T_{z,0} = -\frac{FE_r Z^2}{RE_Z} + T_{0,0} \qquad [A5.25]$$

Assuming that the film thickness at the wall is very small, therefore the temperature at the liquid–film interface is given by:

$$T_{z,R} = \frac{FR}{2} - \frac{FE_r Z^2}{RE_Z} + T_{0,0} \qquad [A5.26]$$

The temperature difference is therefore given by:

$$T_{z,R} - T_{z,0} = \frac{FR}{2} \qquad [A5.27]$$

At $r = R$, the rate of heat transfer is given by:

$$Q = 2\pi R Z_1 \rho_L C_{PL} E_r \frac{dT_{z,r}}{dZ} \qquad [A5.28]$$

where Q is the rate of heat transfer to the column and Z_1 is the length of the heating section of the bubble column. Therefore:

$$F = \frac{Q}{2\pi R Z_1 \rho_L C_{PL} E_r} \qquad [A5.29]$$

Using the heat input from Table 4.1 for u_G = 0.031 m/s and estimating E_Z from the correlation in Figures 4.15:

$$E_Z = 0.35(D_C)^{4/3}(g \times u_G)^{1/3}$$

$$E_Z = 0.35(0.108)^{4/3}(9.81 \times 0.031)^{1/3}$$

$$E_Z = 0.012\ m^2/s$$

It mostly reported that the value of E_r is 1/100th of the value of E_r (Abdulrazzaq, 2010 and Camacho Rubio et al., 2004), therefore:

$$E_r = 0.01 \times 0.012 \ m^2/s$$

$$E_r = 0.00012 \ m^2/s$$

Substituting the value of E_r into Equation 5.29.

$$F = \frac{2703.2 \ W}{2\pi \times 0.054\,m \times 1.05\,m \times 1000\,kg.m^{-3} \times 4180\,J.kg^{-1}.^{o}C \times 0.00012\,m^2/s}$$

$$F = 15 \ ^{o}C.m^{-1}$$

Substituting the value of F into Equation 5.27.

$$T_{z,R} - T_{z,0} = \frac{15 \ ^{o}C.m^{-1} \times 0.054\,m}{2}$$

$$T_{z,R} - T_{z,0} = 0.4^{o}C$$

The temperature difference could be greater than this value if the assumption that the axial and radial dispersion coefficient is constant was not made.

Appendix 6: Derivation of gas holdup equation

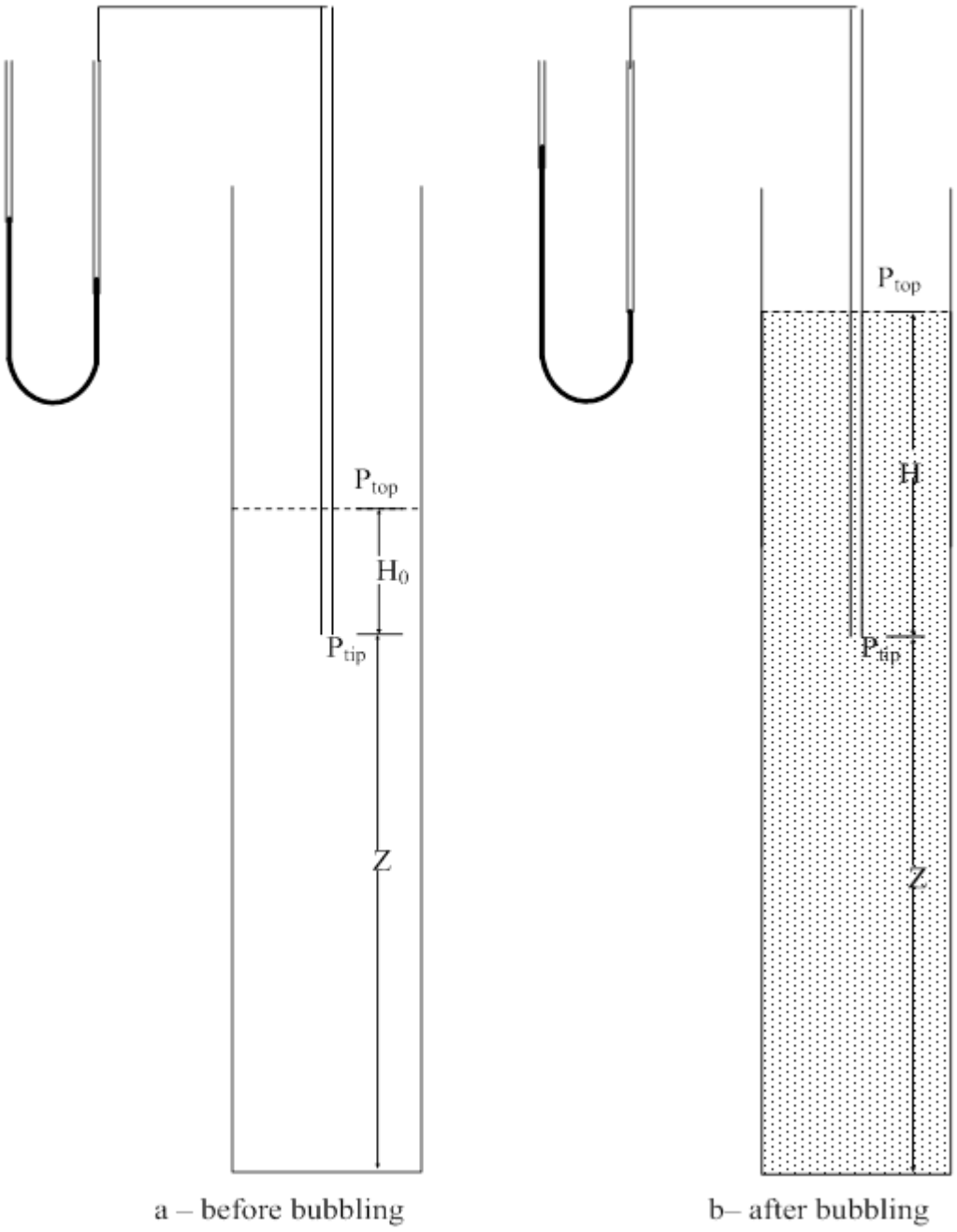

Figure A6.1: Column level before and after bubbling

Gas holdup can be calculated from both the level expansion method. All the necessary equations were derived, as given below.

The equations derived here are based on a single bubbler tube, as shown in Figure A6.1. Pressure at the tip of the bubbler tube is given by:

$$P_{top} = P_{tip} + \rho_{disp} g H \qquad [A6.1]$$

where P_{tip} is the pressure at the tip of the bubbler, P_{top} is the pressure at the surface of the liquid, ρ_{disp} is the density of the gas–liquid dispersion, H is the depth of the dip tube in the gas–liquid dispersion. Also, as the pressure difference in the bubbler tube is the same as that of the manometer, Equation A6.1 is equivalent to:

$$P_{top} - P_{tip} = \rho_{disp} g H = \rho_{water} g H_{mano} \qquad [A6.2]$$

where ρ_{water} is the density of water in the manometer and H_{mano} is the head of the manometer. The density of the dispersion is given by:

$$\rho_{disp} = \rho_L (1 - \bar{\varepsilon}_G) + \rho_G \bar{\varepsilon}_G \qquad [A6.3]$$

where ρ_L is the density of the liquid in the bubble column and ρ_G is the gas density. The gas density is very small compared with that of a liquid, and therefore Equation A6.3 can be reduced to:

$$\rho_{disp} \approx \rho_L (1 - \bar{\varepsilon}_G) \qquad [A6.4]$$

The average gas holdup is given by:

$$\bar{\varepsilon}_G = \frac{(H + Z) - (H_0 + Z)}{h_2 + Z} \qquad [A6.5]$$

Simplifying Equation A6.5 yields:

$$\bar{\varepsilon}_G = \frac{H - H_0}{H + Z} \qquad [A6.6]$$

where Z is the distance from the tip of a dip tube to the bottom of the column. From Equation A6.2:

$$H = \frac{\rho_{water} H_{mano}}{\rho_{disp}} \qquad [\text{A6.7}]$$

Substituting Equation A6.4 into Equation A6.7:

$$H = \frac{\rho_{water} H_{mano}}{\rho_L (1 - \bar{\varepsilon}_G)} \qquad [\text{A6.8}]$$

Gas holdup can be calculated by solving Equations A6.6 and A6.8 simultaneously, as shown below.

Substituting Equation A6.6 into Equation A6.8 gives:

$$H = \frac{\rho_{water} H_{mano}}{\rho_L \left[1 - \left(\frac{H - H_0}{H + Z}\right)\right]} \qquad [\text{A6.9}]$$

$$H = \frac{\rho_{water} H_{mano} (H + Z)}{\rho_L (H_0 + Z)} \qquad [\text{A6.10}]$$

$$H = \frac{\rho_{water} H_{mano} Z}{\rho_L H_0 + \rho_L Z - \rho_{water} H_{mano}} \qquad [\text{A6.11}]$$

Gas holdup can be calculated from Equation A6.6 once the value of H is known.

Appendix 7: Calibration

A7.1 Temperature difference calibration

The temperature difference from thermocouples connected in series was calibrated by inserting the thermocouples into a brass block, as shown in Figure A7.1.

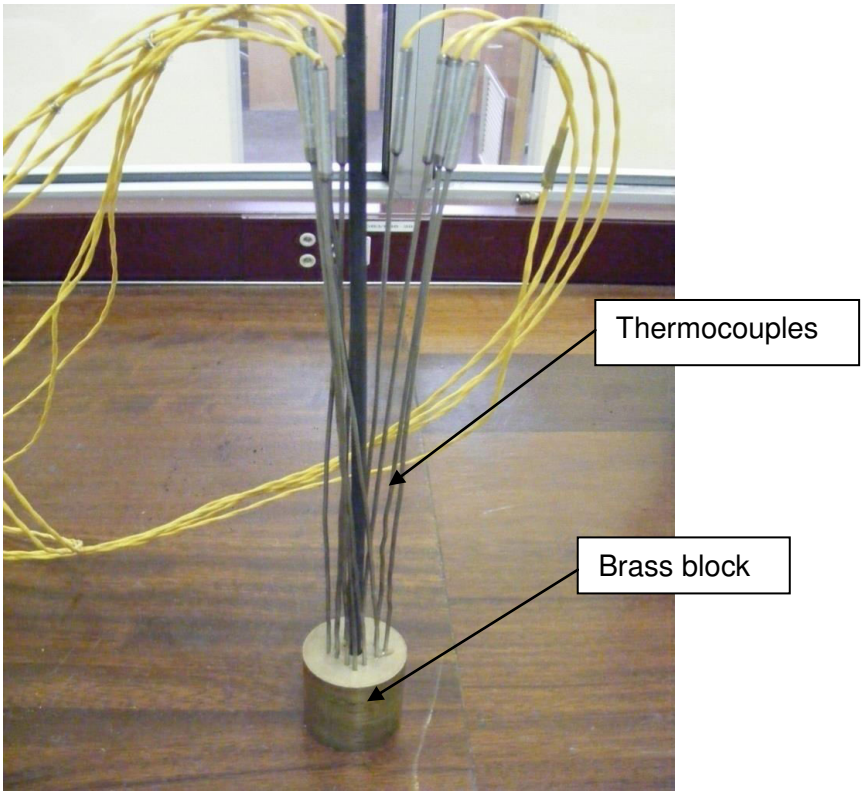

Figure A7.1: Brass block that ensures uniform temperature

A standard thermocouple has a red wire and a yellow wire. To measure the temperature difference using two thermocouples, yellow wires were joined together and red wires were connected to the data logger. However, it does not matter which wire (red/yellow) is joined. If the thermocouples have been perfectly manufactured, they will read a zero temperature difference if inserted into water that is at uniform temperature. However, there will be some small error due to imperfection in their manufacturing. The calibration is therefore done in order to check for a few small errors in the measured temperature difference.

The brass block was inserted into the water bath at different temperatures, as shown in Figure A7.2.

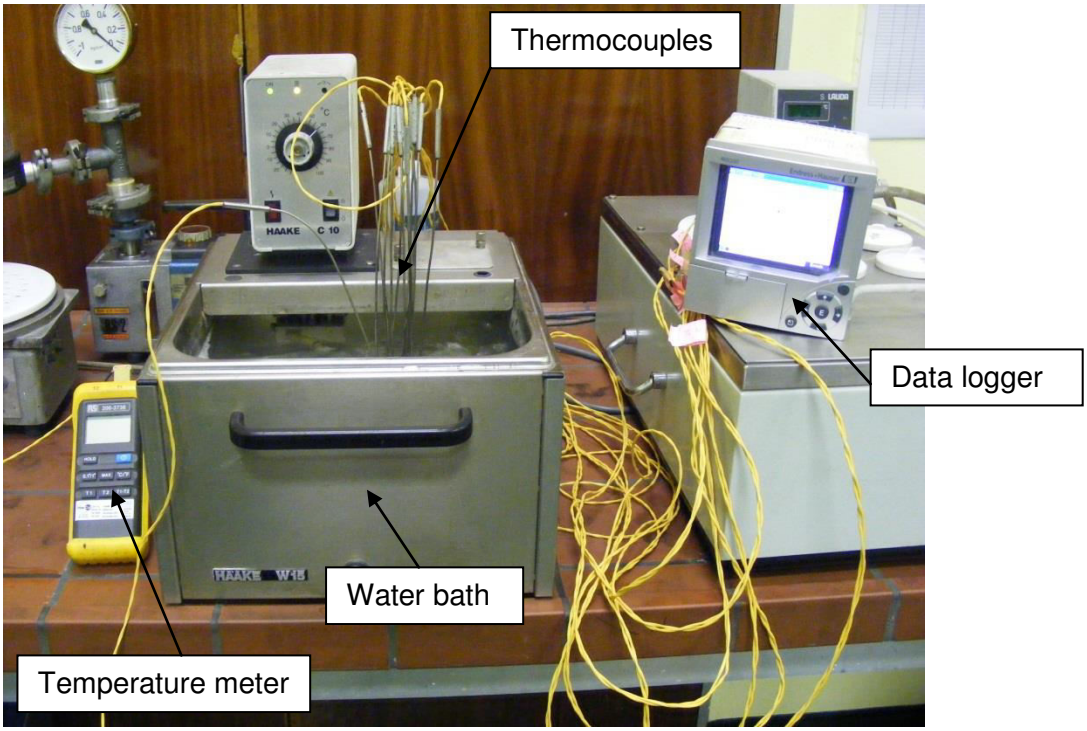

Figure A7.2: Water bath used for calibrating the thermocouples

The water bath has water circulation to keep the temperature uniform. The millivolt reading from the thermocouples was recorded on the data logger. The results are given in Table A7.1.

Table A7.1: Temperature difference for thermocouples inserted into water

First run							
T **(°C)**	ΔV_1 **(mV)**	ΔV_2 **(mV)**	ΔV_3 **(mV)**	ΔV_4 **(mV)**	ΔV_5 **(mV)**	ΔV_6 **(mV)**	
30	-0.00995 -0.25	-0.00784 -0.20	-0.00634 -0.16	-0.01443 -0.36	-0.0087 -0.22	-0.01113 -0.28	Average ΔT (°C)
60	-0.00886 -0.22	-0.00892 -0.22	-0.00543 -0.13	-0.01294 -0.32	-0.01189 -0.29	-0.01306 -0.32	Average ΔT (°C)
90	-0.00751 -0.18	-0.01127 -0.28	-0.00686 -0.17	-0.01428 -0.35	-0.01196 -0.29	-0.0168 -0.41	Average ΔT (°C)
Second run							
T **(°C)**	ΔV_1 **(mV)**	ΔV_2 **(mV)**	ΔV_3 **(mV)**	ΔV_4 **(mV)**	ΔV_5 **(mV)**	ΔV_6 **(mV)**	
30	-0.01568 -0.39	-0.01269 -0.32	-0.00992 -0.25	-0.01896 -0.48	-0.0129 -0.32	-0.01433 -0.36	Average ΔT (°C)
60	-0.00907 -0.23	-0.01072 -0.27	-0.00559 -0.14	-0.01277 -0.32	-0.01152 -0.29	-0.01246 -0.31	Average ΔT (°C)
90	-0.00875 -0.22	-0.01264 -0.31	-0.00635 -0.16	-0.01208 -0.30	-0.01217 -0.30	-0.0135 -0.33	Average ΔT (°C)
Third run							

T (°C)	ΔV_1 (mV)	ΔV_2 (mV)	ΔV_3 (mV)	ΔV_4 (mV)	ΔV_5 (mV)	ΔV_6 (mV)	
30	-0.01187 -0.30	-0.00977 -0.25	-0.00662 -0.17	-0.01438 -0.36	-0.01386 -0.35	-0.01076 -0.27	Average ΔT (°C)
60	-0.01088 -0.27	-0.01079 -0.27	-0.006 -0.15	-0.01393 -0.35	-0.01272 -0.32	-0.01279 -0.32	Average ΔT (°C)
90	-0.00694 -0.17	-0.01156 -0.28	-0.0063 -0.16	-0.01201 -0.30	-0.01152 -0.28	-0.01639 -0.40	Average ΔT (°C)

A7.2 Thermowell calibration

The thermowells were calibrated using boiling water to check the temperature difference when the temperature is measured with the aid of a thermowell and when the thermocouple is inserted directly into water. One thermocouple was used for all the experiments. Data were collected for 60 seconds for each experiment, using the data logger. The results in Table A7.2 show that a thermocouple inserted to a thermowell will still give a close representation of the temperature to be measured.

Table A7.2: Calibration of a thermowell

	Run 1		Run 2		Run 3	
	V_{t_well} (mV)	V_{water} (mV)	V_{t_well} (mV)	V_{water} (mV)	V_{t_well} (mV)	V_{water} (mV)
Average V	2.988	2.990727	2.990	2.988	2.982	2.984
ΔV (mV)	0.002785		-0.001464		0.002226	
ΔT (°C)	0.08		0.03		0.05	

Appendix 8: Gas distributor design

The design of the perforated plate is carried out to ensure that the gas flows into all orifices. The calculations below are for the column operated with water. The design begins by calculating the critical weep velocity. The following equations can be used to calculate the critical weep velocity for small and large hole diameters respectively (Kulkarni, 2010).

$$We_o = \frac{\rho_G d_o V_o^2}{\sigma} \geq 2 \qquad [A8.1]$$

where We_o is the Weber number at the critical weep point, ρ_G is the gas density, d_o is the hole diameter, V_o is the critical weep velocity and σ is the surface tension.

$$Fr' = \frac{V_o^2}{d_o g}\left[\frac{\rho_G}{\rho_L - \rho_G}\right]^{5/4} \geq 0.37 \qquad [A8.2]$$

where Fr' is the modified Froude number.

The demarcation between small and large bubbles can be calculated by equating Equations A8.1 and A8.2, which yields the following equations for small and large holes respectively.

$$d_o \leq 2.32\left[\frac{\sigma_L}{\rho_G g}\right]^{1/2}\left[\frac{\rho_G}{\rho_L - \rho_G}\right]^{5/8} \qquad [A8.3]$$

$$d_o \geq 2.32\left[\frac{\sigma_L}{\rho_G g}\right]^{1/2}\left[\frac{\rho_G}{\rho_L - \rho_G}\right]^{5/8} \qquad [A8.4]$$

The minimum superficial velocity to ensure no-weep conditions can be calculated by equating the gas flowrate in the column and the total gas flowrate through all the plate holes.

$$\frac{\pi D_C^2}{4} \times u_{mG} = N \times \frac{\pi D_o^2}{4} \times V_o \qquad [A8.5]$$

where u_{mG} is the minimum superficial gas velocity for no weeping, D_C is the column diameter, D_o is the orifice diameter, N is the number of holes and V_o is the critical weep velocity.

Step I

The density of water at 40 °C is:

$$\rho_L = 992.2 \text{ kg/m}^3$$

The surface tension of water at 40 °C is:

$$\sigma = 6.96 \times 10^{-2} \text{ N/m}$$

Argon density can be calculated from the following equation.

$$\rho_{gas} = \frac{PMr}{RT} \qquad \text{[A8.6]}$$

$$\rho_{gas} = \frac{1.2 \times 10^5 \, Pa \times 39.948 \, gmol^{-1}}{8.314 JK^{-1} mol^{-1} \times 313.15 K}$$

$$\rho_{gas} = 1841.3 \text{ g/m}^3$$

$$\rho_{gas} = 1.84 \text{ kg/m}^3$$

Step II

The demarcation for small and large perforated plate hole diameters can be predicted as follows:

$$d_o \leq 2.32 \left[\frac{6.96 \times 10^{-2} N/m}{1.84 kg/m^3 \times 9.81 m/s^2} \right]^{1/2} \left[\frac{1.84 kg/m^3}{992.2 kg/m^3 - 1.84 kg/m^3} \right]^{5/8}$$

$$d_o \leq 2.83 \text{ mm}$$

The plate hole diameters are less than 2.83 mm and thus Equation A8.1 must be used to calculate the critical weep velocity.

For a 0.5 mm hole gas distributor, the critical weep velocity is given by:

$$V_o = \sqrt{\frac{2 \times \sigma}{\rho_G \times d_o}}$$

$$V_o = \sqrt{\frac{2 \times 6.96 \times 10^{-2} N/m}{1.84 kg/m^3 \times 0.5 \times 10^{-3} m}}$$

$$V_o = 12.29 \text{ m/s}$$

Step III

Lastly, the minimum superficial velocity for no-weep conditions is calculated for the given number of holes of 0.5 mm diameter in the gas distributor.

$$\frac{\pi D_C^2}{4} \times u_{mG} = N \times \frac{\pi D_o^2}{4} \times V_o$$

$$u_{mG} = N \times \frac{D_o^2}{D_C^2} \times V_o$$

$$u_{mG} = 17 \times \left(\frac{0.5 \times 10^{-3} m}{0.108 m} \right)^2 \times 12.29 m/s$$

$$u_{mG} = 0.0045 \text{ m/s}$$

Appendix 9: Calculations of the mass of LiCl and KCl in the eutectic mixture

The volume of salt to be melted is calculated as follows:

$D_C = 0.108$ m

$L = 1.2$ m

$$A = \pi \times \frac{D^2}{4}$$

$$A = \pi \times \frac{(0.108m)^2}{4}$$

$A = 9.161 \times 10^{-3}$ m^2

$V = A \times H$

$V = 9.161 \times 10^{-3} m^2 \times 1.2m$

$V = 0.01099$ m^3

$V = 11$ litres

The density of salt eutectic at 450 °C was determined using the data from Janz (1988).

$\rho_{LiCl(l)} = 2.0286 - 5.2676 \times 10^{-4} T$ in g/cm^3 for a KCl mole fraction of 41.2–58.8 %

$\rho_{LiCl(l)} = 2.0286 - 5.2676 \times 10^{-4} \times 723.15K$

$\rho_{euctectic}$ = 1.648 g/cm^3

In kg/m^3, $\rho_{euctectic}$ = 1648 kg/m^3

Hence, the mass of salt eutectic is given by:

$m_{euctectic} = \rho_{euctectic} \times V$

$$m_{euctectic} = 1648 kg/m^3 \times 0.0109 m^3$$

$m_{euctectic}$ = 17.96 kg

The mole fraction of LiCl at eutectic is 0.592:

$$n_{LiCl} = 0.592 \times n_{total}$$

$$n_{KCl} = 0.418 \times n_{total}$$

$$m_{LiCl} = 0.592 \times n_{total} \times 42.394$$

$$m_{KCl} = 0.592 \times n_{total} \times 74.55$$

$$n_{total} = \frac{17.96}{(0.592 \times 42.39) + (0.418 \times 74.55)}$$

n_{total} = 0.319 kmol

m_{LiCl} = 8.01 kg

m_{KCl} = 9.95 kg

Appendix 10: Photograph of the bubble column test rig

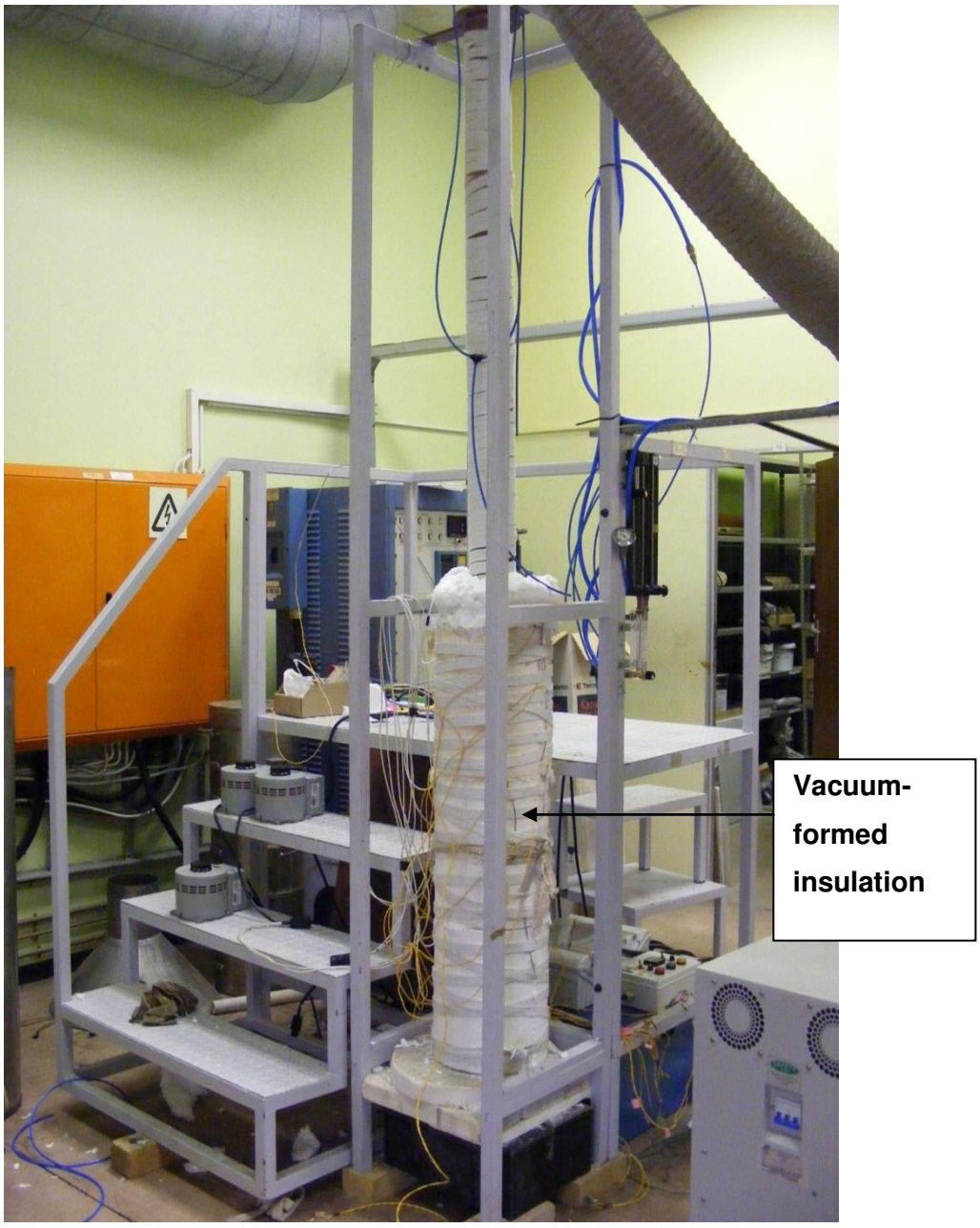

Figure A10.1: Photograph of the bubble column test rig with thermal insulation